

Secondary Pyrrhotite as a Recorder of Earth Magnetic Field Variations

Dissertation
zur Erlangung des Grades eines Doktors der Naturwissenschaften

der Geowissenschaftlichen Fakultät
der Eberhard-Karls-Universität Tübingen

vorgelegt von
Florian Wehland
aus
Mutlangen

2004

Tag der mündlichen Prüfung: 08. Dezember 2004

1. Berichterstatter: Prof. Dr. Erwin Appel,
Eberhard-Karls-Universität Tübingen
2. Berichterstatter: Prof. Pierre Rochette,
Université d'Aix-Marseille III
3. Berichterstatter: Prof. John Shaw,
University of Liverpool

„Die Wissenschaft fängt eigentlich erst da an, interessant zu werden, wo sie aufhört“

*Justus Freiherr von Liebig
(1803-1873), deutscher Chemiker*

Acknowledgement

First of all I like to thank Prof. Erwin Appel and Dr. Viktor Hoffmann for their supervision, the project management, their patience and for the support of my ideas. Dr. Christian Crouzet introduced me in the field of pTRM acquisition and gave a lot of support during field and laboratory work. Prof. Pierre Rochette guidance during my time in France and his final revision of the thesis is greatly acknowledged. Prof. Soffel opened the way for using the magnetic laboratory and supported the development of the TRM furnace at the LMU.

Significant contribution to the thesis came from my two diploma students Steffi Braun und Ulrich Alt-Epping. Florian Wellmann helped realizing the software for the furnace device. Prof. Dr. Oliver Eibl made the TEM pictures of pyrrhotite during his weekends. Further technical and scientific support came from Dr. Christoph Berthold, Hermann Kurz, Dr. Roman Leonhardt, Horst Stumpp, Fabienne Vadeboin and Manuela Weiß.

Encouragement and support came from the members of the geophysical group in Tübingen and CEREGE, my friends and family.

Summary:	I
Introduction:	I
Principle of pTRM recording:	II
Pyrrhotite Formation in metamorphic environments (Chapters I and II):	III
Pyrrhotite and its suitability as a pTRM recorder (Chapter II and IV):	IV
Instrumental development (Chapters V+IV):	V
Time estimation (Chapters II + IV):	VI
Methodical Approach:	VI
Paleointensity determination:	VIII
An example from Elba Island:	IX
Chapter I: <i>Pyrrhotite pTRM acquisition in metamorphic limestones in the light of microscopic observations</i>	1
1.1 Introduction:	1
1.2 Samples and methods:	2
1.3 Results:	3
<i>Regional Metamorphism:</i>	3
<i>Contact metamorphism:</i>	4
1.4 Discussion:	8
<i>Regional Metamorphism:</i>	8
<i>Contact metamorphism:</i>	9
1.5 Conclusion:	10
1.6 References:	11
Chapter II: <i>Quality of pTRM acquisition in pyrrhotite bearing contact-metamorphic limestones: Possibility of a continuous record of Earth magnetic field variations</i>	13
1.1 Introduction:	13
2.2 Geological Settings:	14
<i>Manaslu area (Nepal):</i>	14
<i>Isle of Skye (Scotland):</i>	16
<i>Elba Island (Italy):</i>	17
2.3 Sample treatment and analytical procedure:	18
2.4 Results:	18
<i>Magnetic mineralogy and rockmagnetic properties in a spatial context:</i>	18
<u>General magnetic mineralogy and the pyrrhotite window:</u>	19
<u>Rockmagnetic properties in their spatial context:</u>	22

<i>PTRM experiments and recording ability:</i>	24
<i>Time-temperature relationship:</i>	26
<i>Directional behaviour:</i>	28
2.5 Discussion:	29
2.6 Conclusions:	31
2.7 References:	34
Chapter III: <i>Experimental evaluation of magnetic interaction in pyrrhotite bearing samples</i>	37
3.1 Introduction:	37
3.2 Theory:	38
3.3 Samples and methods:	40
3.4 Results and discussion:	41
<i>Sized dispersed fractions:</i>	41
<i>Natural samples:</i>	47
3.5 Conclusion:	52
3.6 References:	54
Chapter IV: <i>Magnetic interaction analysis of basaltic samples</i>	57
4.1 Introduction:	57
4.2 Samples and Methodology:	58
4.3 Results and Discussion:	59
<i>Continuous thermal demagnetisations:</i>	59
<i>Interaction analysis:</i>	60
4.4 Conclusion:	63
4.5 References:	65
Chapter V: <i>How to measure in a Cryogenic Magnetometer at elevated temperatures?</i>	67
5.1 Introduction:	67
5.2 Technical design:	68
5.3 Control and Calibration:	69
5.4 Demagnetisation Results:	70
<i>Demagnetization of a single- component TRM:</i>	70
<i>Demagnetisation of two antiparallel components:</i>	72
5.5 Conclusions:	74
5.6 References:	75

Chapter VI: <i>One inch of reversal or how a single sample can hold variations of the Earth magnetic field</i>	77
6.1 Introduction:	77
6.2 Remanence directions:	78
6.3 Quality of pTRM recording:	79
6.4 Thermal Modeling:	80
6.5 Paleointensity determination:	81
6.6 Conclusions:	83
6.7 References:	85
<i>Appendix</i>	
1. TRM furnace	i
2. Patent	iv
3. Glossary	xiii
4. Figure Captions	xvii
5. Table Captions	xix

Chapter I: Pyrrhotite pTRM acquisition in metamorphic limestones in the light of microscopic observations

Florian Wehland¹, Oliver Eibl², Stefanie Braun¹, Ulrich Alt-Epping³, Erwin Appel¹

¹Institut für Geowissenschaften, Sigwartstraße 10, 72074 Tübingen, Germany

²Institut für Angewandte Physik, Auf der Morgenstelle 10, 72076 Tübingen, Germany

³Forschungszentrum "Ozeanränder", Postfach 330440, 28334 Bremen, Germany

Journal: Physics of the Earth and Planetary Interiors

Status: Accepted

Keywords: pyrrhotite, TEM, pTRM acquisition, metamorphic limestone, Skye, Elba, Manaslu

a) Idea:	90%
b) Sample acquisition:	60%
c) Laboratory work:	40%
d) Data interpretation:	70%
e) Writing up (Publication):	90%

Chapter II: Quality of pTRM acquisition in pyrrhotite bearing contact-metamorphic limestones: Possibility of a continuous record of Earth magnetic field variations

Florian Wehland¹, Ulrich Alt-Epping², Steffi Braun¹, Erwin Appel¹

¹Institut für Geowissenschaften, Sigwartstraße 10, 72074 Tübingen, Germany

²Forschungszentrum "Ozeanränder", Postfach 330440, 28334 Bremen

Journal: Physics of the Earth and Planetary Interiors

Status: Accepted

Keywords: pTRM recording, pyrrhotite, contact metamorphism, Elba, Isle of Skye, Manaslu

a) Idea:	90%
b) Sample acquisition:	60%
c) Laboratory work:	50%
d) Data interpretation:	70%
e) Writing up (Publication):	90%

Chapter III: Experimental evaluation of magnetic interaction in pyrrhotite bearing samples

F. Wehland¹, A. Stancu², P. Rochette³, M.J. Dekkers⁴, E. Appel¹

¹Institut für Geowissenschaften, Universität Tübingen, Sigwartstr. 10, 72076 Tübingen, Germany.

²Faculty of Physics, ‘Alexandru Ioan Cuza’ University, Blvd. Carol I, 11, 700506, Iași, Romania

³CEREGE, Europôle Méditerranéen de l'Arbois, BP 80, Aix en Provence cedex 04, France

⁴Paleomagnetic laboratory ‘Fort Hoofddijk’, Universiteit Utrecht, Netherlands

Journal: Physics of the Earth and Planetary Interiors

Status: Accepted

Keywords: magnetic interaction, ΔM analysis, irreversible susceptibility, FORC analysis, pyrrhotite

a) Idea:	90%
b) Sample acquisition:	80%
c) Laboratory work:	100%
d) Data interpretation:	90%
e) Writing up (Publication):	90%

Chapter IV: Magnetic Interaction analysis of basaltic samples

Florian Wehland¹, Roman Leonhardt², Erwin Appel¹, Vabienne Vadeboin³

¹Institut für Geowissenschaften, Sigwartstr. 10, 72074 Tübingen, Germany

²Department for Earth and Environmental Sciences, Theresienstr. 41, 80333 München, Germany

³CEREGE, Europôle Méditerranéen de l'Arbois, BP 80, Aix en Provence cedex 04, France

Journal: Geophysical Journal International

Status: Accepted

Keywords: magnetic interaction; palaeointensity; basalts; FORC

a) Idea:	90%
b) Sample acquisition:	0%
c) Laboratory work:	60%
d) Data interpretation:	80%
e) Writing up (Publication):	90%

Chapter V: How to measure in a Cryogenic Magnetometer at elevated temperatures?

Florian Wehland¹, Erwin Appel¹

¹Institut für Geowissenschaften, Sigwartstr. 10, 72074 Tübingen, Germany

Journal: none

Status: in preparation

Keywords: none

a) Idea:	80%
b) Realization:	80%
c) Data interpretation:	100%
d) Writing up (Publication):	90%

Chapter VI: One inch of reversal or how a single sample can hold variations of the Earth magnetic field

Florian Wehland¹, Ulrich Alt-Epping², Erwin Appel¹

¹Institut für Geowissenschaften, Sigwartstraße 10, 72074 Tübingen, Germany

²Forschungszentrum "Ozeanränder", Postfach 330440, 28334 Bremen

Journal: Science or Geophysical Research

Status: in preparation

Keywords: paleointensity, pTRM, pyrrhotite, contact metamorphism, Elba

a) Idea:	50%
b) Sample acquisition:	70%
c) Laboratory work:	70%
d) Data interpretation:	85%
e) Writing up (Publication):	90%

Introduction:

At the beginning of the last century Albert Einstein called the Earth magnetic field (EMF) one of the last unsolved problems of classical physics. Progress during the last decades in the field of paleomagnetism and in the application of computational dynamo models lead to large steps forward in the understanding of the structure and origin of the Earth magnetic field.

In the view of the paleomagnetic record of the EMF it is now well established that its dominant dipolar part has changed the polarity hundreds of time during the past 160Ma (Merrill et al., 1995). Although the polarity sequence of the EMF is well known since Cretaceous and widely used for stratigraphic correlations, the polarity reversals themselves remain one of its most enigmatic properties. This depends mainly on the short time-interval estimated for such a transition between 1000-8000 yrs (Merrill, 1997) and the intrinsic problems of the recording media used. Moreover, the nature of the EMF itself, which can be described by dipole and non-dipole sources at the Earth's outer core (Merrill, 1997), hampers the interpretation of intensity and directional data obtained by paleomagnetic studies.

The latter case can only be improved if the number of synchronous independent measurements well distributed over the Earth's surface is large enough to sufficiently solve the spherical harmonics describing the EMF (Merrill and McFadden, 1999). The recording media have their specific problems as well. Reversal results from basaltic rocks, which are used to assess directional and absolute paleointensity data, can be hardly correlated within a convincing time frame as the time between the individual lava layers is poorly known. This may lead to the frequently observed VGP clusters. Hoffman (2000) stated that – based on spatial palaeomagnetic field data associated with the Matuyama-Brunhes reversal – such clusters can be related to dynamo processes and possible reflect energy barriers during a reversal. In contrary, Valet & Herrero-Bervera (2003) comparing VGPs of five detailed records concluded that such clusters are observed in most records at various geographical locations without preference for specific longitudes, which most likely result from intense volcanism during short time periods rather than from transitional dipolar states. This interpretation is supported by the work of Riisager et al. (2003).

In sedimentary sections, which allow estimating relative paleointensities, the directional as well as the intensity results are blurred by the uncertainties of the remanence acquisition

process i.e. the lock-in depth-problem caused by the diagenesis of the rock, grain-size distribution and sedimentation rates.

This work focuses on an additional record of the EMF using partial thermoremanent magnetisation (pTRM) in single samples (Ménard & Rochette, 1990; Rochette et al., 1992; Crouzet et al., 1997, 2001) to gain more insight in its temporal variation. Records of pTRM from suitable rocks have the advantage of a quasi-continuous time axis. There is some similarity with the work on intrusive rocks carried out by Dodson et al. (1978) and Williams & Fuller (1982), who studied TRMs at different levels within a pluton, and the recent work of Keating et al. (2002) who found a quasi-continuous record of a field transition in a contact metamorphic aureole. Experimentally, the recording potential of hydrothermally grown magnetite was investigated by Cairanne et al. (2003); it is based on partial chemical remanences, i.e. the analogue to pTRM.

The new method described in this thesis – i.e. recording of EMF variations, especially reversals, by using secondary pyrrhotite in metacarbonates - adds a new source of data. It allows revealing a continuous record of the EMF and, hence, improves the knowledge about the duration of a reversal.

Principle of pTRM recording:

An assemblage of single domain grains different in size and coercivity have blocking temperatures (Fig.1), which expand far below the Curie Temperature T_c . During cooling in a varying external field, this assemblage will continuously record the mean field changes within individual pTRMs.

Crucial for the quality of the record is the Thellier law of reciprocity ($T_{ub}=T_b$), which is only valid of non-interacting single domain grains. Earlier studies of Crouzet et al. (1999, 2001) have shown that pyrrhotite in marly metacarbonates is able to carry independent pTRMs and, thus, mainly crystallizes in the SD particle range ($<2\mu\text{m}$; Soffel, 1977).

As these studies concentrate on regional metamorphic rocks, much effort had been made to investigate the pyrrhotite formation in terms of its geological surrounding and its relevance as a recording media of pTRMs in a contact metamorphic environment.

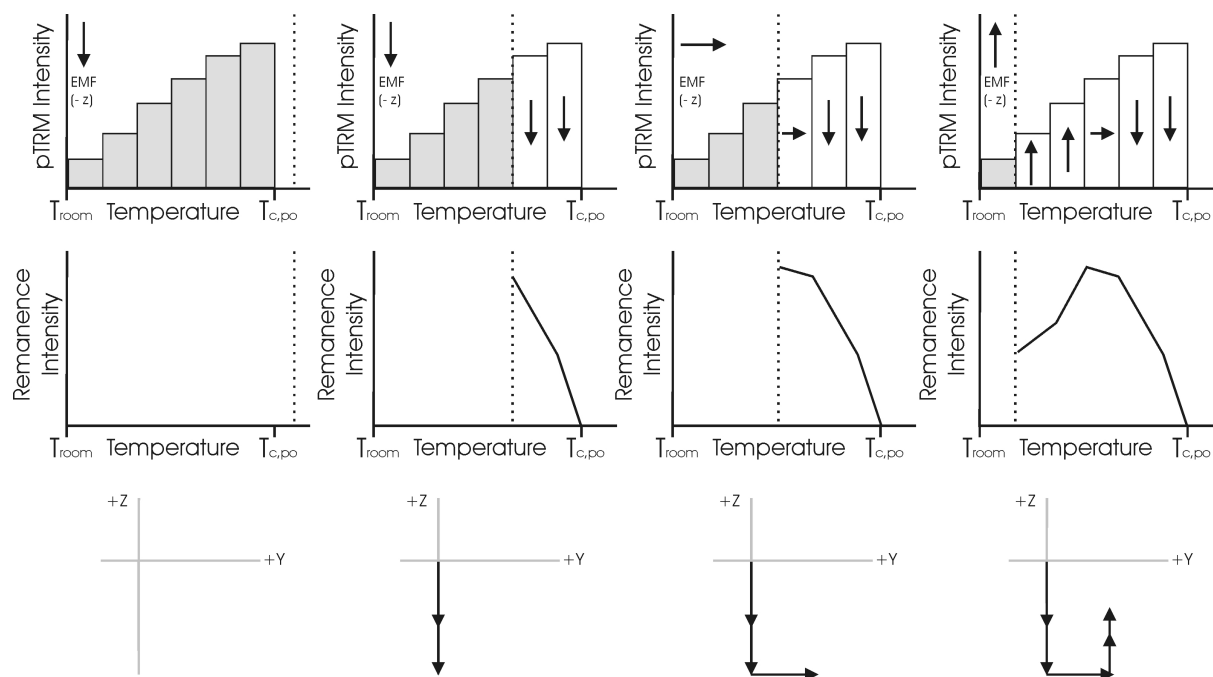
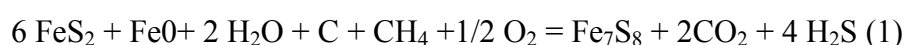


Figure I.1: Principle of pTRM recording in a single sample during metamorphic cooling (from left to right): the different directions of the EMF are recorded in the respective pTRMs. The direction of the EMF is marked with the arrow in the left upper half of the diagram. Gray boxes stand for individual unblocked pTRMs, white for blocked ones. The dashed line indicates the actual metamorphic temperature during cooling. The middle diagrams demonstrates the resulting net-intensity of the sample. $T_{c,po}$ is the Curie temperature of pyrrhotite. The lower diagram represents an orthogonal vector plot for demagnetisation.

Pyrrhotite Formation in metamorphic environments (Chapters I and II):

The growth of pyrrhotite is generally associated with the breakdown of pyrite and magnetite starting under very low-grade metamorphic conditions. Important in this context is the presence and amount of the C-H-O-S fluid system well described for different P-T conditions by Poulson and Ohmoto (1989). They showed that with increasing temperatures the proportion on H_2S in the fluid is increasing while the one of H_2O is reduced. An intermediate position plays CH_4 , which has its maximum proportion in the fluid at about $500^\circ C$. Incorporating all phases equation (1) attempts to describe the situation in a carbon bearing rock, where iron oxide minerals are expressed by FeO :



How and where pyrrhotite finally crystallizes depends on the amount of fluids involved during the metamorphic event. In a temperature dominated environment (low fluid/rock ratio) like in regional metamorphic rocks, the formation of pyrrhotite occurs as an in-situ process favouring the crystallization of SD-particles (see Chapter I). Such scenarios are favourable to record independent pTRMs. If high fluid/rock ratios are present most of the iron sulfides will dissolve, be transported and crystallize during cooling in large aggregates. Moreover large amounts of metamorphic fluids will lower or completely remove the amount of carbon in the sample and, hence, opens the way for the crystallization of iron oxides. In chapter I and II it is shown, that contact metamorphic environments can produce both extremes and, therefore, thorough investigation is needed before using them for the purpose of pTRM recording.

Pyrrhotite and its suitability as a pTRM recorder (Chapter II and IV):

Different approaches were accomplished to investigate the validity of the reciprocity for pyrrhotite bearing metacarbonates. At first samples taken from Bourg d'Oisans (France) and the Manaslu area (Nepal) were used to impart unidirectional pTRMs with a maximum temperature below $T_{c,po}$. During demagnetisation of these pTRMs the existence of MD particles can be observed by the means of the demagnetisation tails as a consequence for $T_{UB} = f(T_B)$ (Dunlop and Özdemir, 2001). It can be seen that most of the samples exhibit a well-defined pTRM with only minor demagnetisation tails indicating SD-PSD behaviour. Although these experiments give a first indication on the domain state of the particle assemblage, their value to assess the pTRM recording quality is restricted.

Therefore selected samples from all localities (Nepal, Isle of Skye, France, Elba) were subjected to Thellier like experiments (Coe, 1967) on a laboratory induced TRM (TRM1). Comparison of the determined and applied intensities and pTRM checks allow the evaluation of the recording qualities over a wide temperature range (see Chapter II for more details). The experiments have shown that pyrrhotite in samples from Elba and Bourg d'Oisans is able to record independent pTRMs and, hence, paleointensities over a wide temperature range.

The second precondition for the record of independent pTRMs is the absence of interaction in the particle assemblage. Presence of interaction would violate the law of independent pTRMs and, in the extreme case, leads to phenomena like partial self reversal during (p)TRM acquisition as reported for pyrrhotite by Bina and Daly (1994). The importance of

investigating interaction effects was evident because the samples from the Isle of Skye showed anomalous behaviour during thermal demagnetisation of IRM.

The recently developed FORC (Pike et al., 1999; Roberts et al., 2000) method as well as the ΔM method (Petrovsky et al., 1993, and ref. therein) were applied on selected samples from all localities and compared with the results of artificial samples of distinct grain size fractions provided by M. Dekkers (see Chapter III). Low magnetic interaction and broad coercivity spectra in the samples from the Manaslu area, Bourg d'Oisans and Elba support the results from the TRM experiments, whereas the abnormal behaviour of the Isle of Skye samples could be attributed to strong negative mean interaction fields which increase the possibility of self reversals.

Coinciding results derived from the magnetic interaction tests (FORC and ΔM) and the TRM experiments lead to the idea of using interaction methods as a fast tool for the selection of samples suitable for paleointensity studies. This idea was also applied using basaltic samples where the recording qualities – SD/MD particles, presence of self reversals – had already been investigated by Thellier experiments and observations of remanence measurements at elevated temperatures (see Chapter IV). It could be shown that interaction measurements – FORC as well as ΔM -plot - can serve as a fast preselective tool for paleointensity measurements.

Instrumental development (Chapters V+IV):

Two different types of furnace devices were developed in order to investigate the ability to record multidirectional pTRMs in pyrrhotite bearing samples and to enhance the options and quality of thermal experiments, i.e. pTRM formation and demagnetisation. The first furnace system (TRM furnace) had to be equipped with external field coils able to change the direction of the field within a plain and an accurate temperature control. Only such an arrangement allows imparting and recording artificial reversal paths within a sample (see Appendix and Chapter VI). The second system, an optical furnace, was envisaged to implant a heating device inside the cryogenic magnetometer, which allows measuring the remanence of a sample continuously while heating (see Chapter IV).

Time estimation (Chapters II + IV):

The cooling times of the metamorphic rocks determine the duration the paleofield being recorded by means of successive pTRMs within a sample. Moreover, the peak temperatures during metamorphism at the sampling position are crucial whether or not a full TRM is recorded. For peak temperatures below the Curie temperature of the remanence carrier the record cannot be regarded as a continuous one.

These considerations make it necessary to model the time-temperature behaviour at the sampling site caused by the metamorphic event of the adjacent intrusion. An important precondition of such a model is the knowledge of the shape, intrusion depth and process of the magmatic body. This is known from the Beinn an Dubhaich granite at the Isle of Skye and the laccolithic bodies of central Elba. Their relative small size of these intrusions ensure the absence of multiple pulsed magma injection (like in the Manaslu granite, Nepal) over a longer time period and favours a more rapid cooling, i.e. a higher time resolution of the pTRM record.

Another aspect for the time-temperature model is the existence of hydrothermal activity. For central Elba this can be neglected for the contact metamorphic zone of the laccolithic bodies, whereas at Skye – based on field and microscopic investigations – hydrothermal activity is evidenced and has to be taken into account. Therefore, different models are used for the time temperature paths at the Isle of Skye (Chapter II) and central Elba (Chapter VI).

These models provide information on cooling times within the pTRM spectra of pyrrhotite (325° to ~150°C) and the maximum distance from the contact to acquire a full TRM.

Methodical Approach:

The tests used to investigate the recording abilities and, therefore, interpret the NRM demagnetisation spectra as a record of an Earth magnetic field reversal can be summarised as shown in Fig.2.

The **TOOLBOX** for quality control

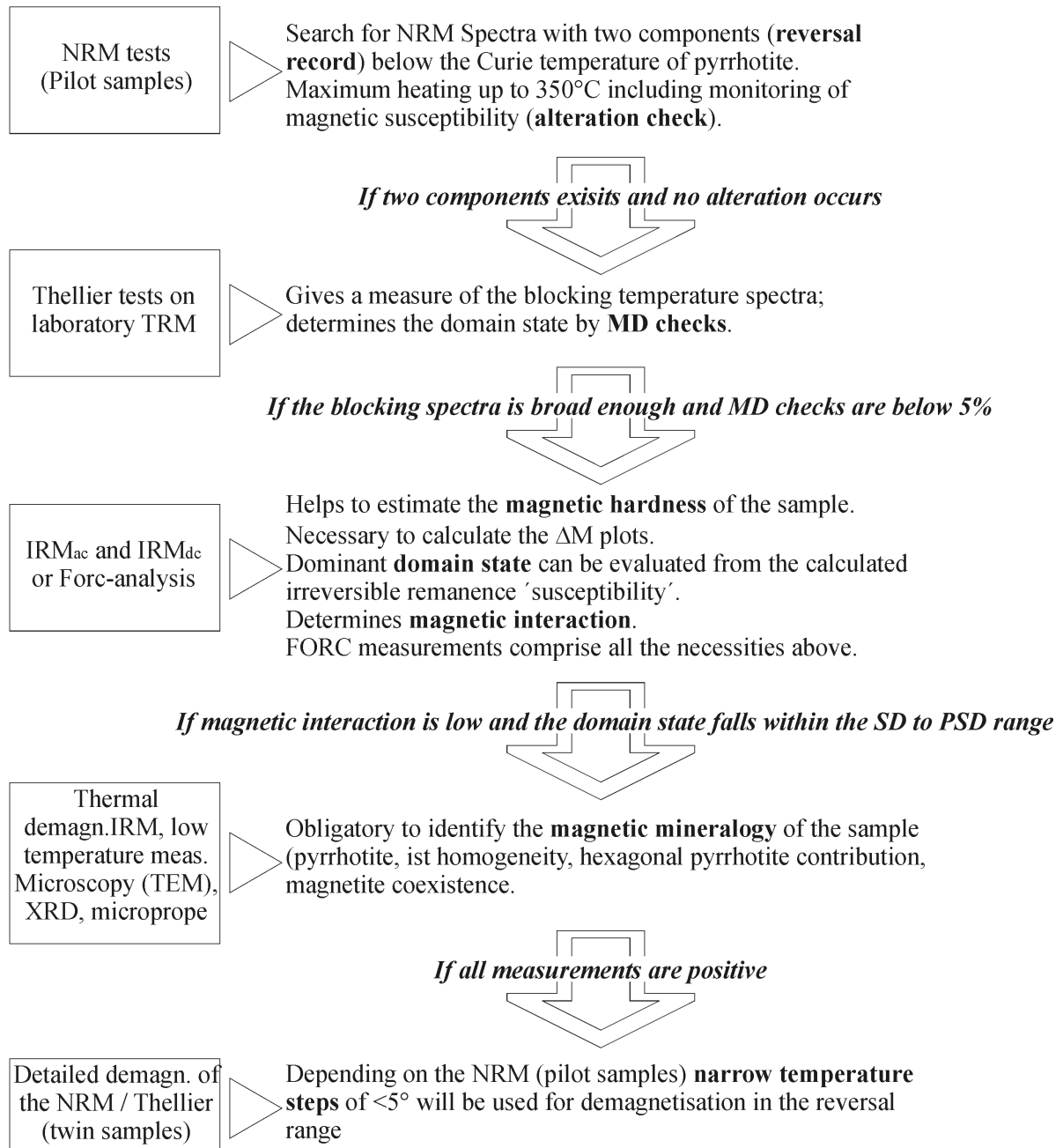


Figure I.2: Steps to be taken in order to ensure pTRM recording within a single sample

The initial step (pilot measurements) also includes the aspect of reversal studies. In a more common attempt like the study of long term investigations of the EMF in regional metamorphic rocks or short term variations like in basalts antiparallel components are not obligatory as the study of EMF reversals is only one possibility of using this technique. For

Summary

regional metamorphic rocks the time enveloped in the record will be much longer. This means that reversals cannot be sufficiently resolved even with very narrow demagnetisation steps, as this will exceed the experimental capability (very narrow blocking temperature range). However, the record can be used for intensity studies of the EMF over a period equivalent the cooling times of the rock.

Paleointensity determination:

In general, the paleointensity determination is based on the relation $NRM/H_{paleo} = TRM/H_{lab}$. This means that the paleofield during NRM acquisition (H_{paleo}) can be recalculated, if a laboratory TRM in a known field (H_{lab}) is compared with the NRM for discrete demagnetisation temperatures. This relation works because the NRM acquisition times in samples like basalts (days) are similar to the ones used during laboratory TRM acquisition (hours).

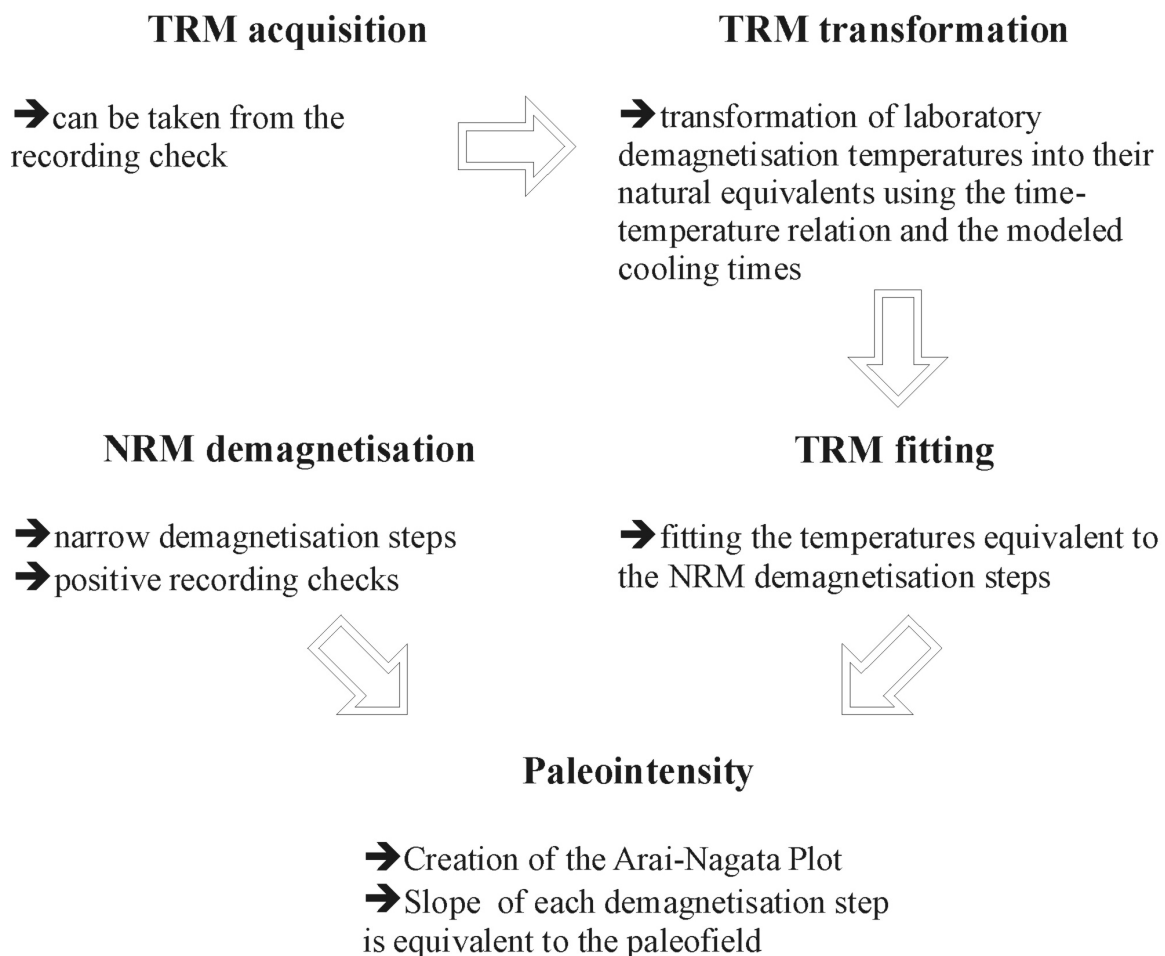


Figure I.3: Processing of metamorphic data.

In the case of successive pTRM acquisition in contact metamorphic limestones such a simple approach is not valid as cooling times during NRM acquisition are much higher (~100kyrs) than the ones used during laboratory TRM acquisition.

This problem can be solved by transforming the temperatures of the laboratory TRM acquisition steps into their natural equivalents using the time-temperature relationship for the recorder mineral (for pyrrhotite: Dunlop et al., 2001). The numerical model as described above provides the cooling times. For comparison with the NRM demagnetisation corresponding temperature steps have to be interpolated on the transformed laboratory curve before the determination of paleointensities from individual pTRMs (Fig. 3).

An example from Elba Island:

In chapter VI the method described above was applied on samples from the central part of Elba Island (Italy). The preliminary recording checks show that samples from this location fulfill the requirements for recording successive independent pTRMs. Additionally, the relatively flat magmatic bodies in central Elba allows to model the cooling times and temperatures by the means of a simple one-dimensional model.

In addition, the folded host rock made it possible to apply field test on the different components in the NRM spectra. This made clear that the TRM in this sample is a secondary remanence, which formed after the folding of the host rock.

For the paleointensity determination 18 samples from one specific site have been used, where seven of them fulfilled the quality criteria. The focus on a specific site is necessary as the cooling times in such an environment depend on the distance towards the contact and the thickness of the specific intrusion. Therefore records of different locations cannot be simply compared.

The results shown in Figure 5 (chapter VI) demonstrate that the transition in the NRM record is equivalent with a decrease in the paleointensity of the pTRM record. An estimate of the duration of the recorded reversal is hampered by the fact that only a part of the reversal is recorded. Taking into account the positions of the VGPs, which indicates the polarity change of the dipole field, it can be argued that most of the reversal process has taken place. The duration for this record based on the different models (chapter VI) is smaller than 20 kyr and, thus, lies in the range of other reversal records observed.

References:

- Bina M. and Daly L., 1994, Mineralogical change and self-reversal magnetizations in pyrrhotite resulting from partial oxidation; geophysical implications. *Phys. Earth Plan. Int.*, 85, 83-99.
- Crouzet, C., Menard, G., and Rochette, P. 1999. High-precision three-dimensional paleothermometry derived from paleomagnetic data in an Alpine metamorphic unit. *Geology*, 27: 503-506.
- Crouzet, C., Stang, H., Appel, E., Schill, E., and Gautam, P., 2001. Detailed analysis of successive pTRMs carried by pyrrhotite in Himalayan metacarbonates: An example from Hidden Valley, Central Nepal, *Geophys. J. Int.*, 146: 607-618.
- Coe, R. S., 1967. Paleointensities of the Earth's magnetic field determined from Tertiary and Quaternary rocks, *J. Geophys. Res.*, 72, 3247–3262
- Dunlop, D.J., Özdemir, Ö., Clark and D.A., Schmidt, P.W. 2000. Time-temperature relations for the remagnetization of pyrrhotite (Fe₇S₈) and their use in estimating paleotemperatures, *Earth Planet. Science Lett.*, 176 (1), 107-116
- Dunlop, D. J. and Özdemir, Ö., 2001. Beyond Néel's theories: thermal demagnetization of narrow-band partial thermoremanent magnetizations, *Physics of the Earth and Planetary Interiors*, 126. 43–57
- Merrill, R T. and McElhinny, .W., McFadden, P.L., 1996: *The Magnetic Field of the Earth: Paleomagnetism, the Core and the Deep Mantel*, Academic, San Diego.
- Merrill, R.T., 1997. The magnetic reversal record, *Nature*, 389, 178-679
- Merrill, R. T. and McFadden, P. L ., 1999: Geomagnetic Polarity Transitions, *Rev. of Geophys.* 37, 201-226.
- Petrovský, E., Hejda, P., Zelinka, T., Kropáček V., and Šubrt, J., 1993. Experimental determination of magnetic interaction within s system of synthetic haematite particles, *Phys. Earth Planet. Inter.*, 76: 123-130.
- Pike, C.R., Roberts, A.P., and Verosub, K.L., 1999. Characterizing interactions in fine magnetic particle systems using first order reversal curves, *J. appl. Phys.*, 85: 6660-6667.
- Roberts, A. P., Pike, C.R. and Verosub, K.L., 2000. First-order reversal curve diagrams: A new tool for characterizing the magnetic properties of natural samples, *J. Geophys. Res.*, 105: B12: 28,461 – 28,475.
- Soffel, H.C., 1977. Pseudo-single domain effects and single-domain multidomain transition in natural pyrrhotite deduced from domain structure observations. *J. Geophys.*, 42: 351-359

*Pyrrhotite pTRM acquisition in metamorphic limestones in the light of
microscopic observations*

Abstract:

The potential of pyrrhotite as a recorder of successive, independent pTRMs in graphite bearing metacarbonates depends on the amount and composition of metamorphic fluids. During its formation very low amounts of H₂S dominated fluids will favour an in situ epitaxy of pyrrhotite by the expense of iron bearing minerals in its surrounding. The resulting particle assemblage of pyrrhotite is within the single domain grain-size range and exhibits a broad blocking temperature spectrum. With increasing fluid content the desulfidation of pyrite controls the pyrrhotite formation and results in large crystals up to several mm, where independent pTRMs cannot be expected. As both types are present in regional and contact metamorphic rocks, the existence of pervasive fluids determines whether or not pyrrhotite will be able to record successive pTRMs, i.e. changes of the Earth magnetic field (EMF) during metamorphic cooling.

1.1 Introduction:

During the last two decades the relevance of pyrrhotite as the main carrier of paleomagnetic information in very low to low grade metamorphic limestones has been demonstrated (Rochette, 1987; Appel et al., 1991; Ménard and Rochette, 1992; Schill et al., 1998; Crouzet et al., 1999; Gillett, 2003). The formation of pyrrhotite in such rocks is generally connected with the breakdown of pre-metamorphic pyrite and/or magnetite in the presence of low oxygen fugacity ($f(\text{O}_2)$). In its simplest form this transformation can take place as a desulfidation reaction of pyrite as proposed by Carpenter (1974) and Ferry (1981) valid for green schist metamorphic conditions. According to Lambert (1973), this reaction may start already around 200°C in presence of carbonate and water. After Crerar et al. (1978) pyrrhotite can also be formed by reduction of magnetite due to sulphur or pyrite, if there is either a decrease in oxygen fugacity or an increase in sulphur fugacity ($f(\text{H}_2\text{S})$) for the reactions to start. Based on thermodynamic modelling and magnetic data, Gillette (2003) suggests that this reaction also starts at ~200°C. Alternatively, iron might come from silicates and/or oxides as proposed by Thompson (1972), Ferry (1981) and Tracy and Robinson (1988). Nevertheless, Ferry (1981) assumes that this reaction is negligible as the amount of iron in silicates and oxides is low.

Taking the C-H-S fluid system into account, Ferry (1981) proposed two possible reactions including CH₄ and H₂O, whereas H₂O dominates at higher temperatures. Poulson and Ohmoto

(1989) favour H₂S at higher temperatures (>500°C), low pressure and low f(O₂). The dominance of H₂S at higher temperatures leads to a decrease in the H₂O contingent <<1, followed by the dehydration of hydrous minerals. In a contact metamorphic environment, such H₂S rich fluids are in direct vicinity to the contact and enable selective transfer of sulphur from pelites into the pluton.

Studying variations and intensities of the EMF requires that the magnetic assemblage comply with the Thellier laws of additivity and independence of successive pTRMs (Thellier and Thellier, 1959). In other words, the blocking temperature should be the same as the unblocking temperature. As only single domain (SD) - and to a lesser amount smaller pseudo single domain (PSD) - particles fulfill these laws the grain-size of pyrrhotite should not exceed a few μm (SD-MD transition 1-2 μm according to Soffel, 1977). It also implies that magnetic interaction between neighbouring SD particles can be neglected. Using magnetic techniques this was already verified for regional metamorphic limestone of the Western Alps (Crouzet et al., 1999; Wehland et al., *subm.a*). The aim of our study is to investigate the process of pyrrhotite formation and its appearance in different metamorphic settings under the light of its relevance as a magnetic remanence carrier. Here we focused on the microscopic indications whereas magnetic experiments are described in another paper (Wehland et al., *subm.b*)

1.2 Samples and methods:

Sampling was performed from contact metamorphic limestones from the Isle of Skye (Scotland) and Elba Island (Italy) and on regional metamorphic limestones from the area of Bourg d'Oisans (France, Crouzet et al., 1997) and the Tethyan Himalaya (Manaslu area, Nepal; Schill et al., *in press*). The latter one has a twofold nature as near the Manaslu Intrusion the limestone has a clear contact metamorphic overprint.

Pyrrhotite in these samples was detected by the means of rockmagnetic methods like thermal demagnetisation of the Saturation Isothermal Remanent Magnetisation (SIRM) and thermomagnetic measurements of the susceptibility. Magnetite or hematite can exist in low amounts (Wehland et al., *subm.b*).

For the microscopic investigation samples from the contact metamorphic areas were taken with an increasing distance to the respective intrusion and subjected to scanning electron microscopy (SEM), transmission electron microscopy (TEM) and light microscopy

(transmission and reflected). For the SEM analysis the surface of the polished samples were treated with diluted (5%) hydrochloric acid for 10 seconds. The etching was necessary as the high competence contrast between the ore minerals and the calcareous matrix lead to a smeared surface of calcite. The competence contrast was also responsible that the TEM analysis was only successfully performed on samples from Bourg d'Oisans.

1.3 Results:

Regional Metamorphism:

Using transmitted and reflected light microscopy, pyrite is identified as the dominant ore mineral and appears in aggregates of up to 0.5 mm. Magnetite and pyrrhotite could not be found by such means. Nevertheless, as the existence of pyrrhotite in these samples is evidenced from rockmagnetic studies, it has to exist in a submicroscopic size of smaller than $\sim 2 \mu\text{m}$.

SEM analysis on the regional metamorphic rock from Bourg d'Oisans revealed a high content of iron sulfides arranged in large complexes of framboidal clusters (Fig. 1.1a). The individual crystals all have a diameter around $1 \mu\text{m}$ and showing a minor resorbation at their corners. Several EDX analyses underlines that the framboidal iron sulfides consist of pyrite only.

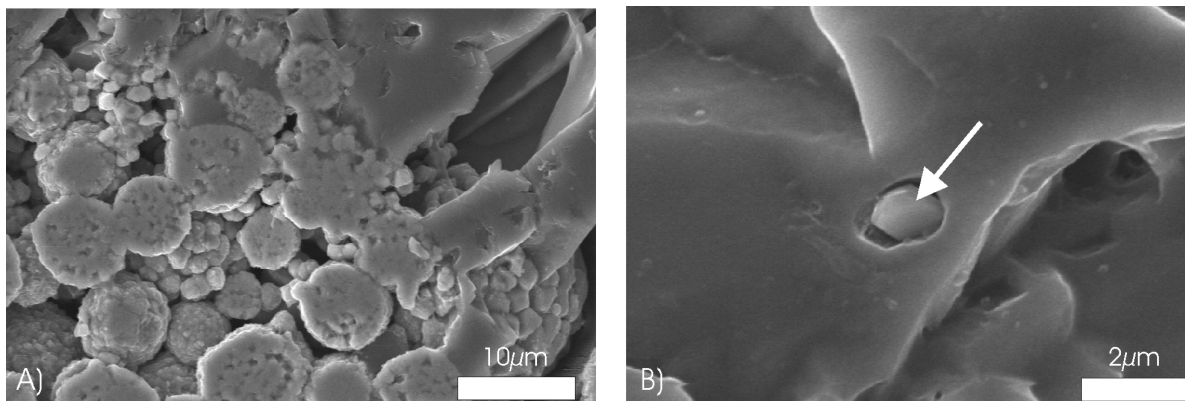


Figure 1.1: (A) Cluster of framboidal pyrite grains (partly polished), (B) individual idiomorphic pyrrhotite grain (white arrow). Both pictures were made by SEM analysis.

Pyrrhotite was directly observed (confirmed by EDX analysis) as sparsely distributed, idiomorphic crystals (Fig. 1.1b) in the range of single domain threshold (Soffel, 1977). Shape and fresh appearance of the grains suggest that it was formed during regional metamorphism. Compositional homogeneity of the pyrrhotite grains is demonstrated by the means of TEM (Fig. 1.2). Homogeneity is inferred by the physical patterns spanning through the grain. The

matrix in direct vicinity of the sulfide consists of pure calcite, whereas in further distances it has a dolomitic composition with a minor sideritic component. The grain-size of the sulfide grain lies within the SD threshold (Soffel, 1977).

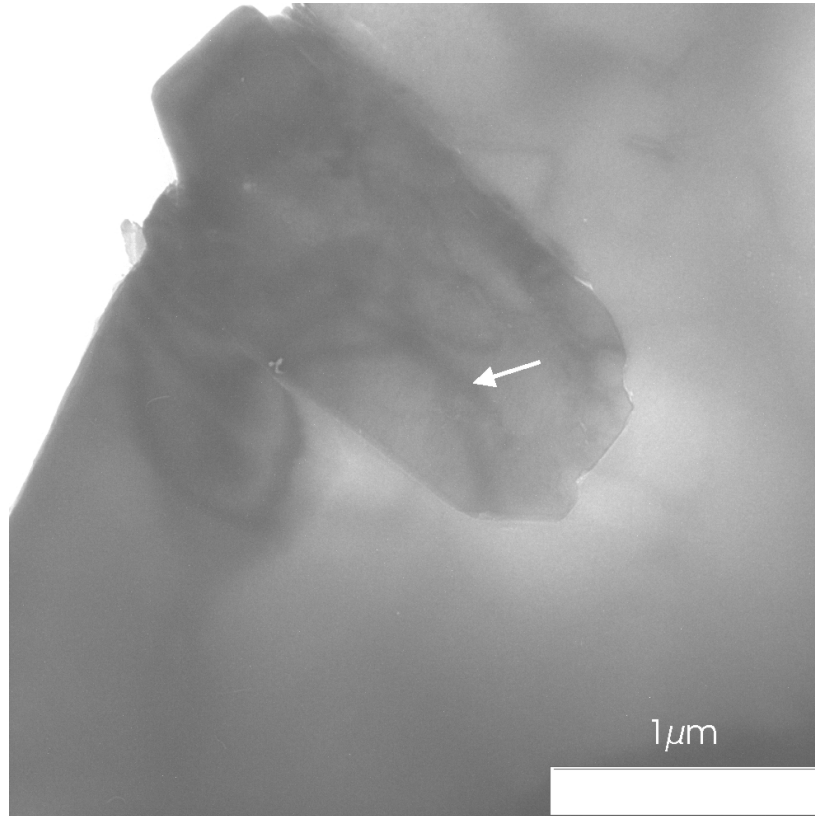


Figure 1.2: Pyrrhotite under TEM. The continuous structure (white arrow) in the pyrrhotite grain indicates chemical homogeneity.

Contact metamorphism:

Using transmitted light microscopy the samples of central Elba appear as micritic biogenetic limestones with a varying fraction of quartz. The blurry matrix, indicating a grain-size smaller than the optical resolution ($<2\mu\text{m}$), contains irregular brownish streams and patches possibly originating from a high ore content of the rock. Occasionally ore phenocrysts with cubic shape are observed (Fig. 1.3a). Noticeable are sporadic bioclasts of mostly foraminifera shells. The specimens are infused of veins of sparry, twinned calcite of more than one generation (Fig. 1.3b). The veins had no visible effect on the adjacent rock suggesting that fluid circulation was not pervasive. Reflected light microscopy reveals a high content of organic carbon, which in parts is completely transformed into graphite. Ti-oxides like rutile are abundant in all specimens. Pyrite, which often occurs as inclusions in biogenetic

structures, can have a limonitic envelope. The observed pyrrhotite is close to optical resolution.

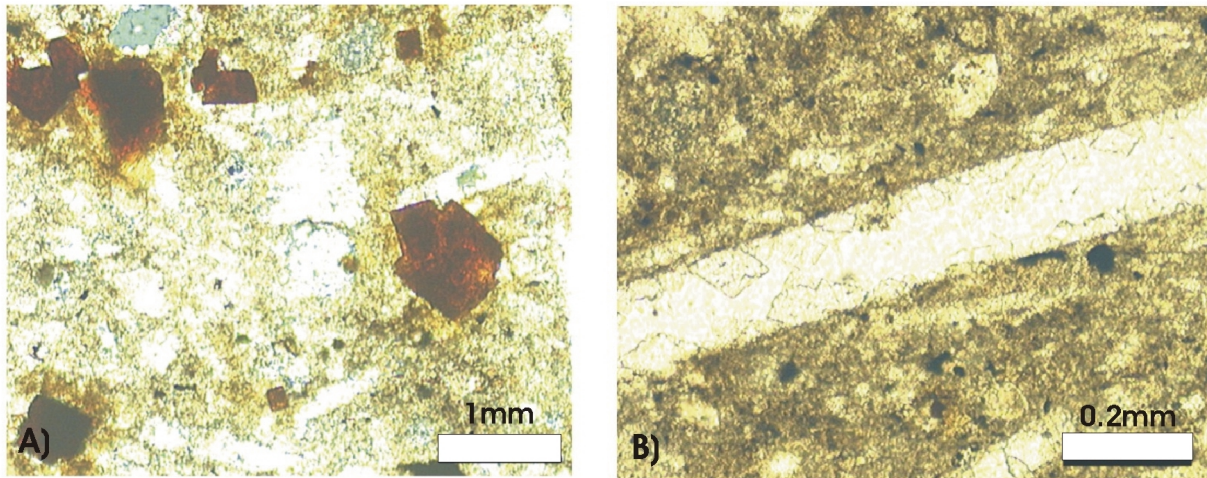


Figure 1. 3: Elba limestones in transmitted light microscopy: A) large idiomorphic ore crystals in a blurry matrix. B) refilled crack with two generations of calcite crystals.

Observation with EDX during SEM analysis indicates a compositional spectrum of the iron sulfides from pyrite to pyrrhotite via greigite. The pyrrhotite grain-size is below $10\mu\text{m}$ (Fig. 1.4a). It has to be kept in mind however, that EDX analysis is only semi-quantitative and conclusion about molar composition has to be drawn with care. On contrary the proportions of FeO to TiO, which would allow a distinction of the iron oxide minerals, is too mutual to be interpreted in a reliable way. Nevertheless, the enrichment of titanium is striking and can explain that contribution of the magnetite during rockmagnetic investigations was very low (Wehland, et al., subm.b).

In contrast to central Elba, the contact metamorphic samples from the Isle of Skye and the Manaslu area have a slightly different petrology. In direct vicinity of the contact the samples are composed out of nearly pure marble. The presence of olivine and/or epidote in a distance up to 10 m from the contact indicates a metamorphic temperature at around 600°C (Bucher and Frey, 1994). In parts dolostones were altered to dolomitic marble containing graphite, olivine and ore minerals like rutile, which represents a typical mineral composition for contact metamorphism at temperatures between 500°C and 600°C degree (Bucher and Frey, 1994).

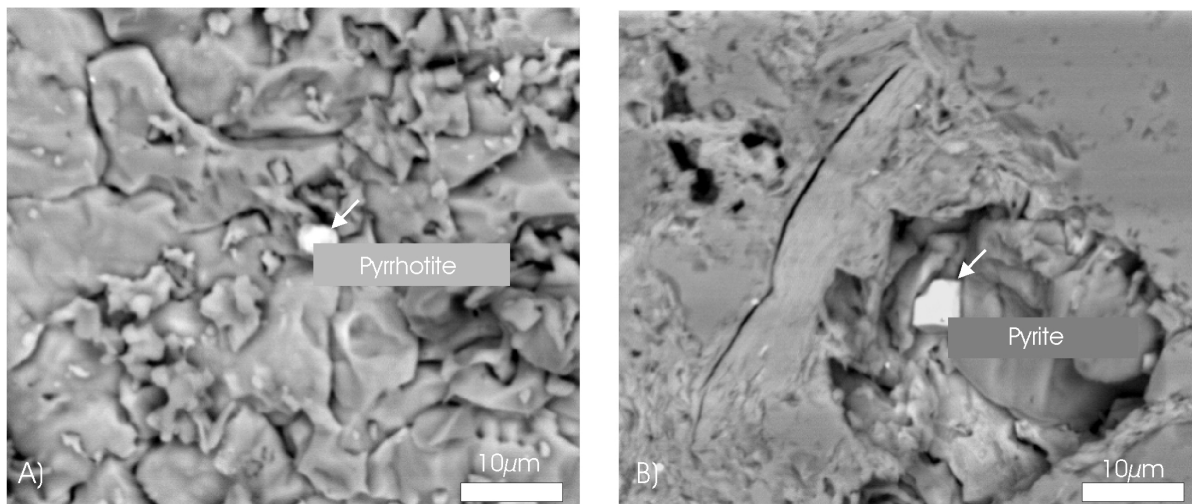


Figure 1.4: Pyrrhotite (A) and pyrite (B) in the samples from Central Elba (Italy) using SEM.

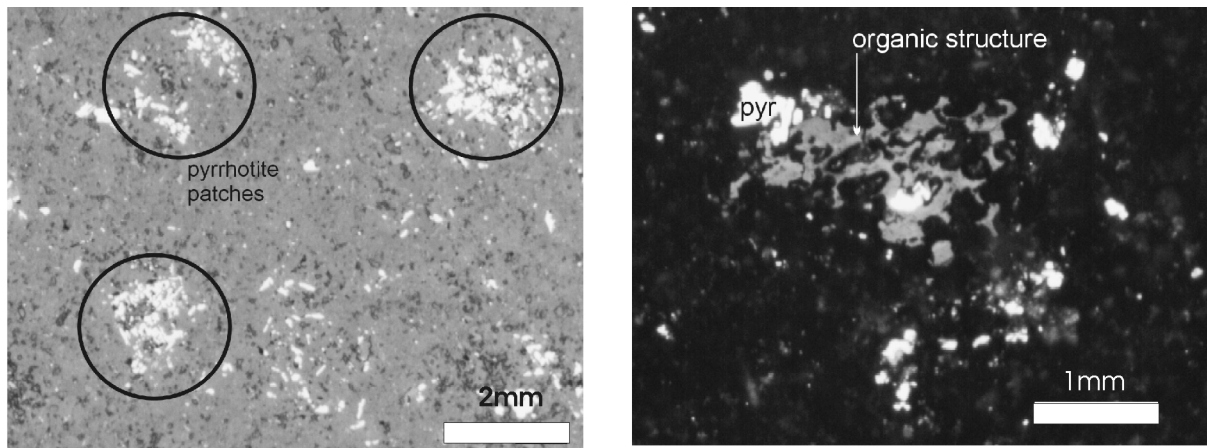


Figure 1.5: Reflected light microscopy of the samples of Isle of Skye. A) Large aggregates of pyrrhotite patches. B) Preserved cell structure of a plant. The carbon is transformed to graphite.

In the contact metamorphic area of the Isle Skye iron sulfides appear abundantly in a distance of 100 m up to 1 km. In this transitional zone pyrrhotite crystals are formed in large aggregates up to some mm (Fig. 1.5a). Graphite impregnates the whole rock. Additional minerals are rutile and chalcopyrite.

Depending on the location a weak degree of metamorphism – indicated by fine-grained calcite and/or quartz, a high content of organic matter (Fig. 1.5b) or preserved bioclast – starts in a distance of around 150 m from the contact. Although evidenced by rockmagnetic means, pyrrhotite could not always be directly observed.

Using SEM analysis the abundance and grain-sizes of pyrrhotite in the transitional zone is even more obvious (Fig. 1.6a). Additionally, pyrrhotite can also exist as an envelope around iron-rich grains (Fig. 1.6b). The close side by side of magnetic phases underlines the

existence of strong magnetic interaction in these samples as reported by Wehland et al. (subm).

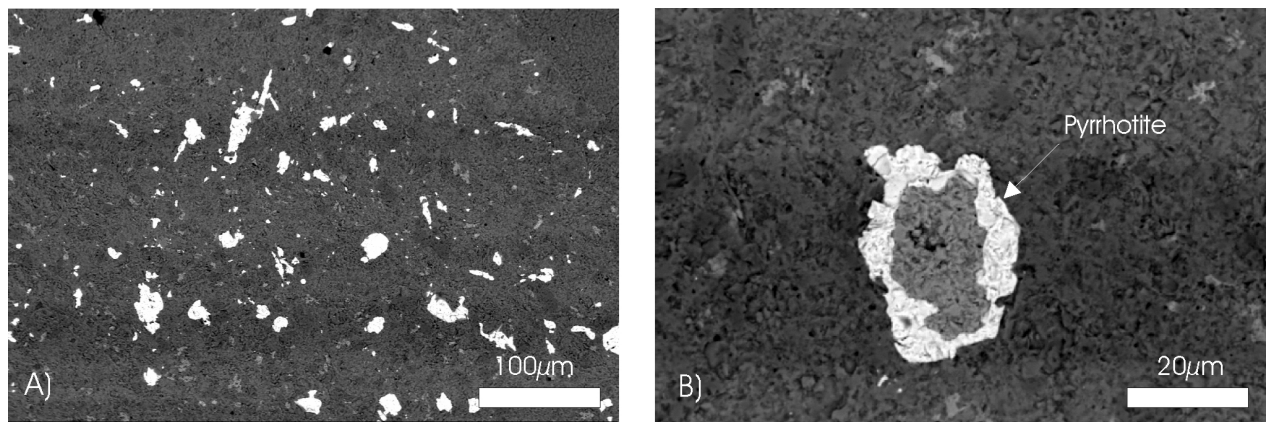


Figure 1.6: Pyrrhotite in the samples from Isle of Skye. A) Abundance and grain-size spectrum. B) Pyrrhotite around an iron rich grain (possibly an iron carbonate).

In the Manaslu area the metamorphic limestones near the contact consist of pure marble with sparsely distributed idiomorphic ore crystals (Fig. 1.7a). The occurrence of calcite twin lamellas stands for a peak temperature above 300°C (Burkhard, 1993). In the regional metamorphic part the rocks appears as a dark, carbon rich marly limestones (Fig. 1.7b).

In samples affected by contact metamorphism framboidal iron sulfides appear similar to the ones in Bourg d'Oisans with a Fe/S ratio of 2/3 (Fig. 1.8a). Such a composition is identical with a mixture of pyrite and pyrrhotite in the proportions of the desulfidation reaction given by Carpenter (1974) and Ferry (1981). Besides framboidal structures, pyrrhotite also exists as individual grains (Fig. 1.8b) in the size of the single domain threshold ($\sim 1\mu\text{m}$).

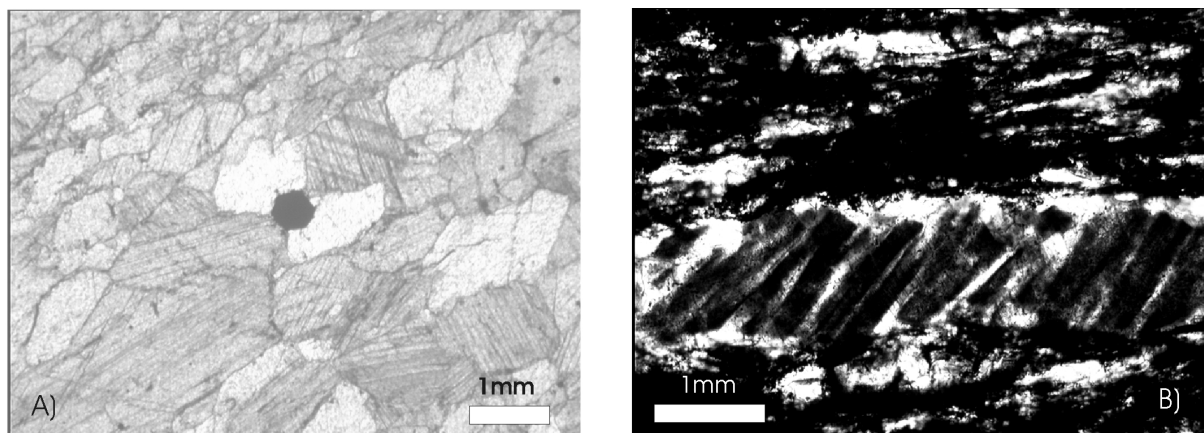


Figure 1.7: Transmitted light microscopy on samples from the contact metamorphic (A) and the regional metamorphic part (B).

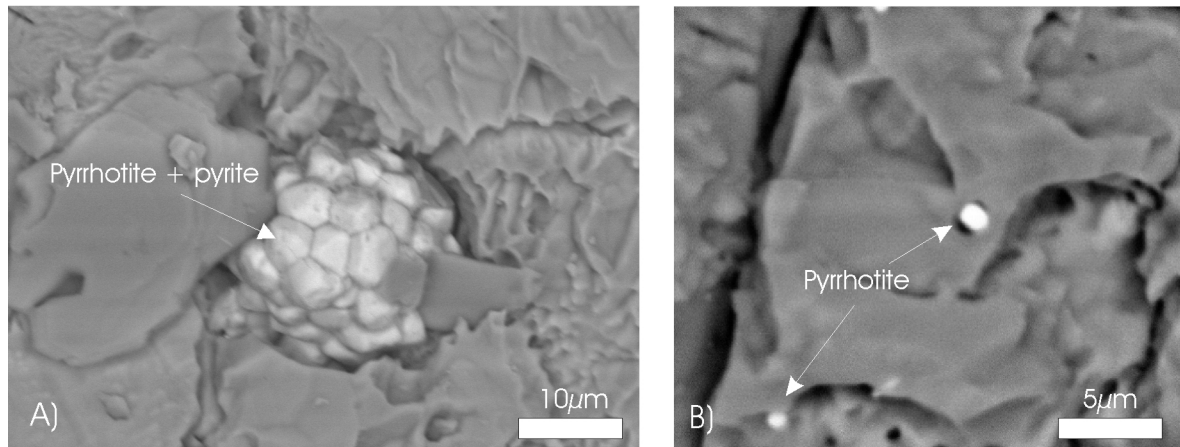


Figure 1.8: Cluster iron sulfids (A) and individual pyrrhotite grains (B) from the Manaslu area.

1.4 Discussion:

The microscopic investigations allow tentative conclusions about the different formation processes of pyrrhotite in the regional and contact metamorphic environments and its potential as a recorder of successive pTRM.

Regional Metamorphism:

The observed coexistence of carbon, pyrite and pyrrhotite and the lack of magnetite is in conformity with the thermodynamic calculations of Gillett (2003) and the study of Ferry (1981) on metamorphic schists, where most of the iron is stored in pyrite. As the paleomagnetic data (Crouzet et al., 1999; Schill et al., in press) indicates peak temperatures above the Curie temperature of pyrrhotite, the expected process for the formation of pyrrhotite under such conditions would be the breakdown of pyrite (Lambert, 1973; Ferry, 1981). But the relatively fresh appearance of the diagenetically grown, framboidal pyrite implies, that the desulfidation process was hampered. A suppression of the desulfidation process requires a low amount of metamorphic fluids (Ferry, 1981).

The idiomorphic pyrrhotite – as observed by TEM analysis - probably formed insitu by the expense of the iron bearing carbonate in its surrounding. Sulphur was made available by a H₂S enriched fluid phase wetting the grain surfaces. In carbon bearing metasediments, such fluids exists for low $f(\text{O}_2)$ compared to the graphite maximum, whereas the H₂S component is favoured by low pressure, low oxidation and increasing temperatures (calculation and examples: Poulson and Ohmoto, 1989, and ref. therein).

The relevance of this formation process for the pTRM acquisition lies in the grain size distribution of pyrrhotite. Depletion of iron in the surrounding matrix during the epitaxy favours the growth of a higher number of smaller grains instead of individual bigger ones. Consequently, the blocking temperature spectra in such rocks will be brought, as grains grow from the small, superparamagnetic (SP) to the larger SD and/or PSD range. This is in accordance with the blocking temperature spectra investigated by Thellier like experiments on laboratory induced TRMs (Fig. 1.9, Wehland et al., *subm.b*).

The blocking temperature spectra spans over the entire temperature range (Fig. 1.9A). The growth from SP to SD particles can be seen in Figure 9B, where the blocking temperature spectra is large at low temperatures and stops below the Curie temperature of pyrrhotite. The lack of MD particles (low MD checks and negligible pTRM tails, see Wehland et al., *subm.b*) goes along with the microscopic observation of pyrrhotite grains with a size $<3 \mu\text{m}$. As clustering of grains is unlikely due to the availability of iron, magnetic interaction can be excluded (Wehland et al., *subm.a*).

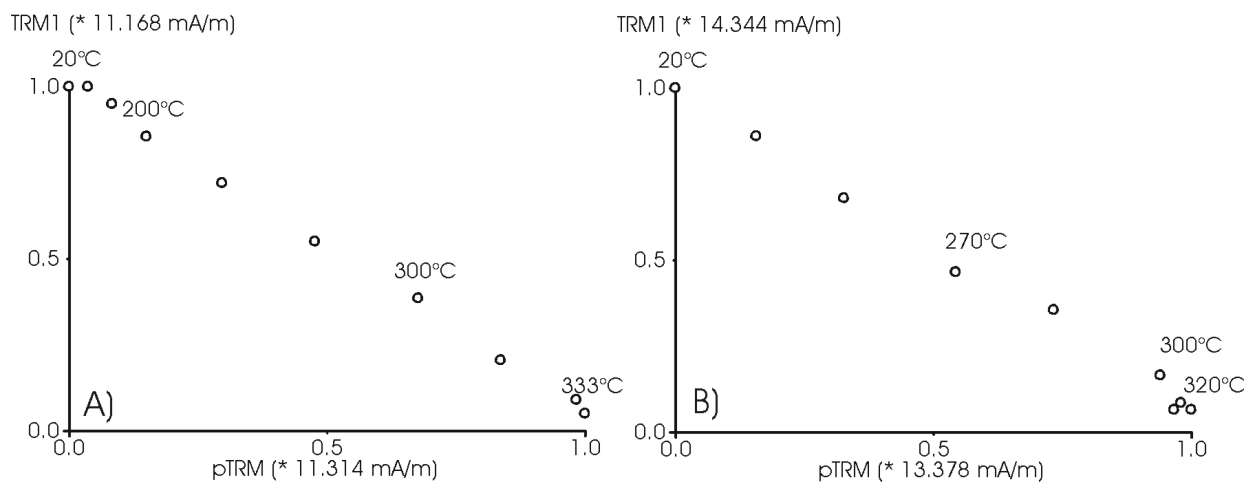


Figure 1.9: Relative blocking temperature spectra derived from Thellier experiments on a laboratory induced TRM. A) Wide spectrum up to the Curie temperature of pyrrhotite. B) Narrow blocking temperature spectrum restricted to the lower unblocking range.

Contact Metamorphic Rocks:

Size and appearance of pyrrhotite in contact metamorphic rocks is more complex and ranges from μm scale crystals up to mm large patches and depends strongly on the nature and degree of metamorphism.

In direct vicinity of the contact the abundance of pyrrhotite and pyrite are extremely low at all sampling locations. With a matrix consisting mostly of pure marble one can assume a

significant amount of fluids involved, which - at these temperature - would be rich in H₂S as long as sulfides were available. These fluids can either migrate into the magma (Poulson and Ohmoto, 1989) or into the country rock.

At larger distances to the contact (up to 1 km), cooling would force the H₂S to fall out either as pyrite or pyrrhotite. If carbon is present the $f(\text{O}_2)$ will be low enough to favour the crystallisation of pyrrhotite (Gillett, 2003) at temperatures higher than 350°C. This can explain size and shape of the large pyrrhotite minerals in the transitional zone at the Isle of Skye.

Due to a lack in the outcrop availability (Wehland et al., subm.b) such a zone is missing in the Manaslu area. Nevertheless, the influence of a higher fluid content is demonstrated by a higher degree of desulfidation, where pyrite is partly transformed into pyrrhotite. A higher fluid content will also promote the dissolution of disseminated iron sulfides (Hall, 1986), where smaller grains will be more affected due to their greater surface/volume ratio.

For magnetic studies it has the consequence, that the blocking temperature spectra will be reduced at lower temperature. This can explain the reported square shoulder demagnetisation curves for pyrrhotite (Gillett, 2003)

In contrary, the situation in the samples of central Elba favours the in situ growth of pyrrhotite. Fluid circulation exists, but not in a pervasive style and the observed grain-size lies in the SD range.

1.5 Conclusion:

The formation of pyrrhotite under low-grade metamorphic conditions depends on the amount of fluids involved. In regimes, where thermal conductivity is dominating, the epitaxy is an in situ process resulting in a broad grain-size distribution within the SP to SD particle range. If the fluid content is high pyrrhotite will be a product of the desulfidation of pyrite forming crystals of up to several mm. As Ferry (1981) reported also larger pyrrhotite aggregates in regional metamorphic schists, both types are possible in contact and regional metamorphic rocks. In the light of pTRM acquisition the in situ growth does provide the necessary grain-size distribution within the SD range to record variations of the EMF during cooling within a single sample.

1.6 References:

Appel, E., Müller, R., and Widder, R.W., 1991. Palaeomagnetic results from the Tibetan Sedimentary Series of the Manang area (north central Nepal). *Geophys. J. Int.*, 104: 255-266.

Bucher, K., and Frey, M., 1994. *Petrogenesis of metamorphic rocks*. Springer Verlag, Berlin.

Burkhard, M., 1993. Calcite twins, their geometry, appearance and significance as stress/strain markers and indicators of tectonic regime: a review. *J. Struct. Geol.*, 15(3-5): 352-368.

Carpenter, R. H., 1974. Pyrrhotite isograd in the SE Tennessee and SW North Carolina. *Geol. Soc. Am. Bull.*, 85: 451-456.

Crerar, D. A., Susak, N. J., Borsik, M. and Schwartz, S., 1978. Solubility of the buffer assemblage pyrite + magnetite in NaCl solutions from 200 to 350 °C. *Geochim. Cosmochim. Acta*, 42: 1427-1437.

Crouzet, C., Rochette, P., Ménard, G., and Prévot, M., 1997. Acquisition d'aimantations thermorémanentes partielles successives portées par la pyrrhotite monodomaine lors du refroidissement de la zone dauphinoise interne (Alpes occidentales, France). *Compte rendu Acad. Sci. Paris, II*, 325: 643-649

Crouzet, C., Ménard, G., and Rochette, P., 1999. High precision three dimensional paleothermometry derived from paleomagnetic data in an Alpine metamorphic unit. *Geology*, 27 (6): 503-506.

Ferry, J. M., 1981. Petrology of graphitic sulfide-rich schists from south-central Maine: an example of desulfidation during prograde regional metamorphism. *Am. Mineral.*, 66: 908-930.

Gillett, S.,L., 2003. Paleomagnetism of the Notch Peak metamorphic aureole, revisited: Pyrrhotite from magnetite+pyrite under submetamorphic conditions. *J. Geophys. Res.*, 108 (B9), 2446, doi:10.1029/2002JB002386

Hall, A. J., 1986. Pyrite-pyrrhotite redox reactions in nature. *Mineral. Mag.*, 50: 223-229.

Lambert I. B., 1973. Post-depositional availability of sulphur and metals and formation of secondary textures and structures in stratiform sedimentary sulphide deposits. *J. Geol. Soc. Australia*, 20: 205-215.

Ménard, G., and Rochette, P., 1992. Utilisation de réaimantation postmétamorphique pour une étude de l'évolution tectonique et thermique tardive dans les Alpes occidentales (France). *Bull. Soc. Géol. France*, 163 (4): 381-392.

Poulson, S., R., and Ohmoto, H., 1989. Devolatilization equilibria in graphite-pyrite-pyrrhotite bearing pelites with application to magma-pelite interaction. *Contrib. Minerl. Petrol.*, 101: 418-425.

Rochette, P., 1987. Metamorphic control of the magnetic mineralogy of black shales in the Swiss Alps, toward the use of "magnetic isograds". *Earth Planet. Sci. Lett.*, 84: 446-456.

Schill, E., Appel, E., Gautam, P. and Singh, V.K., 1998. Preliminary palaeomagnetic results from medium-grade metacarbonates of the Lesser Himalaya. *J. Nepal Geol. Soc.*, 18: 205-215.

Schill, E., Appel, E., Crouzet, C., Gautam, P., Wehland, F., and Staiger, M, in press. Oroclinal bending and regional significant clockwise rotations of the Himalayan arc - constraints from secondary pyrrhotite remanences. *Geol. Soc. Am.*

Soffel, H.C., 1977. Pseudo-single domain effects and single-domain multidomain transition in natural pyrrhotite deduced from domain structure observations. *J. Geophys.*, 42: 351-359.

Thellier E., and Thellier O., 1959. Sur l'intensité du champ magnétique terrestre dans le passé historique et géologique, *Ann. Geophys.*, 15: 285-376.

Thompson, J. B. Jr., 1972. Oxides and sulfides in regional metamorphism of pelitic schists. *Proceeding of the 24th International Geological Congress, Section, 10: 27-35.*

Tracy, R.J., and Robinson, P., 1988. Silicate-sulfide-oxide-fluid reactions in granulite grade pelitic rocks. *Central Massachusetts. Am. J. Sci.*, 288: 45-74.

Wehland, F, Stancu, A., Rochette, P., Dekkers M.J., and Appel, E., *subm.a.* Experimental evaluation of magnetic interaction pyrrhotite bearing samples, *Phys. Earth Planet. Inter.* 2004.

Wehland, F., Alt-Epping, U., Braun, S., and Appel, E., *subm.b.* Potential and quality of pTRM recording in pyrrhotite bearing contact-metamorphic limestones, *Phys. Earth Planet. Inter.*, 2004.

Quality of pTRM acquisition in pyrrhotite bearing contact-metamorphic limestones: Possibility of a continuous record of Earth magnetic field variations

Abstract:

The rockmagnetic and palaeomagnetic signal in pyrrhotite bearing limestones of different contact metamorphic settings were investigated related to intrusions ranging from small sills to large magmatic complexes. Magnetic susceptibility, the pyrrhotite/magnetite ratio and thermal modelling serve as an investigative tool to define three metamorphic zonation: a contact zone of a mixed magnetic assemblage and low susceptibilities, a pyrrhotite bearing transitional zone, where full TRMs are acquired due to temperatures above the Curie temperature of pyrrhotite ($T_{c,po}$), and a marginal zone containing pyrrhotite and magnetite at temperatures below $T_{c,po}$. The fact that TRMs can consist of independent pTRMs is successfully tested by modified Thellier experiments. It is shown that a metamorphic environment with low fluid circulation provides a scenario for the recording of independent pTRMs. Multicomponent behaviour of the NRM residing in samples from the transitional zone can therefore be interpreted as a continuous record of Earth magnetic field variations.

1.1 Introduction:

Using conventional methods to record changes of the Earth Magnetic Field (EMF) one has to deal with intrinsic problems of the time axis such as unknown time gaps in lavas and the lock-in-depth problem in sedimentary rocks. Continuous records based on the acquisition of successive partial thermoremanent magnetisations (pTRMs, Fig. 1) at one site during metamorphic cooling in a single sample could provide additional information.

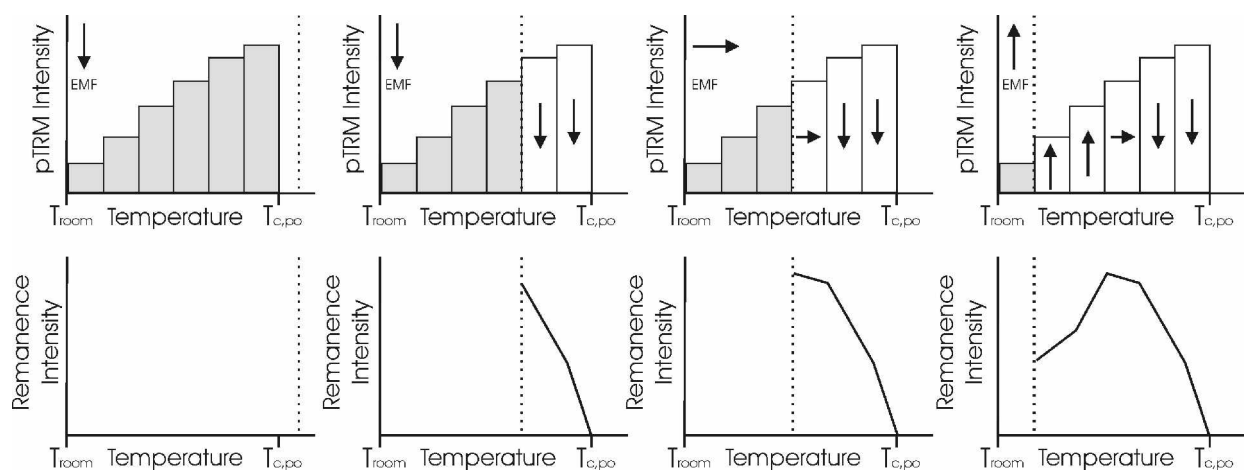


Figure 2.1: Principle of pTRM recording in a single sample during metamorphic cooling (from left to right): the different directions of the EMF are blocked in the respective pTRMs. The direction of the EMF is marked with the arrow in the left upper half of the diagram. Gray boxes stand for individual unblocked pTRMs, white for blocked ones. The dashed line indicates the actual metamorphic temperature during cooling. The lower diagrams demonstrates the resulting net-intensity of the sample along the axis parallel to the primary EMF direction. $T_{c,po}$ is the Curie temperature of pyrrhotite.

During the last two decades the relevance of pyrrhotite as the main carrier of paleomagnetic information in very low to low grade metamorphic limestones has been well established (Rochette, 1987; Appel et al., 1995; Ménard and Rochette, 1992; Schill et al., 1998, 2001; Crouzet et al., 1999, 2001; Gillett, 2003). For regional metamorphic limestones Crouzet et al. (1999, 2001) demonstrated that pyrrhotite is able to acquire successive, independent pTRMs during cooling. As the temporal resolution of such a continuous record of the EMF depends on the cooling rate contact metamorphic rocks would be more appropriate. This is underlined by a recent study of Keating et al., (2002) who reported the recording of transitional fields carried by pyrrhotite in the vicinity of an intrusive body.

In this paper we assess the potential of pyrrhotite for pTRM acquisition in contact metamorphic settings in dependence of their spatial relation to the magmatic contact.

2.2 Geological Settings:

The selection of the geological settings followed the idea to obtain samples from marly limestones near intrusions of different size, and hence different cooling rates and different contact-metamorphic conditions such as the amount of fluids involved. All selected magmatic bodies have a shallow intrusive depth, which ensures a low initial temperature of the intruded rocks. This is important as deep burial would decrease the contact metamorphic influence and would favour a more regional metamorphic setting. Under these conditions samples were selected from three locations as followed: Manaslu (Nepal), Isle of Skye (Scotland), Elba (Italy)

Manaslu area (Nepal):

The Manaslu Granite (Fig. 2.2) is one of the best studied intrusives of the Himalayan Orogen. It can be described as a lenticular body of ~10km in thickness with a gentle dip towards NNE. Formed during two major pulses of magmatism (Harrison et al., 1999), ca 23 Ma (Larkya La phase) and 19 Ma (Bintang phase), the intrusion has grown by lateral expansion (following a model proposed by Lagarde et al., 1990).

Limestones eastwards adjacent to the Manaslu Granite, near the Tibetan border, form part of the Tethyan Sedimentary Series (TSS), comprising Ordovician to Jurassic sediments of low grade metamorphism (Fuchs and Paudel, 1998). Cooling of the Manaslu Granite and its aureole, as based on $^{40}\text{Ar}/^{39}\text{Ar}$ measurements (Guillot et al., 1994), has mainly taken place at the period ~16-19 Ma. This age corresponds to the Bintang phase. Palaeomagnetic directions

of the TSS sampled to the east of the contact area carry a regional metamorphic signal (Schill et al., in press; see arrows Fig. 2.2).

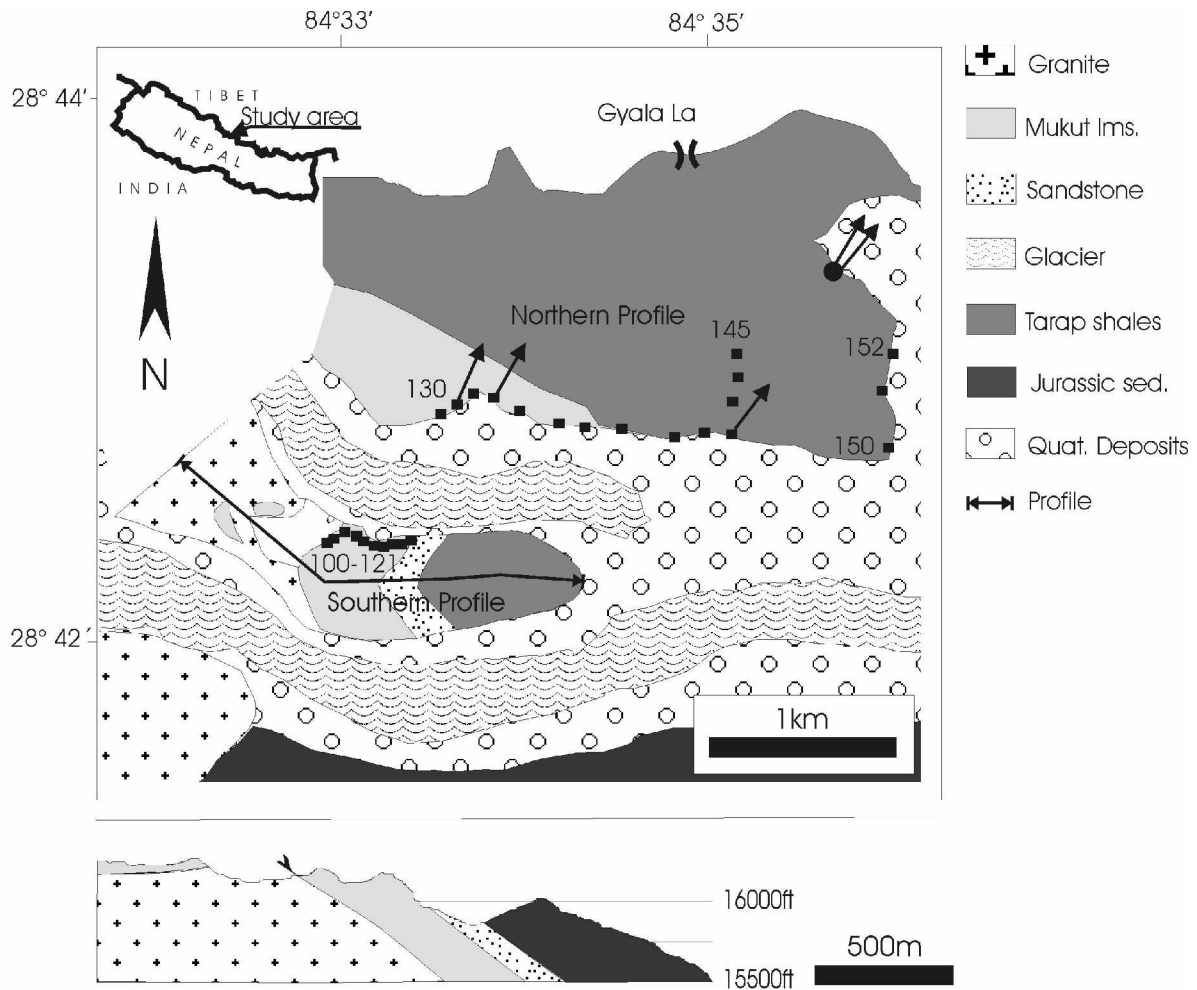


Figure 2.2: Geological map of the eastern contact metamorphic area of the Manaslu granite (Nepal) modified after Fuchs and Paudel (1998). The geological profile of the central ridge (sampling positions 100-121) is made by own observation. Sampling positions are indicated with square boxes. The circles and arrows represent sampling sites and remanence directions as reported by Schill et al. (inpress).

The sampling area (Fig. 2.2) covers the limestones (Mukut lms.; Tarap Shales) from the contact with the intrusion up to a distance of about 3 km (site 152). Although a displacement of unknown distance occurs along the contact at the southern profile (Guillot, pers. com.; and own observations), the highly metamorphosed rocks indicate a direct vicinity to the intrusion. The widespread presence of thick (~0.5m) veins in the Mukut limestone of the northern profile indicates its vicinity to the intrusion. Moreover, its stratigraphic analogy with the southern profile suggest that the northern profile is the continuation of the southern profile in respect of the distance towards the intrusion. The tectonic style of the sequence changes from nearly undisturbed limestone (Mukut Limestone) towards strongly folded shales (Tarap Shales) at greater distance from the contact.

Isle of Skye (Scotland):

The southern part the Isle of Skye is dominated by the large igneous complex of the Red Hills granite (~10 km in diameter). Emplacement into the Paleozoic and Mesozoic rocks in the study area (Fig. 2.3) occurred between 58.7 ± 0.9 Ma (western Red Hills) and 53.5 ± 0.9 Ma (Beinn an Dubhaich granite) (Dickin, 1981; Harris, 1985).

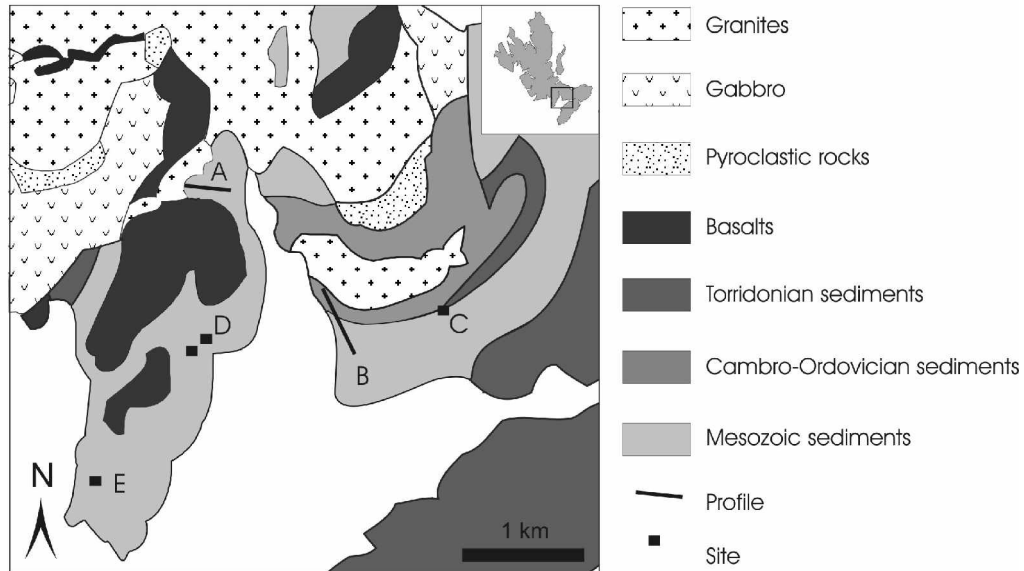


Figure 2.3: Overview of the sampling area at the Isle of Skye (Scotland). A and B are profiles sampled with increasing distance towards the contact. C is the position of the conglomerate. D and E are individual sites.

Contemporary fissure feeders and dykes of basaltic composition penetrated the sediments and plutons of the whole island and are now visible in the NW-SE trending dyke swarms (England, 1994; Bell and Jolley, 1997). Beside some petrological alteration at magmatic temperatures (650°C - 700°C), most of the mineral alteration has taken place at the hydrothermal stage of pluton cooling (Ferry, 1985; Holness et al., 1989; Holness, 1992; Holness and Fallick, 1997). Due to indications favoring a depletion of stable isotopes of oxygen and hydrogen, Bell and Harris (1986) suggested that an extensive convective flow of heated groundwater existed in the volcanic and subvolcanic units as well as in the surrounding country rock within a distance of 4 km of the center of the isle of Skye.

The western part of the sampling area (A-D-E, Fig. 2.3) is made up of unfolded Middle Jurassic to Upper Cretaceous limestones and sandstones, which were intruded in the northern part by a large gabbroic and granitic complex. The intrusion of the NW-SE trending basaltic dykes crosscuts all other features and can therefore be seen as the youngest geological event (England, 1994). The eastern part of the sampling area (B and C, Fig. 2.3) is dominated by the

Beinn an Dubhaich Granite, which is surrounded by Cambro-Ordovician limestones of the Ben Suardal Formation (Durness Group). These sediments are part of an anticline formed during the Cambrian Orogeny whose southern limb is overlain by Triassic conglomerates and Liassic limestones (Bell and Harris, 1986). Tertiary dykes and faults are abundant in the Liassic limestones

Elba Island (Italy):

The island of Elba envelops a variety of different contact metamorphic scenarios: The dominant, nearly circular intrusive body of the Mt. Capanne Granite in the western part of the island is surrounded to the east by highly metamorphosed skarns and serpentinites (Fig. 2.4). According to U/Pb data from Juteau et al. (1984) the 600°C isotherm was crossed by cooling at 6.2 Ma. A comparison with the 120°C isotherm (apatite fission track dated of Bouillin et al., 1994),

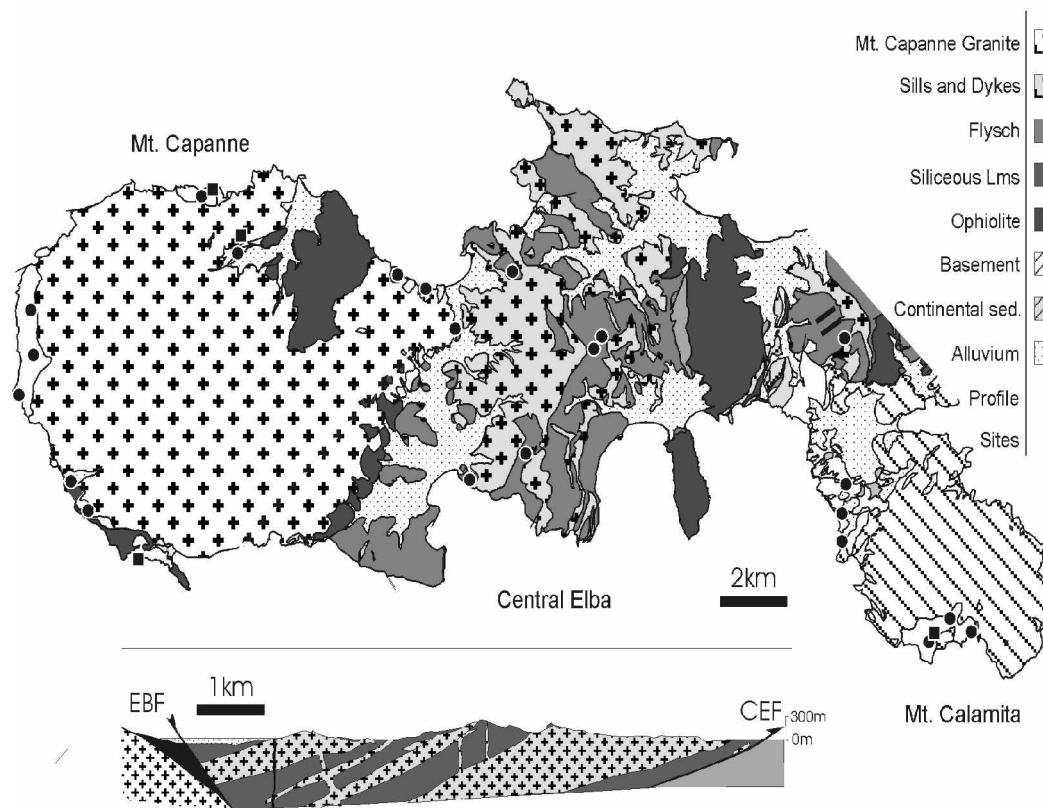


Figure 2.4: Simplified geological map of the contact metamorphic parts of Elba Island (from W to E): Mt. Capanne, central Elba and Mt. Calamita. The cross-section through central Elba is redrawn after Rocchi et al. (2002), EBF- Eastern Border Fault; CEF – Central Elba Fault.

which was crossed at an age of 5.4 Ma, indicates that the cooling rate of the body was relatively high. Adjacent to the east lie the aplitic dykes and sills of central Elba, the latter being relatively flat bodies of up to 500m thickness intruded into Middle Jurassic to early

Creataceous limestones and sandstones (complex IV after Trevisan, 1950). In all probability emerging from the roof of the Mt. Capanne, this sequence was detached along the Central Elba Fault (CEF) and the Zucchale Detachment Fault (ZDF) after initial pluton emplacement, and experienced a second downward movement relative towards the Mt. Capanne Granite during stretching at approximately 2 Ma (Daniel and Jolivet, 1995). The Capanne Granite was dated at 6.2 Ma using Rb/Sr in mica (Venzlaff and Waldeck, 1974). Although remaining in a genetic relationship with the Mt. Capanne pluton, the difference in ages can be explained by a slower cooling of the larger Mt. Capanne pluton.

Separated by the ZDF the schists (belonging to complex 1 after Trevisan, 1950) and skarns of the southeast belong to the intrusion of the Mt. Calamite pluton. This intrusion is slightly younger (5.2 Ma after Daniel and Jolivet, 1995) than the Mt. Capanne Granite and does not crop out at the surface.

2.3 Sample treatment and analytical procedure:

In general, sites were selected at increasing distance from the intrusion. At each site three samples were drilled, each with a diameter of 2.5 cm. Samples were orientated using a magnetic compass and sliced into specimens of 2.2 cm length. In the Manaslu region orientated block samples were also taken and later on cut into cubes of 2.2 cm aside. Measurements were performed in the palaeomagnetic laboratory of the University of Tübingen. For each site the natural remanent magnetization (NRM) one of the two pilot specimens was demagnetised using a MMTD1 thermal demagnetiser (Magnetic Measurements) and the other specimen by alternating field demagnetisation (AF) using a 2G600 (2G Enterprise) automatic degaussing system. Remanence was measured using a 2G Enterprise RF SQUID magnetometer. AF treated samples were subsequently subjected to isothermal remanent magnetisation (IRM) analysis (acquisition, backfield and thermal demagnetisation). Susceptibility during thermal treatment was monitored using a KLY2 Kappabridge (AGICO). Thermomagnetic curves were measured in air using a KLY3 Kappabridge with a CS temperature unit (AGICO). For Thellier experiments the applied field (in the MMTD1) was set at 90 μ T.

2.4 Results:

Magnetic mineralogy and rockmagnetic properties in a spatial context:

Knowledge about the magnetic mineralogy in their respective spatial relationships to the contact is important in order to understand the genetic process of pyrrhotite formation and alteration in contact-metamorphic limestones. This enables us to select suitable sampling sites for studying EMF variations by pTRM recording. Our assessment is based on the model that pyrrhotite is formed under low grade metamorphic conditions above a critical lower temperature boundary and is stable until an upper temperature boundary, together defining the so-called pyrrhotite window.

General magnetic mineralogy and the pyrrhotite window:

The occurrence of primary, authigenic pyrrhotite in fresh sediments is rare (Menard & Rochette, 1989). In general, it is assumed that pyrrhotite in low grade metamorphic limestones is a secondary accessory forming during progressive metamorphism by a simple desulfidation reaction (Carpenter, 1974, Ferry, 1981) or the breakdown of primary pyrite and magnetite (Ferry, 1981; Tracy & Robinson, 1988) under reducing conditions (Hall, 1986) above 200°C (Lambert, 1973; Gillett, 2003). We regard this temperature as the lower boundray of the pyrrhotite window. With increasing metamorphism pyrrhotite can be stable up to higher temperatures (700°C; see Ferry, 1981), as long as carbon is present to ensure reducing conditions (Poulson & Ohmoto, 1989). To assess the pyrrhotite stability under

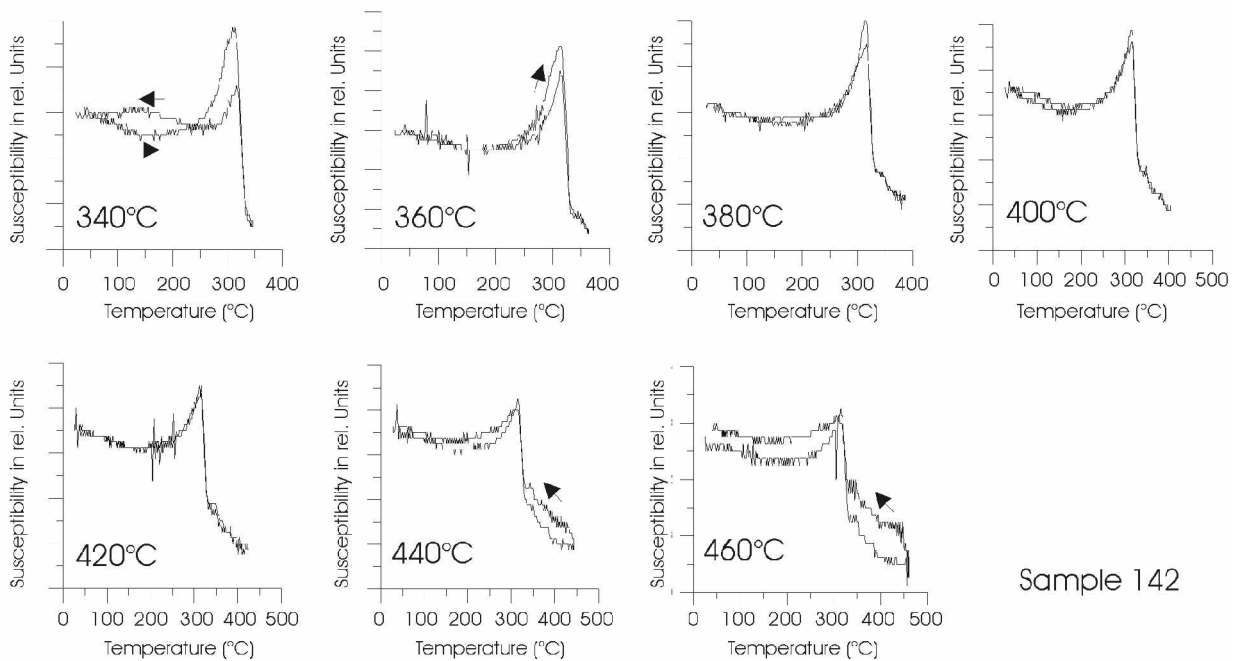


Figure 2.5: Successive thermomagnetic runs of sample 142 from the northern profile of the Manaslu area showing that besides initial differences pyrrhotite destruction starts at temperatures greater 420°C.

highly oxidizing conditions, we detected the alteration of pyrrhotite in our samples using thermomagnetic measurements. The existence of pyrrhotite is supported by a clear Hopkinson Peak just below its Curie temperature (Fig. 2.5). Alteration of pyrrhotite towards magnetite does not start before 440°C, which corresponds to the results from Crouzet et al. (2001). Under metamorphic conditions in the presence of carbon, the oxygen fugacity $f(\text{O}_2)$ will be much lower (Poulson and Ohmoto, 1989; Gillett, 2003) than in the laboratory experiments and the stability of pyrrhotite can rise to higher temperatures. Thus the laboratory results can be seen as the lower limit for the pyrrhotite instability (upper boundary of the pyrrhotite window). As a consequence the presence of pyrrhotite can be expected to have formed between metamorphic peak temperatures of 200°C and ~450°C. (more details are found in the companion paper of Wehland et al., *subm.*).

Acquisition and thermal demagnetisation of IRM (Fig. 2.6) indicates that pyrrhotite is the dominant magnetic phase in most of the samples. Magnetite and hematite also occur in lesser amounts. The relative occurrences of these magnetic phases depend on their distance from the magmatic contact, that is the degree and nature of metamorphism. For example, the Manaslu samples from the southern profile contain hematite and a lesser amount of pyrrhotite, whereas pyrrhotite is the dominant phase in the northern profile and the amount of magnetite is negligible (Fig. 2.6a,b). This is supported by the acquisition of the IRM showing the co-existence of a low and a high coercivity component in samples near the contact. In contrast, in the northern profile pyrrhotite exists in two different coercivities. Whereas the high coercivities are typical for SD pyrrhotite, such low coercivities can be related to larger grains with true MD behaviour (O'Reilly et al., 2000).

The results from the Mt. Calamite contact-metamorphic area (Elba) samples are comparable, with hematite dominating in highly metamorphosed samples (Fig. 2.6c). The small shift to lower temperatures (600°C) in the thermal demagnetisation of the IRM in the hematite bearing samples can be explained by maximal unblocking temperatures of the grain-size assemblage below the Curie temperature of hematite. Therefore, the grain-size assemblage should consist of SD particles only, which can be inferred by the high coercivity as shown in the IRM acquisition curve. In Central Elba (Fig. 2.6d) the magnetic mineralogy is composed of pyrrhotite and - to a lesser extent - magnetite. Hematite is rare and can only be found in some samples close to the magmatic contact. In the samples around the Mt. Capanne Granite, pyrrhotite again is the dominant magnetic phase besides a minor contribution of magnetite. At

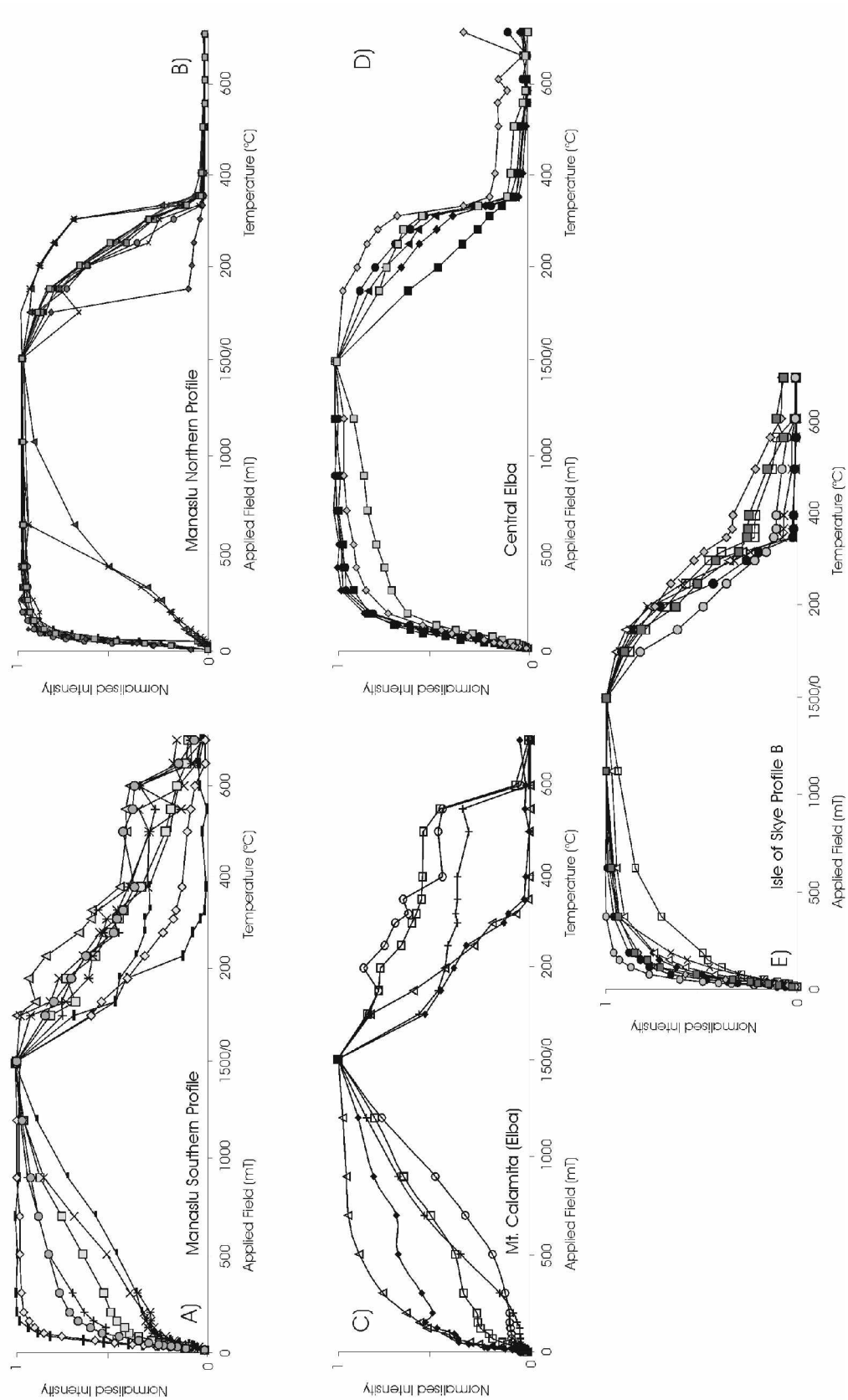


Figure 2.6: Examples of normalised IRM acquisition and thermal demagnetisation of the SIRM from different locations. The maximum applied field is 1500mT.

the Isle of Skye (Fig. 2.6e) the result from thermal demagnetisation indicates that pyrrhotite is the major magnetic phase, besides magnetite and a lesser amount of hematite. Samples of high coercivities are very rare, as found in the other locations close to the contact.

Rockmagnetic properties in their spatial context:

The idea of the pyrrhotite window allows to use the pyrrhotite/magnetite ratio for geothermometry. Therefore, the magnetic mineral content can be assessed by a PCA analysis using the thermal demagnetisation of of NRM and IRM. Thereby, results from the NRM analysis should be treated with care as the mineral content and the NRM remanence acquisition process do not stand in a direct relationship. So far, the methods was tested by Schill et al. (2001) in regional metamorphic rocks of the Tethyan Himalaya.

At the Isle of Skye the relative pyrrhotite/magnetite contribution calculated from thermal demagnetisation of SIRM and NRM after Schill et al. (2002) for profile B shows an increase of magnetite with increasing distance (<1500m) following a linear trend (Fig. 2.7a,b). Magnetic susceptibility, measured on untreated samples and after heating up to 330°C, gradually increases with increasing distance from the intrusional contact along profile B. As magnetite has a higher susceptibility than pyrrhotite, this behaviour suggests the formation of pyrrhotite at the expense of magnetite in the vicinity of the contact. Profile A-D-E (Fig. 2.7c,d) shows different behaviour of the pyrrhotite/magnetite ratio and the magnetic susceptibility along the profile. Pyrrhotite is the only ferro(i)magnetic phase along profile A at distances to the pluton below 1500m. At larger distances (site D and E) magnetite also occurs, with a decrease of the pyrrhotite/magnetite ratio with increasing distances. The increase of magnetic susceptibility at distances below 1500 m (Fig. 2.7c,d) is followed by a decrease at site D and E. As pyrrhotite is the only ferro(i)magnetic phase in profile A, the variation in magnetic susceptibility indicates the degree of pyrrhotite formation due to desulfidisation of pyrite. It appears from the complete profile A-D-E that the pyrrhotite/magnetite ratio depends on whether or not the sites are affected by younger dykes. It seems that reheating of the rocks during dyke intrusion enhanced the amount of pyrrhotite in the rocks (Fig. 2.7c). This is underlined by the high pyrrhotite content along profile A where dykes are abundant.

The behaviour of magnetic susceptibility and the pyrrhotite/magnetite ratio in central Elba is similar to profile B at the Isle of Skye: in close vicinity of the contact magnetic susceptibility is low, indicating the lack of ferro(i)magnetic phases. The relative increase of pyrrhotite with increasing distance to the center compared to magnetite combined with a decreasing trend in

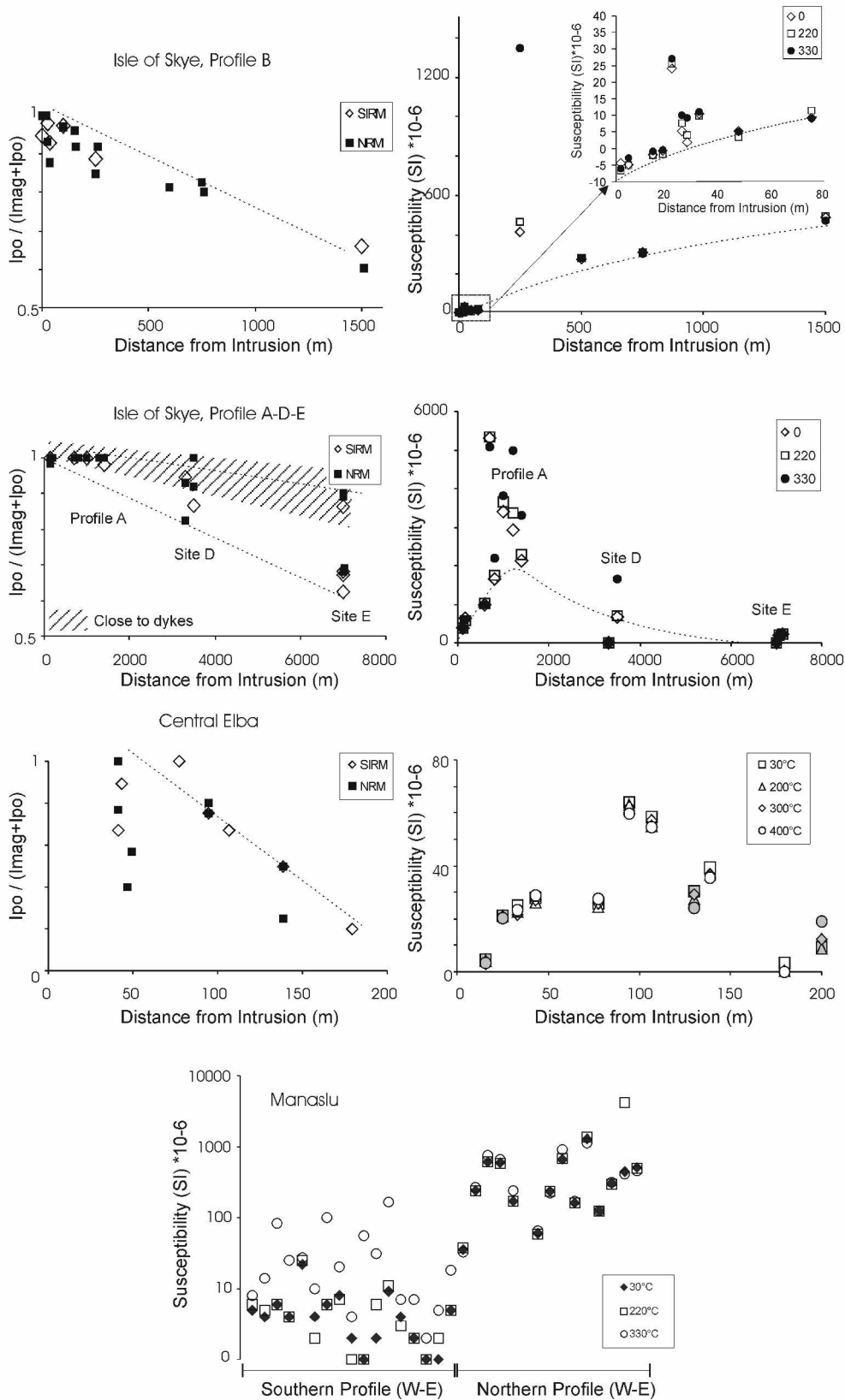


Figure 2.7: Magnetic susceptibility and pyrrhotite/magnetite ratio (I_{po}/I_{mag+po}) derived from thermal demagnetisation of the NRM and SIRM along different profiles. Dashed lines show inferred trends in respect to the distance of the intrusion.

magnetic susceptibility with increasing distance to the center suggests the formation of pyrrhotite at the expense of pyrite and magnetite closer to the contact.

The two profiles from the Manaslu area do not fit the above scheme. The pyrrhotite/magnetite ratio cannot be determined because primary magnetite is absent. This can be attributed to the consumption of magnetite during the earlier regional metamorphism. Moreover, the discontinuity of the profile does not permit an interpretation in terms of trends in the magnetic susceptibility (Fig. 2.7e).

PTRM experiments and recording ability:

The recording ability of pyrrhotite bearing samples depends on the domain state of the grains, the presence of magnetic interaction in the magnetic particle assemblage and the blocking temperature spectrum of the assemblage. This was tested on selected samples by Thellier-type experiments (Coe, 1967) on laboratory-imparted TRMs including the determination of multidomain (MD) tails (Riisager and Riisager, 2001). It allows the identification of the blocking temperature spectrum and to use the sensibility of the Arai-Nagata plot (Nagata et al., 1963) in order to determine contribution of MD grains and magnetic interaction.

The quality of the recorder was evaluated using the following criteria:

Class A: all specimens have MD checks (MD tail contribution expressed in % as Δmag) lower than 5% and a standard deviation for the palaeointensity determination lower than 10%. The directional deviation (directional deviations from a straight line expressed as Δang) is less than 3° .

Class B: all specimens have either MD checks (Δmag) lower than 5% or a standard deviation for the palaeointensity determination lower than 10%. The directional deviation (Δang) is less than 3° .

Class C: all specimens have MD checks (Δmag) higher than 5% and a standard deviation for the palaeointensity determination higher than 10%.

An additional qualitative criterion is the appearance of the blocking temperature spectrum, which should be broad to allow pTRM recording over a wide temperature range.

The Manaslu samples have a relatively narrow (Fig. 2.8) blocking temperature spectra near $T_{c,po}$. MD checks indicate that the grain size assemblage can range from a relatively restricted SD assemblage to a mixed assemblage of SD and MD grains. The changes in the direction in some of the samples suggest minor alteration during the repeated heating steps (Leonhardt et

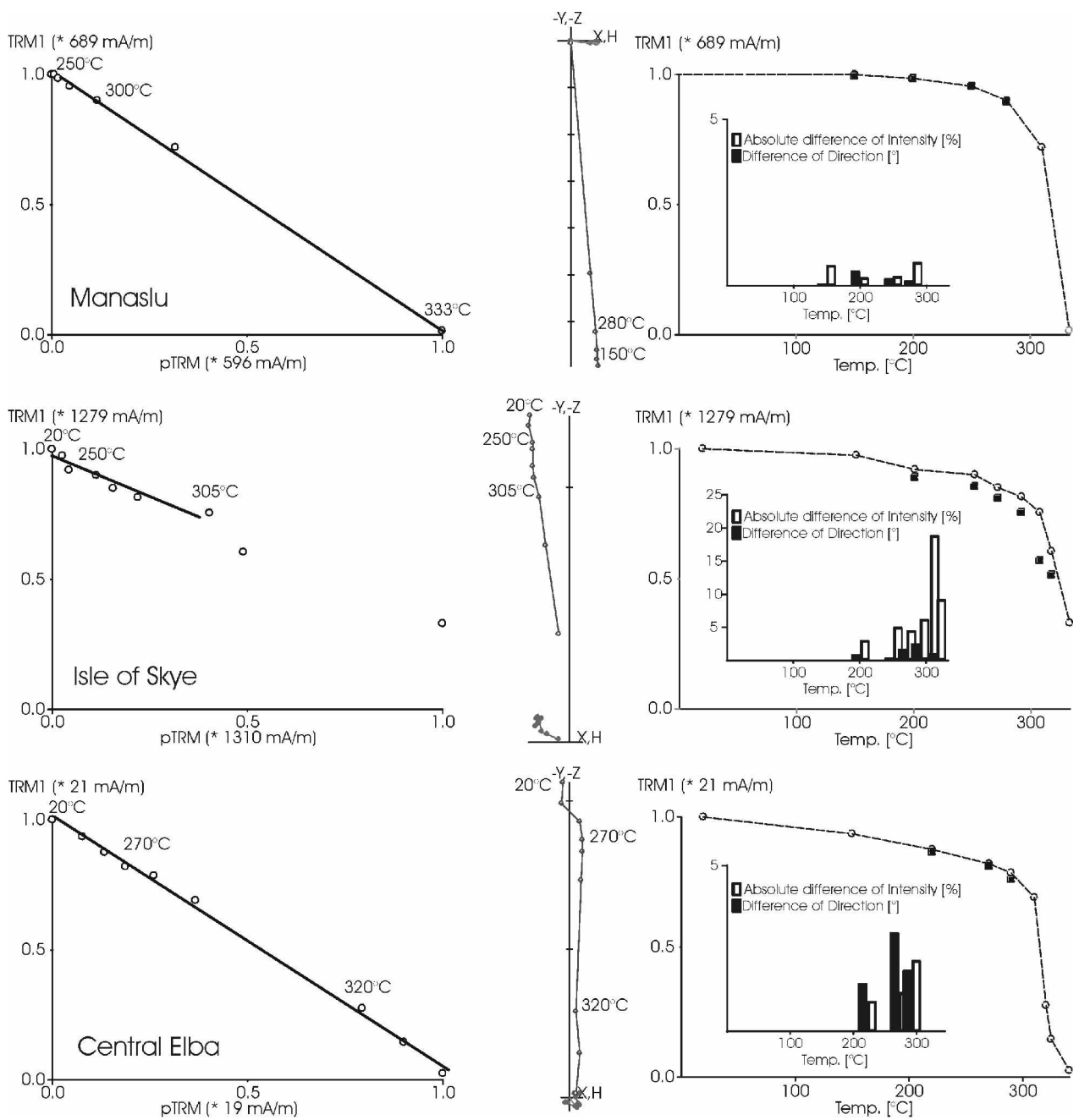


Figure 2.8: Thellier type experiments on laboratory TRMs: Arai-Nagata plot (left side), corresponding Zijderveld diagram (middle) and the intensity during demagnetisation (right). Histograms showing intensities of MD checks (white bars) and directional deviations of pTRMs from the external field directions (gray bars).

al., 2000). Three out of five samples of the northern profile fall into class A and B (Table 1). Samples from the southern profile were too low in intensity. Additionally, coexisting magnetite/hematite, low coercivities of pyrrhotite, and alteration hamper the results.

The Thellier experiments on the samples from the Isle of Skye demonstrate that pyrrhotite in these samples exists in the SD to MD range. Alteration during thermal treatment is observed. The blocking temperature spectra are relatively broad. In general, the TRM intensities in these samples, as calculated from the Arai-Nagata-plot, are higher ($\Delta\text{mag} > 10\%$) than the laboratory applied field. Because of the relatively restricted recording quality further pTRM tests were not performed. Thellier experiments on the Elba samples exhibit good recording quality. Blocking temperature spectra are relatively broad. MD checks and directional deviation are low. Eight out of twelve samples were classified into class A and B.

Time-temperature relationship:

The metamorphic history from larger intrusions is difficult to assess due to the uncertainties of the shape of the intrusives and the pulses of magmatic events. The shape of the Beinn an Dubhaich Granite is quite well known from gravity and structural data (Hoersch, 1979,1981; Longman and Coward, 1979; Tantrigoda, 1988; Butler and Hutton, 1994; England, 1994; Gouly et al., 1996). Suggesting that the granitic body intruded during the Tertiary into the Cambro-Ordovician carbonates up to 2 km below the palaeosurface (Hoersch, 1979) and using the modelled shape of the intrusion after Gouly et al. (1996), the time-temperature relation can be modelled using the program HEAT, a 2-D finite difference, graphically interfaced code (for more information, see: www.ees1.lanl.gov/Wohletz/Heat.htm). With a grid space of 200 m and a top level of the pluton at 1.8 km (Hoersch, 1979) the model was run with the following parameters: surface temperature 25°C (estimated), magma temperature 800°C (Ferry, 1985; Holness, 1992), thermal gradient of 30°C/km (England,1994), density of the magma of 2580 kg/m³ (Gouly et al., 1996), density of country rock of 2720-2600 kg/m³ (Gouly et al., 1996), conductivity of the magma of 3.1 W/(mK) (defined by the Heat program) and a conductivity of the country rock of 3.0 W/(mK) (www.geo.tu-freiberg.de/tektono/interactivescripts/heatflow.htm). Because the present level of erosion is unknown the model was carried out at depths of 2.0 km , 2.4 km and 3.2 km.

The time-temperature paths for three different distances from the contact (directly at the contact with the intrusion at a distance of 200 m and a distance of 1000 m) and three different depth-levels (2.0 km, 2.4 km and 3.2 km) are derived from 19 vertical thermal profiles produced by the HEAT program (Fig. 2.9). For the kinetic process of pyrrhotite formation

during contact metamorphism, the temperature and the duration of the metamorphism are important. This means, that the amount of pyrrhotite produced under ideal conditions (presence of magnetite, pyrite, carbon and fluids) is equivalent to integral over the time-temperature path in the pyrrhotite window (200°C - 440°C). For a better comparison of the results, the maximal value reached for 3.2 km depth of intrusion at a distance of 200m is used for normalisation (100% of the relative potential of pyrrhotite growth, see Table 2). It becomes obvious that distance and depth both play an important role in pyrrhotite production. Only the assumption of an erosion of more than 2 km would allow the production of pyrrhotite at distances greater than 1000 m.

To acquire a full TRM metamorphic temperatures have to be above the Curie temperature of pyrrhotite ($T_{c,po}$). In the model, such temperatures are reached at distances < 200 m to the contact and an intrusion depth of more than 2.4 km. As peak temperatures increase with increasing depths of the intrusion it becomes clear that $T_{c,po}$ can also be reached to a minor extent beyond 200 m.

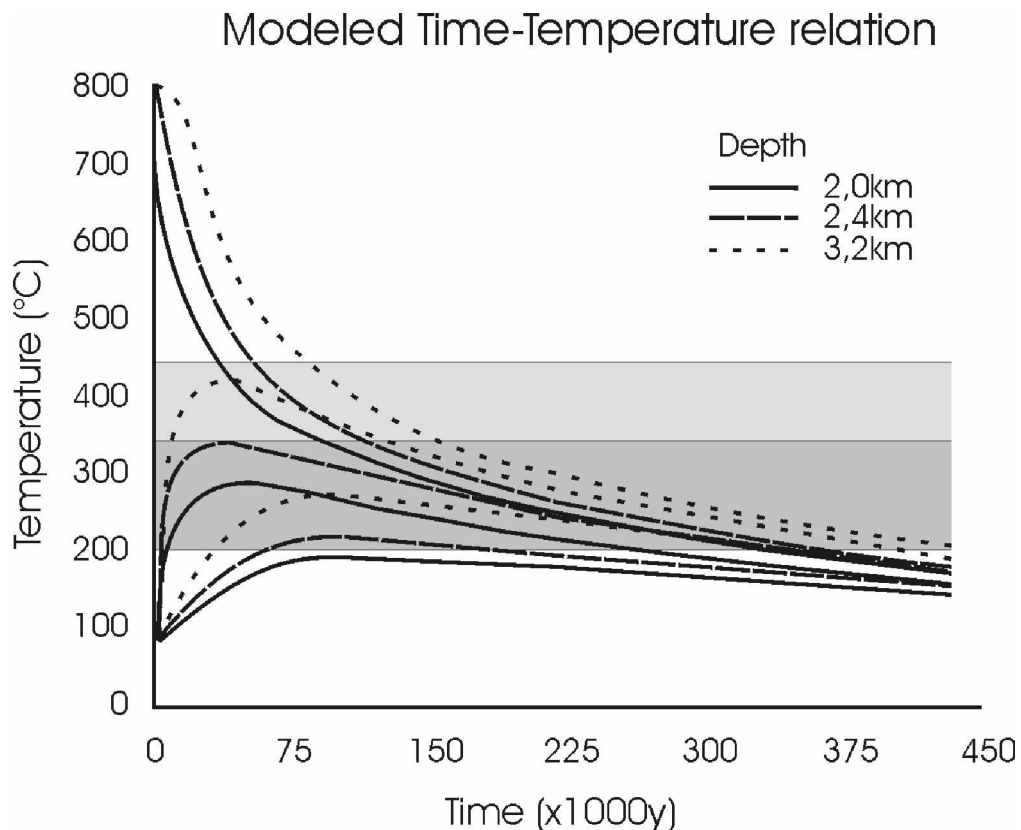


Figure 2.9: Time temperature relation for different depths and positions: in the centre the intrusion (upper curves), in a distance of 200 m from the contact (middle curves) and in a distance of 1000 m from the contact (lower curves). The gray boxes marks the pyrrhotite window (Schill et al., 2002). Lighter gray stands for the temperatures above the Curie temperature of pyrrhotite (where a full TRM is acquired).

Directional behaviour:

The directional analysis of the Manaslu samples of the southern profile is hampered by their low intensities. As a consequence only 10 out of 40 measured samples gave reasonable results. In general, pyrrhotite-dominated samples yield the same general direction, although the blocking temperature spectra are very different. In samples where magnetite is present the pyrrhotite component is generally subordinated as a viscous remanent magnetisation .

Some of the pyrrhotite bearing samples from both profiles contain multiple, partly antiparallel components (Fig. 2.10). Although such features are not reproducible on a site level due to the different magnetic mineralogy or/and blocking temperature spectra of pyrrhotite, they can stand for different directions of the EMF recorded during contact metamorphic cooling.

A conglomerate test for the samples at Isle of Skye (Site C) and a fold test for the Elba samples (Wehland et al., in prep.) indicate that the NRM is a TRM induced by the adjacent intrusion (positive contact test). In selected samples from Isle of Skye and from Elba the NRM in the pyrrhotite range consists of two almost antiparallel components. For the Isle of Skye sample, this two component NRM could be the result of a second heating of the rocks after a reversal of the EMF. This assumption is likely, because larger igneous bodies are formed by multiple magma injection - a process which spans over a certain period of time. Moreover, dyke intrusion could also lead in parts to a reheating of the contact-metamorphic rocks. At central Elba, the sills show no visible sign of multiple magma injections. Moreover, the good recording quality of these samples (mainly SD particles) would cause a sharp peak, if the low temperature component was recorded during a second heating. The broad transition (about 40°C) between the two components indicates that the TRM was recorded during one cooling event. In this case the two components envelope a reversal of the Earth magnetic field. A detailed analysis of this record in terms of paleointensity and directional behaviour of the individual pTRMs will be given in a companion paper (Wehland et al., in prep.).

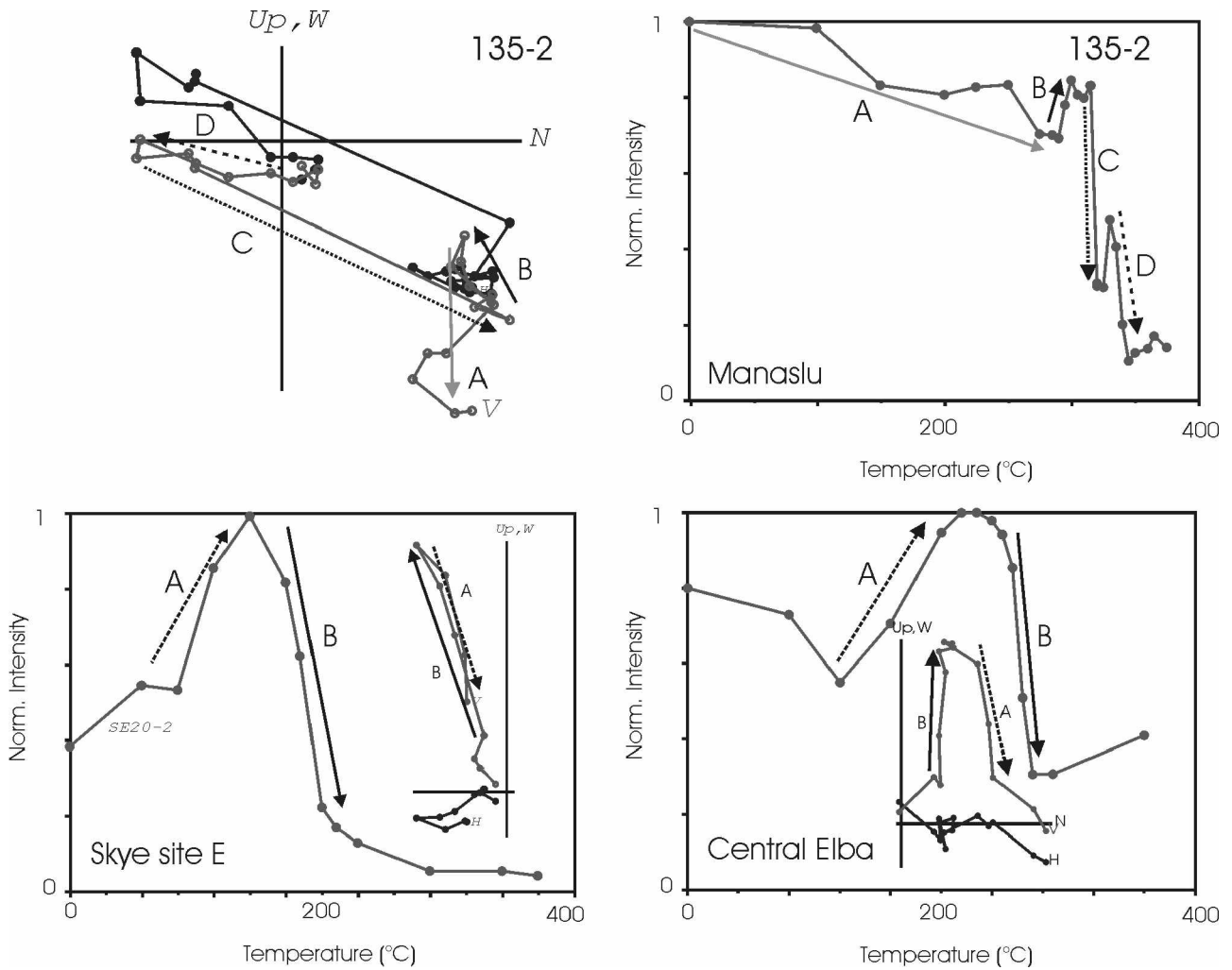


Figure 2.10: Examples of pyrrhotite bearing sample carrying different, partly antiparallel components.

2.5 Discussion:

The formation of pyrrhotite in contact-metamorphic limestones depends on both the metamorphic temperature and the composition and amount of the metamorphic fluids. Contact metamorphic aureoles, therefore, envelope a threefold zonation:

Contact Zone: In direct vicinity of the contact, the rocks were exposed to larger amount of metamorphic fluids as indicated by nearly pure marble. This is supported by low values of magnetic susceptibility, as most of the pre-existing sulphides will be dissolved. The existence of hematite and magnetite stand for higher $f(O_2)$ and the absence of carbon as a sink of oxygen. Consequently, most of the iron will be hosted in hematite or pyrite, as pyrrhotite is

unstable under such conditions (Hall, 1986). Depending on the size of the intrusion this contact zone extends from several meters (Elba) up to some ~400-500 m (Manaslu).

Transitional Zone: High pyrrhotite content, high magnetic susceptibility and peak temperatures adequate to record a full TRM (320°C) mark the transitional zone. According to thermal modelling, this isotherm extends up to a distance of about 500 m. These values are only indicative as they depend strongly on the size and depth of the intrusion. Using a one dimensional model of 500 m thickness, the extension of this zone reaches ~150 m (Wehland et al., in prep.). For large intrusions like the Manaslu granite or the Western Red Hill (Isle of Skye), thermal modelling will consequently give much greater distances. Nevertheless, modelling of bigger intrusive bodies can give arbitrary results as multiple phases of magmatism and uncertainties in their geometry lead to unclear starting conditions. Most of the Thellier-type experiments were performed on rocks from such sites as with further distance the magnetite component starts to play an important role.

Marginal Zone: Decreasing values of magnetic susceptibility and a substantial lowering of the pyrrhotite/magnetite ratio is indicative for the marginal zone of contact metamorphic influence. In general, peak metamorphic temperature at this zone will be below $T_{c,po}$, which excludes the acquisition of a full TRM. Consequently, the occurrence of a pyrrhotite component up to $T_{c,po}$ can either be interpreted as a CRM or an earlier component. Multicomponent remanences in such location can therefore only be explained by reheating through metamorphic fluids, dykes (Isle of Skye, site E) or younger thermal events (pulses of magmatism in the Manaslu area).

A direct comparison between the spatial distribution of secondary grown pyrrhotite with the prediction derived from thermal modelling will be difficult. Although the amount of pyrrhotite in the field is constantly decreasing with distance to the pluton it still has a relatively high proportion (60%) at 1500m (at Profile B, Isle of Skye) from the contact. The potential for the formation of pyrrhotite as derived from the thermal model at such distances can only be reached, if the depth of the intrusion is relatively deep or the size of the intrusion is larger than the one in the model. For both the geological evidence is missing. Woods et al. (2000) explained a remagnetisation by the occurrence of pervasive diagenetic fluids, a mechanism which could be enhanced by the intrusion of late to post metamorphic dykes.

Generally it can be assumed that some pyrrhotite has already grown before the contact metamorphic event. This is possible as the temperatures during burial metamorphism can be high enough for the formation of pyrrhotite (Gillett, 2003). As no sample with confirmed initial magnetic mineralogy could be taken the existence of a former metamorphic overprint as in the samples of the Tethyan Himalayan cannot be excluded.

The impact of fluids on pre-existing pyrrhotite can be seen in the Manaslu samples, where a restricted blocking temperature spectrum of SD particles coexists with samples of broader spectra. Such restricted spectra are unlikely to be formed during in situ growth (Wehland et al., *subm.*) or by precipitation from a metamorphic fluid, therefore, it is assumed that the smaller particles of the initial spectra are dissolved during contact metamorphism (Ferry, 1981).

2.6 Conclusions:

Regarding the formation of pyrrhotite contact, metamorphic aureoles can be grouped into three zones: A contact zone of partly oxidising conditions indicated by the existence of hematite and magnetite; a transitional zone with predominantly pyrrhotite and temperatures above $T_{c,po}$, and a marginal zone of coexisting pyrrhotite and magnetite and temperatures below $T_{c,po}$. In the light of successive pTRM recording the transitional zone is the adequate sampling target, as pyrrhotite is the dominant phase and temperatures were above $T_{c,po}$. The recording quality in samples from transitional zones of different locations varies significantly, possibly due to the amount of fluids involved. At places where fluid circulation was low, pyrrhotite exists in a suitable form to record successive pTRMs appropriate for studies of the EMF variations.

Such a scenario could be found in the samples from central Elba, where the recording qualities in terms of pTRM acquisition and magnetic mineralogy allow the recording of successive pTRMs during cooling. If a simple cooling history is assumed, the two component record of the NRM with the broad transition in between could be regarded as a continuous record of the EMF. A detailed analysis of this site in terms of paleointensity determination, remanence acquisition, thermal modelling and the absence of CRM will be given in a companion paper (Wehland et al., *subm.*).

Table 2.1: Results from the Thellier tests on laboratory TRMs

Location	Field	Std.-dev.	T _{Min}	T _{Max}	N	MAD	Class	Δmag	Δang
<i>SkyeB</i>	96,14	13,89	20	330	9	1,91	B	5,50	2,69
<i>SkyeB</i>	88,98	6,36	20	330	8	1,64	B	11,10	3,13
<i>SkyeB</i>	71,93	4,23	20	330	9	0,79	C	9,74	2,28
<i>SkyeA</i>	60,20	5,78	20	330	9	0,99	C	18,90	2,47
<i>SkyeA</i>	Not successful - possible self reversal process								
<i>SkyeA</i>	Not successful - possible self reversal process								
<i>ManaNorth</i>	82,65	4,38	200	320	6	0,60	A	0,67	0,62
<i>ManaNorth</i>	108,20	15,00	200	333	7	0,33	B	3,47	0,39
<i>ManaNorth</i>	103,21	1,99	200	333	5	0,18	B	0,67	0,41
<i>ManaNorth</i>	131,61	9,69	250	333	6	1,43	C	6,39	3,66
<i>ManaNorth</i>	141,47	8,85	250	333	6	2,73	C	4,67	5,43
<i>ManaSouth</i>	Not successful – too low intensities								
<i>Elba</i>	89,79	2,67	20	330	9	0,81	A	1,31	1,50
<i>Elba</i>	91,91	4,25	20	330	9	0,99	A	1,79	1,67
<i>Elba</i>	96,08	6,34	20	290	6	0,93	A	3,99	2,24
<i>Elba</i>	89,41	2,96	20	290	6	0,29	A	2,72	1,05
<i>Elba</i>	89,88	5,35	20	330	9	1,23	A	2,98	2,52
<i>Elba</i>	84,01	3,28	20	305	7	1,50	B	5,29	2,51
<i>Elba</i>	105,91	15,23	20	290	6	0,68	B	2,85	1,30
<i>Elba</i>	94,13	10,67	20	290	6	0,50	B	4,46	1,21
<i>Elba</i>	144,09	7,23	20	330	5	0,93	C	8,90	1,37
<i>Elba</i>	134,39	17,17	20	290	6	1,31	C	5,80	2,43
<i>Elba</i>	219,33	38,85	20	330	9	1,53	C	10,90	1,94
<i>Elba</i>	98,04	12,18	20	290	6	1,09	C	6,16	2,17

Table 2.1: Benchmarks of the thermal modeling. T_{min,po} and T_{max,po} are the lower and upper limit of the pyrrhotite window.

Table 2.2: Results from thermal modelling

Depth (km)	Initial temperature at depth (°C)	Distance to the contact (m)	Maximum temperature T_{max} (°C)	T_{max} reached after time of intrusion (ka)	Duration in pyrrhotite window (ka)	$T_{min,po}$ in the pyrrhotite window reached at (ka)	$T_{max,po}$ in the pyrrhotite window reached at (ka)	Cooling time in pyrrhotite window (ka)	Relative potential of pyrrhotite growth
		1000	190	110	none	none	none	none	0%
2	60	200	280	60	245	5 and 250	none	170	25%
		0 (centre)	800	initial age	230	310	80	230	-
2,4	72	1000	215	110	160	60 and 220	none	70	4%
		200	345	30	327	3 and 330	none	300	56%
3,2	96	0 (centre)	800	initial age	250	350	100	250	-
		1000	270	110	360	30 and 390	none	240	36%
3,2	96	200	420	30	428	2 and 430	10 and 100	390	100%
		0 (centre)	800	initial age	320	435	155	320	-

Table 2.2: Recording potential tested by Thellier type experiments on a laboratory TRM (90 μ T): Field is the calculated field strength derived from the experiments; Std.-dev its standard deviation. T_{Min} and T_{Max} are the lower and upper temperature step, N the number of temperature steps used for field calculation. MAD is the mean angular deviation of the TRM direction. Class is the classification as mentioned in the text. Δmag and Δang are the maximal deviations from the intensity (MD checks) and the direction for an individual temperature step.

2.7 References:

- Appel, E., Patzelt, A., and Chocker, C., 1995. Secondary palaeoremanences of the Tethyan Sedimentary Series of the Manang area (north central Nepal). *Geophys. J. Int.*, 104: 255-266.
- Bell, B.R., and Harris, J.W., 1986. An excursion guide to the geology of the Isle of Skye. Geol. Soc., Glasgow.
- Bell, B. R., and Jolley, D. W., 1997. Applications of palynological data to the chronology of the Palaeogene lava fields of the British Province: implications for magmatic stratigraphy. *J. Geol. Soc.* London, 154: 701-708.
- Bouillin, J.P., Poupeau, G., and Sabh, N., 1994. Etude thermochronologique de la dénudation du pluton du Mte. Capanne (Isle d'Elbe, Italie) par les traces de fission. *Bull. Soc. Géol. France*, 165: 19-25
- Butler, R. W. H., and Hutton, D. H. W., 1994. Basin structure and Tertiary magmatism on Skye, NW Scotland. *J. Geol. Soc. London*, 151 (6): 931-944.
- Carpenter, R.H., 1974. Pyrrhotite isograd in the SE Tennessee and SW North Carolina, *Geol. Soc. Am. Bull.*, 85: 451-456.
- Crouzet, C., Menard, G., and Rochette, P. 1999. High-precision three-dimensional paleothermometry derived from from paleomagnetic data in an Alpine metamorphic unit. *Geology*, 27: 503-506.
- Crouzet, C., Stang, H., Appel, E., Schill, E., and Gautam, P., 2001. Detailed analysis of successive pTRMs carried by pyrrhotite in Himalayan metacarbonates: An example from Hidden Valley, Central Nepal, *Geophys. J. Int.*, 146: 607-618.
- Coe, R.S., 1967. Paleointensity of the Earth's magnetic field determined from tertiary and quaternary rocks. *Geophys. Res.*, 72: 3247-3262.
- Daniel, J.-M., and Jolivet, L., 1995. Detachment faults and pluton emplacement: Elba Island (Tyrrhenian Sea). *Bull. Soc. Géol. France*, 166 (4): 341-354.
- Dickin, A. P., 1981. Hydrothermal fluid pathways at the contact of the Beinn an Dubhaich epigranite, Isle of Skye. *Scottish J. Geol.*, 19 (2): 235-242.
- England, R. W., 1994. The structure of the Skye lava field. *Scottish J. Geol.*, 30 (1): 33-37.
- Ferry, J. M., 1985. Hydrothermal alteration of Tertiary igneous rocks from the Isle of Skye, northwest Scotland: II. Granites. *Contrib. Min. Petrol.*, 91: 283-304.
- Fuchs, G., and Paudel, L.P., 1998. Note on the Tethyan Sedimentary Series of the Manaslu region (Northern Nepal). *Jahrb. Geol. Bundesanstalt*, 141: 45-50.
- Gillett, S.L., 2003. Paleomagnetism of the Notch Peak metamorphic aureole, revisited: Pyrrhotite from magnetite + pyrite under submetamorphic conditions. *J. Geophys. Res.*, 108 (B9), 2446, doi: 10.1029/2002JB002386
- Guillot, S., Hodges, K.V., Le Fort, P., and Pêcher, A., 1994. New constraints on the age of the Manaslu leucogranite: Evidence for episodic tectonic denudation in the central Himalayas. *Ecology*, 22: 559-562.

- Gouly, N. R., Darton, C. E., Dent, A. E., and Richardson, K. R., 1996. Geophysical investigation of the Beinn an Dubhaich Granite, Skye. *Geol. Mag.*, 133 (2): 171-176.
- Hall, A. J., 1986. Pyrite-pyrrhotite redox reactions in nature. *Mineral. Mag.*, 50: 223-229.
- Harris, A. L., 1985. The nature and timing of orogenic activity in the Caledonian rocks of the British Isles. *Geol. Soc. London, Memoir*, 9: 1-53.
- Harrison, T.M., Rove, M., McKeegan, K.D., Coath, C.D., Lovera, O.M., and LeFort, P., 1999. Origin and episodic emplacement of the Manaslu Intrusive complex, Central Himalaya, *J. Petrol.*, 40: 3-19.
- Hoersch, A. L., 1979. General structure of the Skye Tertiary igneous complex and detailde structure of the Beinn an Dubhaich Granite from magnetic evidence. *Scottish J. Geol.*, 15(3): 231-245.
- Hoersch, A. L., 1981. Progressive metamorphism of the chert-bearing Durness limestone in the Beinn an Dubhaich aureole, Isle of Skye, Scotland: A reexamination. *Am. Min.*, 66: 491-506.
- Holness, M. B., Bickle, M. J., and Harte, B., 1989. Short paper: Textures of forsterite-calcite marbles from the Beinn an Dubhaich aureole, Skye, and implications for the structure of metamorphic porosity. *J. Geol. Soc., London*, 146: 917-920.
- Holness, M. B., 1992. Metamorphism and fluid infiltration of the calc-silicate aureole of the Beinn an Dubhaich granite, Skye. *J. Petrol.*, 33(6): 1261-1293.
- Holness, M. B., and Fallick, A.E., 1997. Fluid flow paths and mechanisms of fluid infiltration in carbonates during contact metamorphism: the Beinn an Dubhaich aureole, Skye. *J. meta. Petrol.*, 15(1): 59-70.
- Juteau, M., Michard, A., Zimmermann, J.L., and Albarede, F., 1984. Isotopic heterogeneities in the granite intrusion of Mte. Capanne (Elba island, Italy) and dating concepts. *J. Petrol.*, 25: 532-545.
- Keating, G.N., Geissman, J.W., and Zyvoloski, G.A., 2002. Multiphase modeling of contact metamorphic systems and applications to transitional geomagnetic fields. *Earth Planet. Sci. Lett.*, 198: 429-448.
- Lambert, I. B., 1973. Post-depositional availability of sulphur and metals and formation of secondary textures and structures in stratiform sedimentary sulphide deposits. *J. Geol. Soc. Australia*, 20: 205-215.
- Lagarde, J., Brun, J.P., and Gapais, D., 1990. Formation des plutons granitiques par injections et expansion latérale dans leur site de mis en place: une alternative a duapirisme et domaine épizonal, *C.R. acad. Sci. Paris*, 310 (2): 1109-1114.
- Leonhardt, R., Hufenbacher, F., Heider, F., and Soffel, H., C., 2000. High absolute paleointensity during a mid Miocene excursion of the Earth's magnetic field, *Earth Planet. Sci. Lett.*, 184: 141-154.
- Longman, C. D., and Coward, M. P., 1979. Deformation around the Beinn an Dubhaich granite, Skye. *Scottish J. Geol.*, 15 (4): 301-311.
- Ménard, G., and Rochette, P., 1992. Utilisation de réaimanation postmétamorphique pour une étude de l'évolution tectonique et thermique tardive dans les Alpes occidentales (France). *Bull. Soc. Géol. France*, 163 (4): 381-392.

- McClelland, E., and Briden, J.C., 1996. An improved methodology of Thellier-type paleointensity determination in igneous rocks and its usefulness for verifying primary thermoremanences, *J. Geophys. Res.*, 101: 21995-22013.
- Nagata, T., Fisher, R.M., and Momose, K., 1963. Secular variations of the geomagnetic total force during the last 5000 yrs. *J. Geophys. Res.*, 68: 5277-5281.
- O'Reilly, W., Hoffmann, V., Chouker, A.C., Soffel H.C., and Menyeh, A., 2000. Magnetic properties of magnetic analogues of pyrrhotite ore in the grain size range 1-24 μ m, *Geophys. J. Int.*, 142: 669-683.
- Poulson, S., R., and Ohmoto, H., 1989. Devolatilization equilibria in graphite-pyrite-pyrrhotite bearing pelites with application to magma-pelite interaction, *Contrib. Minerl. Petrol.*, 101: 418-425.
- Rochette, P., 1987. Metamorphic control of the magnetic mineralogy of black shales in the Swiss Alps: toward the use of "magnetic isogrades". *Earth Planet. Sci. Lett.*, 84: 446-456.
- Schill, E., Appel, E., Gautam, P., and Singh, V.K., 1998. Preliminary palaeomagnetic results of medium grade carbonates from the Lesser Himalaya. *J. Nepal Geol. Soc.*, 18: 205-215.
- Schill, E., Appel, E., Gautam, P., and Dietrich, P., 2001. Thermo-tectonic history of the Tethyan Himalayas deduced from palaeomagnetic record of metacarbonates from Central Nepal (Shiar Khola), *J. Asian Earth Sci.*, 20 (3): 203-210.
- Schill, E., Appel, E., and Gautam, P., 2002. Towards pyrrhotite/magnetite geothermometry in low-grade metamorphic carbonates of the Tethyan Himalayas (Shiar Khola, Central Nepal). *J. Asian Earth Sci.*, 20: 195-201.
- Schill, E., Appel, E., Crouzet, C., Gautam, P., Wehland, F., and Staiger, M., inpress. Oroclinal bending and regional significant clockwise rotations of the Himalayan arc – constraints from secondary pyrrhotite remanences, *Geol. Soc. Am.*
- Tantrigoda, D. A., 1988. Interpretation of magnetic anomalies over the Skye Tertiary intrusive complex. *Scottish J. Geol.*, 24(3): 215-221.
- Trevisan, L., 1950. L'Elba orientale e la sua tettonica di scivolamento per gravità, 15. Università, Istituto di Geologia e Paleontologia. Memorie, Padua, pp.40.
- Venzlaff, V., and Waldeck, H., 1974. Geochemical Investigations on the Island of Elba: 2. Age Dating of Central and Western Elba Granites – A Comparison. *N. Jahrb. Min. Ab.*, 120 (3): 315-323.
- Wehland, F., Eibl, O., Braun, S., Alt-Epping, U., and Appel, E., subm. Pyrrhotite pTRM acquisition in metamorphic limestones in the light of microscopic observations. *Earth Planet. Sci. Lett.*, 2004a.
- Wehland, F., Stancu, A., Rochette, P., Dekkers M.J., and Appel, E., subm.. Experimental evaluation of magnetic interaction pyrrhotite bearing samples, *Earth Plan. Sci. Lett.*, 2004b.
- Wehland, F., Alt-Epping, U., and Appel, E., in prep. Continuous recording of an Earth magnetic field reversal. 2004
- Woods, S. D., Elmore, R. D., and Engel, M. H., 2000. The occurrence of pervasive chemical remanent magnetizations in sedimentary basins: implications for dating burial diagenetic events. *J. Geochem. Explor.*, 69-70: 381-385.

Experimental evaluation of magnetic interaction in pyrrhotite bearing samples

Abstract

Pyrrhotite bearing metamorphic limestones have recently experienced an increasing relevance in paleomagnetic research. Simple univectorial remanences document the metamorphic uplift whereas more complex multicomponent pTRMs may constrain its age. For a successful application of the latter, it is important to estimate the degree of magnetic interactions to ensure the additivity of individual pTRM segments. We therefore have subjected the sized dispersed suite (<5 to 250 μm) of TTE pyrrhotite to FORC analysis and compared the result with remanence based parameters like the ΔM or the irreversible susceptibility. This is used as a basis to evaluate the response of marly limestone samples from regionally metamorphic areas (Bourg d'Oisans, France) and contact-metamorphic aureoles (Elba, Italy; Skye, Scotland; Manaslu area, Nepal) to these techniques. The results show that the techniques is able to estimate the nature and – to a certain degree – the intensity of the magnetic interaction. The different dominant magnetic states of the assemblage can be unravelled as well. Based on the remanence measurements of the TTE samples, a relationship between grain-size and the irreversible susceptibility is established in order to estimate the mean grain-size fraction in natural particle distribution.

3.1 Introduction:

Secondary pyrrhotite is formed in low-grade metamorphic limestones at the expense of pyrite and magnetite within the 200-450°C temperature range (Lambert, 1973; Rochette, 1987; Schill et al., 2002). The need to investigate magnetic interactions in pyrrhotite bearing metamorphic limestones arose from the use of such rocks as recorder of Earth's Magnetic Field Reversals (Rochette and Menard, 1992; Crouzet et al., 1999; 2001 a,b). Independent partial thermoremanent magnetization (pTRM), i.e. identical blocking and unblocking spectra, are mandatory for such studies. Therefore, the samples should consist of a non-interacting single domain (SD)-particle assemblage (Thellier and Thellier, 1959). The tendency to crystallize mainly below the single domain threshold (< ~2 μm ; Soffel, 1977) favours the use of pyrrhotite as a pTRM recorder. Nevertheless, clustering of pyrrhotite grains, the presence of multidomain (MD) particles, or an incomplete metamorphic reaction can cause magnetic interaction during pTRM recording processes.

During the past, experimental investigation of magnetic interaction was hampered by the lack of fast and reliable experimental methods. For natural magnetite Dunlop (1972) concluded

that ratios of M_{rs}/M_s (saturation remanence/saturation magnetization) of 0.5 and higher are characteristic of non-interacting SD grains. This was supported by Davis and Evans (1976), who showed that this ratio can be lowered due to interaction. Cisowski (1981) used a plot of IRM_r vs. a.f. demagnetised SIRM (acquisition of isothermal remanent magnetisation vs. alternating field demagnetised saturation IRM), where non-interacting grains exhibit symmetrical curves. Other methods to examine magnetic interaction like the off-diagonal Preisach diagram for SD particle interaction (Daniel and Levine, 1960; Woodward and Della Torre, 1960) or the inverse anhysteretic susceptibility (Kneller, 1969; Veitch, 1990) as a measure for magnetic interaction were later on questioned by Dunlop et al. (1990). New input came from studies of magnetic recording media (Spratt et al., 1988; Fearon et al., 1990; Mayo et al., 1990a,b, 1991a,b) where mainly remanence measurements were used to study magnetic interaction. Petrovský et al. (1993) tried to transfer these ideas to natural systems concluding that, despite some promising results, more extensive studies are necessary to decisively delineate texture, concentration, and type of the magnetic carriers as function of the differential remanence behaviour. Nevertheless, the remanence based methods are useful to detect the degree and general character of magnetic interaction. The recently developed FORC (First Order Reversal Curves) diagram (Pike et al., 1999; Roberts et al., 2000) seems to be an appropriate technique to obtain information about switching fields and interactions in magnetic particle systems. For this study we applied the remanence based methods as well as the FORC method on artificial and natural pyrrhotite bearing samples.

3.2 Theory:

The problem of measuring magnetic interaction by a remanence based technique was first discussed by Wohlfarth (1958) who concluded that for a non-interacting uniaxial SD particle assemblage the relationship of the different normalized remanence acquisitions can be described by:

$$IRM_{dc}(H) = 1 - 2 * IRM_r(H), \quad (1)$$

where IRM_r and IRM_{dc} are the normalized remanences acquired from the virgin state and during dc backfield demagnetization of the SIRM, respectively. For MD particles this relationship is not valid as domain wall pinning and domain wall nucleation are not the same for the ascending and descending branch of the remanence curve.

By plotting IRM_r vs. IRM_{dc} (Henkel, 1964) the ideal case of non-interacting uniaxial SD-particles will lead to a straight line with a slope of -2. In 1990, Mayo et al., introduced the deviation from this line expressed by the differential remanence parameter (Speliotis et al., 1991) $\Delta M(H)$, a formulation that has been used since then

$$\Delta M(H) = IRM_{dc}(H) - (1 - 2 IRM_r(H)). \quad (2)$$

For a SD particles assemblage the resulting deviation is ascribed to many-body effects and generally indicates the presence of magnetic inter-particle interaction (Fearon et al., 1990; Mayo et al., 1991a,b). Positive values of ΔM are interpreted as a result of positive interaction, which tends to stabilize the magnetization, whereas a negative value would come from negative interaction yielding a net demagnetising effect (see Petrovský et al., 1993). Nevertheless, one has to take into account that results from MD particles can be congruent with results from SD particles. The differential susceptibility of the remanence χ_r and χ_{dc} can be calculated from IRM_r and IRM_{dc} curves as the first derivative $d(IRM)/dH$. The ratios of χ_r and χ_{dc} (here introduced as W parameter) should follow the Wohlfarth equation giving a value of two for a non-interacting case. The spectra of χ_r and χ_{dc} are quantified by the position of the maxima and the shape parameter FWHH (full-width-at-half-height). It is important here to note the dependence of IRM curves and related parameters on the initial magnetization state (Fearon et al., 1990; Heslop et al., in press). It is conventional to start from a three axial static a.f.-demagnetized state being the most reproducible one (Stancu et al., 2001 and references therein).

The FORC diagram is calculated from a set of partial hysteresis curves (see Mayergoyz, 1986). The measurement of a FORC starts with the saturation of the sample in a high positive field. The field is afterwards decreased to the reversed field H_a , and the FORC is the magnetization curve measured from H_a back to saturation. A set of FORCs is obtained by repeating this measurement for different values of H_a . At the applied field H_b on a FORC starting from H_a the magnetization is denoted as $M(H_a, H_b)$, where $H_b > H_a$. The FORC distribution $\rho(H_a, H_b)$ is then defined as the mixed second derivative:

$$\rho(H_a, H_b) \equiv - \frac{\partial^2 M(H_a, H_b)}{\partial H_a \partial H_b}, \quad (3)$$

where $\rho(H_a, H_b)$ is defined for $H_b > H_a$. It became convenient for plotting the FORC distribution to use the coordinate system $\{H_c=(H_b-H_a)/2, H_u = (H_a + H_b)/2\}$ instead of the original $\{H_a, H_b\}$. As $H_b > H_a$, $H_c > 0$, and the FORC diagram is plotted as a contour plot in the right-hand half plane with H_u and H_c as the vertical and horizontal axis, respectively. The H_c coordinate is referred to microcoercivity. Further details about the derivation of equation (3) and the change of the coordinates can be found in Pike et al. (1999).

Experimental results for monoclinic pyrrhotite gave a single domain threshold at around 1.5-2 μm (Soffel, 1977), a PSD range up to grains of 40 μm , and pure MD behaviour for grains larger 40 μm (Soffel, 1981). Dekkers et al. (1989) as well found a value for the SD threshold of 1-2 μm . Clark (1984) found a slightly higher value of about 3 μm for the single domain threshold.

3.3 Samples and methods:

The sized dispersed fractions of TTE pyrrhotite used in this study had already been subjected to different measurements in the past (Dekkers, 1988; Dekkers et al., 1989; Worm et al., 1993). The material was available as 7 mm cylindrical samples with distinct grain-size fractions of <5 μm , 5-10 μm , 10-15 μm , 15-20 μm , 20-25 μm , 25-30 μm , 30-40 μm , 40-55 μm , 55-75 μm , 75-100 μm , 100-150 μm and 150-250 μm . Material for preparing the samples was selected from a pyrometasomatic pyrrhotite-pyrite-chalcopyrite ore zone at Temperino (Tuscany, Italy). The pyrrhotite fractions contain equidimensional grains. Magnetite is absent in these rocks and the amount of intergrowths is rare. Sample preparation was performed in an inert atmosphere to prevent alteration. The resulting grain-size fractions were checked using transmitted and reflected light microscopy and X-ray diffraction; the grain-size ranges were controlled optically. Monoclinic pyrrhotite has been proven as the dominant magnetic phase; only in the smallest fraction traces of hexagonal pyrrhotite were identified. The grain-size fractions were homogeneously dispersed in an epoxy resin matrix with about 2% pyrrhotite by volume. For more details see Dekkers (1988a,b).

Natural samples were taken from contact-metamorphic limestones of the Isle of Skye, Scotland, the Manaslu area, Nepal (Schill et al., in press) and Elba Island, Italy. Also regional metamorphic limestones near Bourg d'Oisans, France (Crouzet et al., 1999) were selected for

the present study. The samples were cut in cubes or cylinders with an edge length or diameter of 10mm, respectively.

All samples were subjected to a.f.-demagnetization of 120 mT prior to any further treatment using an three axis static 2G600 a.f.-demagnetiser. A Micromag 3900 Vibrating Sample Magnetometer carried out all magnetization and remanence experiments and measurements. Generally, FORC diagrams are based on a set of 100 individuals FORCs with a smoothing factor (SF) of two, an average time of 0.25 s, zero waiting time and a saturation field of 700 mT. For weaker samples the average time was increased up to 5s on a set of not less than 80 FORCs. Due to smoothing not all values down to $H_c = 0$ can be plotted. For imparting high fields of 9T a MPM9 pulse magnetiser has been used.

3.4 Results and discussion:

Sized dispersed fractions:

FORC diagrams of all grain-size fractions are shown in Fig. 3.1. For the smaller grain-size fractions (<5 μm to 30-40 μm) the contours of the plot are generally closed indicating an SD to PSD behaviour. For the coarser fractions the open contour lines stand for their MD behaviour. With decreasing grain size the maximum of the distributions are shifted to higher coercivities with an increasing tendency to deviate from the horizontal line (Fig. 3.2). The deviation from the H_c -axis in combination with a negative slope of the line of contour elongation can be interpreted as a consequence of a positive mean interaction field (Roberts et al., 2000). The asymmetry in the diagrams with respect to the H_c -axis is most pronounced in the small grain-size fractions leading to sharp negative (white) regions in the lower half. These negative regions are always placed at higher coercivities than the peak and are decreasing with increasing grain-size. The negative regions become negligible for coarser grain-sizes (Fig 3.1) Comparing the asymmetries in the FORC diagrams with those obtained by micromagnetic and phenomenological (Preisach-type) modelling of interacting ferromagnetic SD particles systems (Stancu et al., 2003) underlines the presence of positive mean interaction fields.

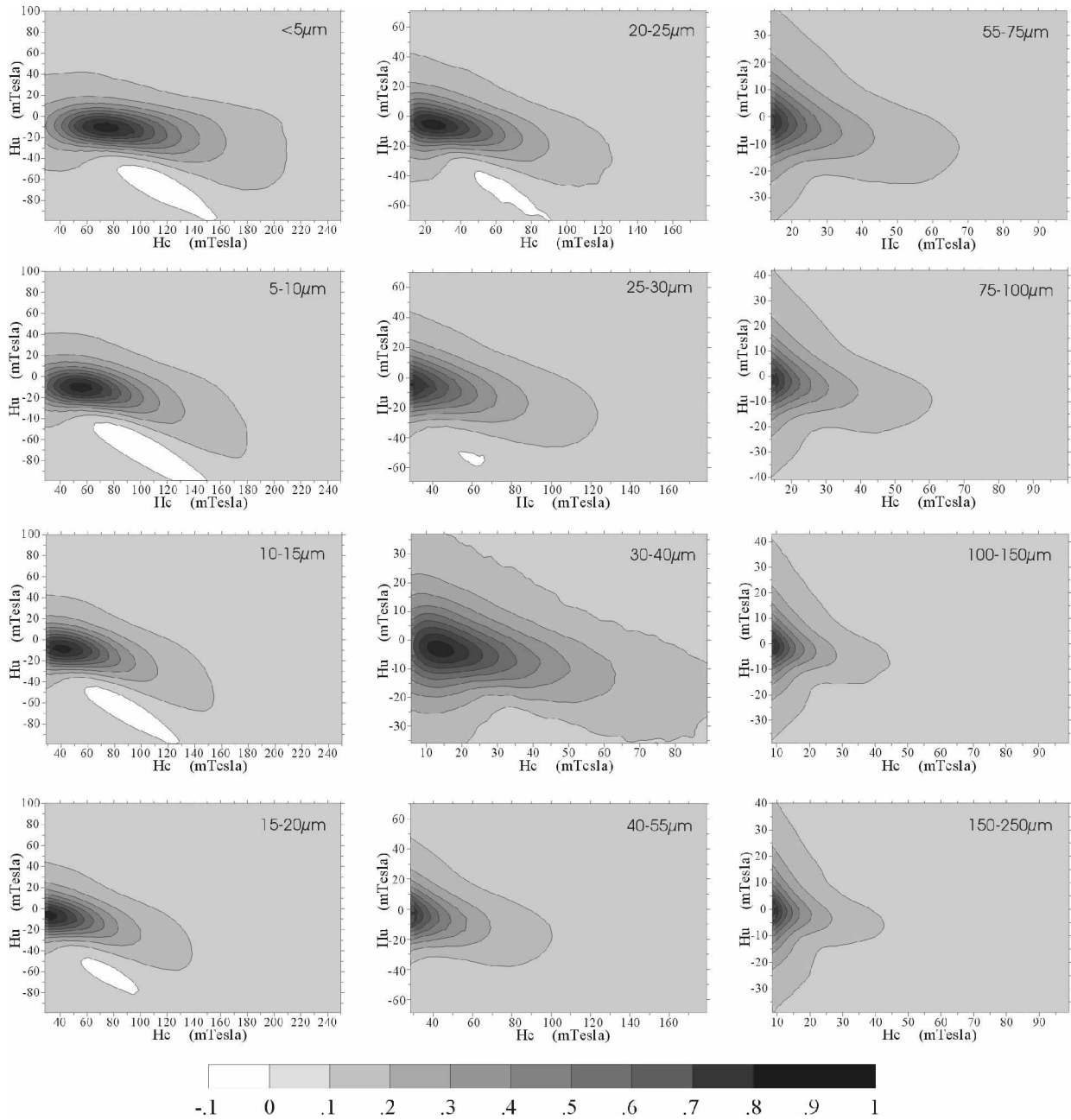


Figure 3.1: FORC diagrams of all grain-size fractions from the TTE series (M. Dekkers, 1988). The samples show a decreasing asymmetry regarding their horizontal axis and a vanishing of the negative area with an increasing grain-size. Note that the coordinates are different for the sake of illustration.

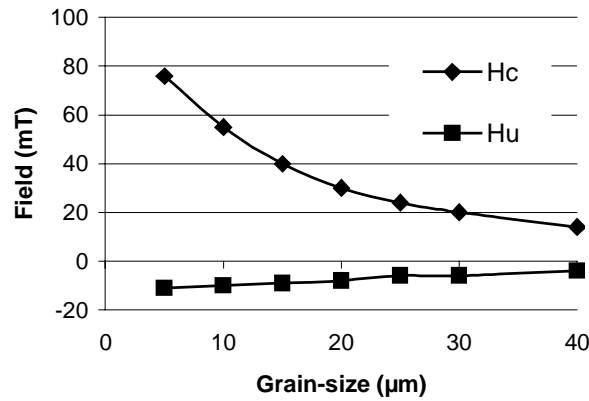


Figure 3.2: Position of the distribution maxima in the FORC diagram. The coercivity (H_c) shows a decrease with increasing grain size. The deviation from the horizontal line (H_u) shows a more linear dependence.

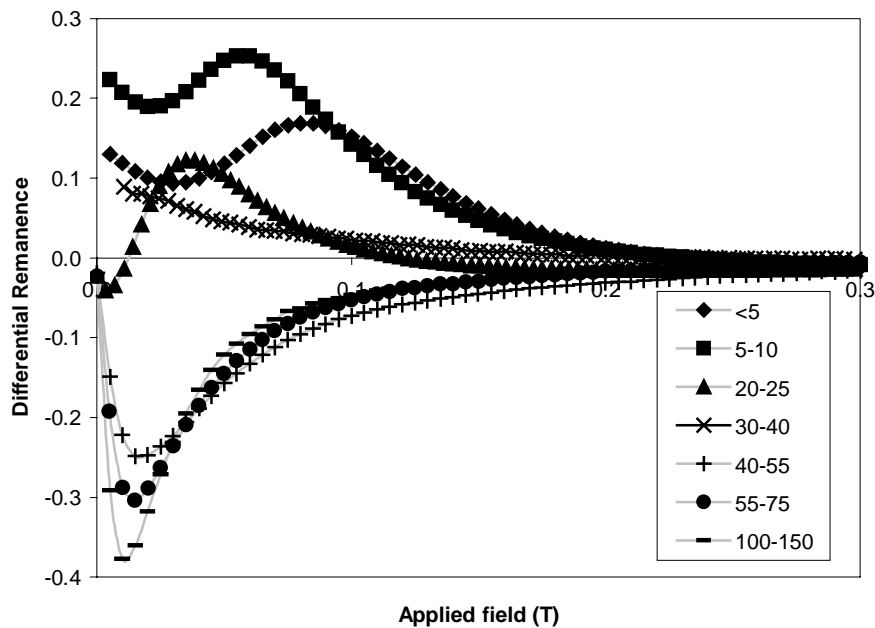


Figure 3.3: Differential remanence parameter ΔM (see text for explanation) as a function of the applied field for selected grain-size fractions (in μm). A clear change in the type of interaction can be seen at the 30-40 μm fraction (upper limit of the PSD range).

The differential remanence parameter ΔM (Fig. 3.3) for the smaller grain-size fractions is positive at lower fields and decreases to a small negative value at fields higher 0.3 T. A pattern like this is characteristic for a system of SD particles with statistical and positive mean

field interaction fields. The positive starting value of the curves (implying local a minimum) is a consequence of the incomplete a.f. demagnetisation; the remanence carried by the high coercive component was not affected (cf. Fig. 3.4). In general, lower coercivities are observed with increasing particle size. In the coarser grain-size fractions (40-55 μm and greater) the ΔMs are negative from the beginning with a minimum at low fields that is most pronounced in the coarsest fraction. The 30-40 μm set, marking the upper limit of the PSD range (Soffel, 1981), has an intermediate shape and it is still positive at lower fields, but without a local minimum. The initial negative values can be linked to the magnetization process related with domain wall motion and, therefore, is expected for MD samples.

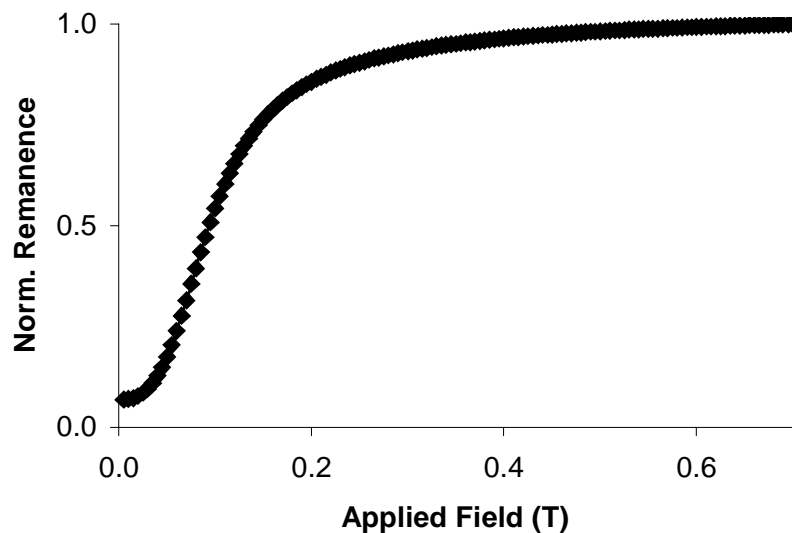


Figure 3.4: Normalized IRM acquisition curve for the $<5 \mu\text{m}$ fraction. The incomplete a.f. demagnetisation causes a residual remanence at zero fields.

The change in shape of the ΔM -plots between the 30-40 μm and 40-55 μm range, which may be interpreted as the transition from a dominant SD/PSD towards a dominant MD behaviour, is more pronounced than in the FORC diagrams, where a gradual opening of the individual contour lines marks the transition.

The appearance of a positive interaction field using the ΔM method is well pronounced in the smaller fractions and strongest in sample 5-10 μm . The lower Ms in the $<5 \mu\text{m}$ fraction is in coincidence with Dekkers (1988b) and can be related to the continual existence of micro twins as a consequence of substantial hammering during sample preparation. Differences

appear in the interaction pattern of the coarser samples, where in the FORC diagram – despite a dominant MD behaviour – the positive mean interaction field can still be detected.

The general trend mentioned above can be made clearer by the comparison of the peak position for χ_r and χ_{dc} . This occurs at higher fields for IRM_{dc} for the smaller fractions as a result of a stabilizing mean interaction field, and changes to lower fields for the coarser fractions due to the destabilizing mean interaction field as expected for multidomain particles (Fig. 3.5). The relationship of the intensities of the calculated susceptibility curves (Table 3.1)

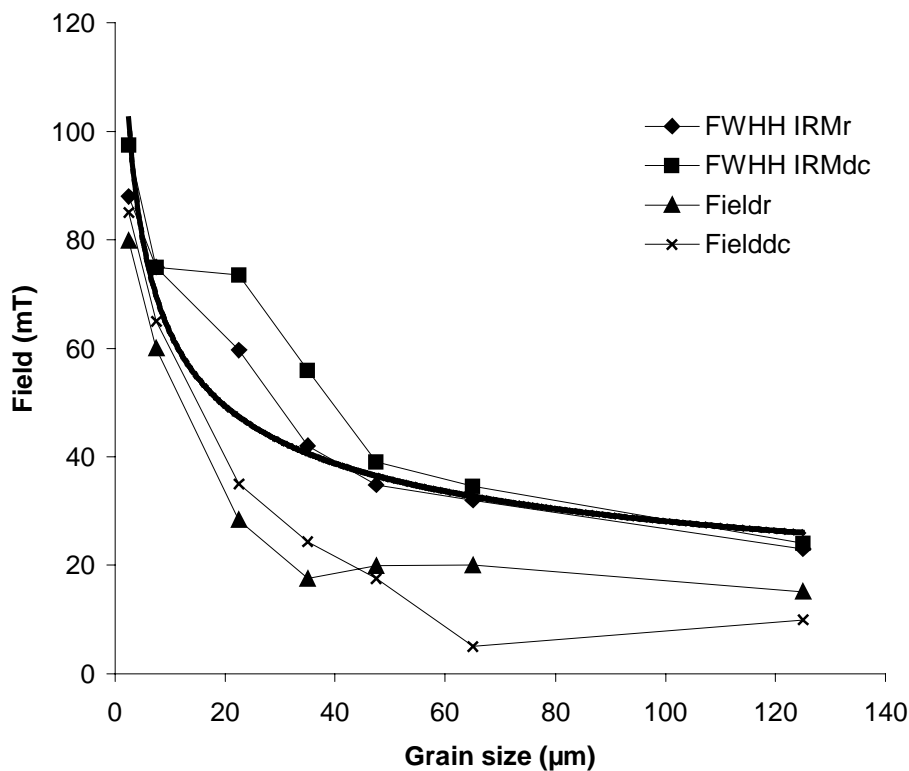


Figure 3.5: FWHH and peak position ($Field_r$ and $Field_{dc}$) of the calculated differential susceptibility. The thick black line is the exponentially fitted trendline for the FWHH IRM_r curves.

is less clear in this matter. After equation (2), $W = 2$ is expected for non-interacting SD particles. In our case the values of the smaller fractions (up to 30-40 μm) are below two with a minimum in the 20-25 μm fraction. For the coarser fractions (40-50 μm and higher) the ratio is greater than 2 due to the demagnetizing effect of the interaction field. In contrast, the FWHH parameter (full width at half height), which can be seen as a measure of the switching field distribution (SFD), is not influenced by the above mentioned transition. The value and difference between the FWHH derived from χ_r and χ_{dc} are decreasing with increasing grain-size related to a narrowing of the SFD.

Due to its direct correlation with the grain-size fractions and independence of the character of the mean interaction field, the FWHH can be used as measure for the grain-size fraction in the natural systems. Derived from χ_r the relationship between FWHH and mean value of the grain-size is expressed by

$$\text{Size \{in } \mu\text{m}\} = 629974 * \text{FWHH \{in mT}\}^{-2.6524} \quad (4)$$

with $R^2 = 0.9296$. The calculated values for the TTE samples are listed in Table 3.1. A function derived from χ_{dc} was abandoned due to the higher noise of the data. The influence of the character of the mean interaction fields on the position of the susceptibility peaks (Field_r in Fig.5) hampers the use of this parameter as an indicator for a mean grain-size. We tried to overcome this problem by taking a mean value ($\text{Field}_{\text{mean}}$) of both peak positions from the IRM_r and IRM_{dc} . The resulting relationship is expressed as

$$\text{Size \{in } \mu\text{m}\} = 7902.7 * \text{Field}_{\text{mean}} \{\text{in mT}\}^{-1.7531} \quad (5)$$

with $R^2 = 0.9581$. An advantage in the use of the peak position is its independence of the shape of the particle distribution. As in the hypothetical case of grains with only one specific coercivity a FWHH derived function does not work, the peak position is still a direct measure of the grain-size. But in general, both for natural and artificial samples this case remains hypothetical.

The results from FORC diagrams and remanence measurements in terms of the domain state are in good agreement with observations described in the literature (Roberts et al., 2000; Pike et al., 1999, 2001; Stancu et al., 2001, 2003). For both techniques, the SD to PSD transition is more gradual whereas the change to the MD behaviour is quite pronounced as a consequence of the change in the mean field interaction fields during this transition. Experiments with high fields (9 Tesla) imparted parallel or perpendicular to the applied field did not change the shape and dimension of the FORC distributions. This could mean that FORC diagrams for this kind of samples are not sensitive for the magnetic history of the sample.

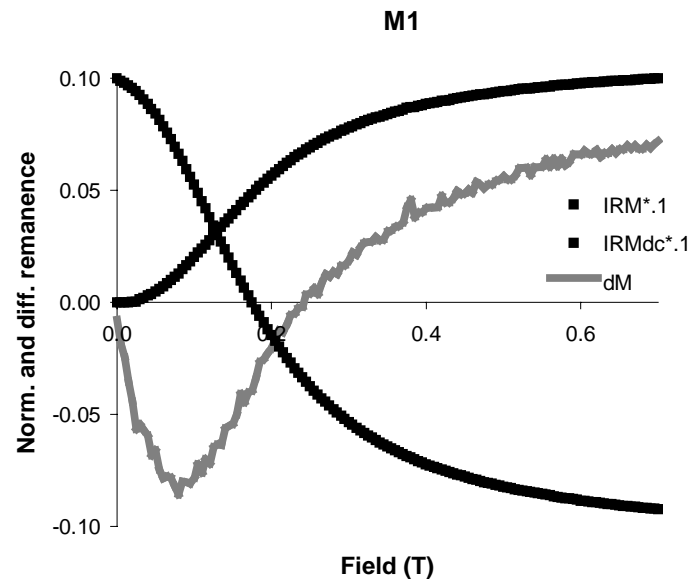


Figure 3.6: IRM, IRM_{dc} and ΔM (grey) for the M1 sample. The IRM-values are reduced by .1 for a better illustration.

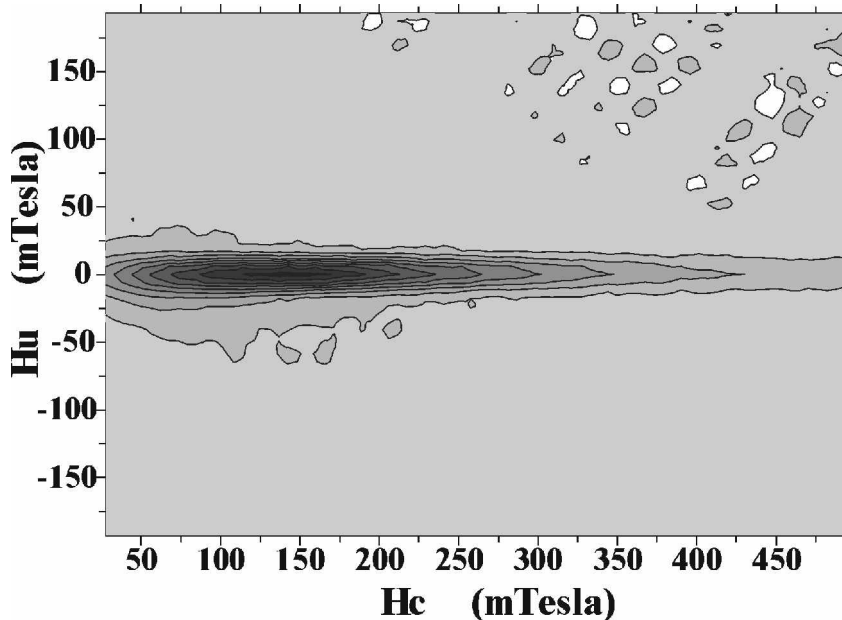


Figure 3.7: FORC diagram of sample M1 ($SF=2$, $t_{avr}=0.25s$, 100 FORCs). The distribution shows a clear SD particle assemblage. Interaction seems to be absent.

Natural samples:

One sample (M1) from the Manaslu area (Nepal) containing only pyrrhotite (proved by thermal demagnetisation of the IRM on a twin sample) was selected. The IRM acquisition curve of M1 is not entirely saturated in 0.7 Tesla (Fig. 3.6) indicating a high coercive part of the pyrrhotite particle distribution. The derived ΔM parameter starts with low negative values changing to positive values at higher coercivities. With a maximal deviation from the Henkel plot of -0.086 magnetic interaction is nearly absent in this sample (Fig. 3.6.). This is

supported by $W = 2.00$. The calculated mean of the grain-size fraction after equation (3) is around $1\mu\text{m}$ (Tab. 3.1) and confirms clear SD behaviour.

In the FORC diagram (Fig.3.7) the distribution is well elongated with a negligible vertical spread, closed contours and no obvious deviation from the horizontal line. This shape stands for a non-interacting SD particle system with high coercivities peak of the distribution at $H_c = 125\text{ mT}$. The extension over the right border is due to the non-saturated parts in the particle system. The result from the FORC analysis coincides with the observation from the remanence measurements.

Similar FORC diagrams are obtained from samples of the western Alps (Fig. 3.8). For the representative sample F9 the shape of the distribution is an elongated one with a maximal coercivity of $H_c \sim 400\text{ mT}$. The contour lines are closed indicating SD behaviour of the assemblage. The enhanced vertical spread ($H_u = 20\text{ mT}$) is due to the higher smoothing factor ($SF = 3$). The FORC diagrams indicate a broad SD particle assemblage and underline the good recording qualities for a pTRM record in samples taken at Bourg d'Oisans as shown by Crouzet et al. (1999).

In the Elba (E) samples the coercivity distribution along H_c as taken from the FORC diagrams (Fig. 3.9) have a maximal extent of 90mT . The shape of the distribution is still elongated and the vertical spread with $H_u < 15\text{mT}$ indicates weak magnetic interactions. The differential remanence parameter exhibits a small negative interaction field ($\Delta M > -1.5$). Together with the other parameters derived from remanence and rockmagnetic measurements (Tab. 3.1) the samples fall into the PSD range.

For the samples of the Isle of Skye (S) thermal demagnetization of IRM discloses that the samples contain large (up mm scale) pyrrhotite and magnetite. This was confirmed by reflected light microscopy and SEM, which reveal intergrowth of pyrrhotite with magnetite,

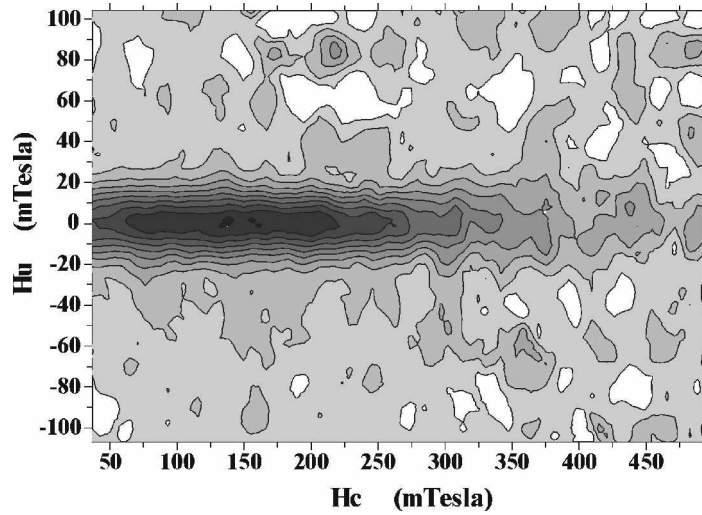


Figure 3.8: FORC diagrams from samples of Bourg d'Oisans. The elongated and closed contours along H_c up to 400 mT standing for a pure SD particles distribution with high coercivities. (picture with SF=3).

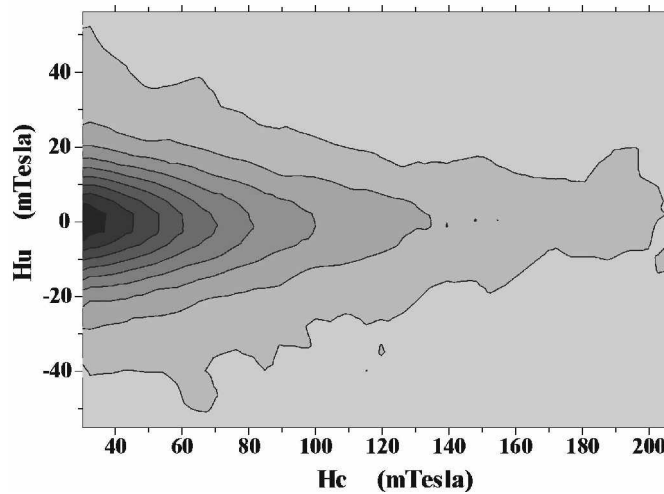
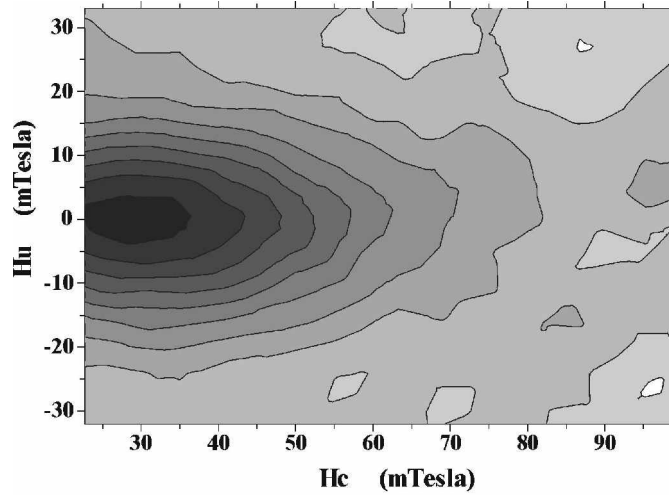


Figure 3.9: FORC diagrams from samples from the Elba. The closed contours and the peak position around 30 mT indicates a dominantly PSD assemblage. Signs of mean interaction field are absent. (both pictures with SF=3).

pyrite and chalcopyrite. Consequently the interaction patterns in the FORC diagrams of these samples are manifold (Fig. 3.10). Sample S3 comes closest to the results from the artificial samples (deviation from the H_c axis, the negative tilt of the distribution, negative region in lower half of the diagram). In the upper half the contours are slightly bended to higher values of H_u . In sample S2 the counters are stronger bended in the upper half of the diagram. The negative region, the deviation and the tilt in the distribution are less pronounced. Additionally

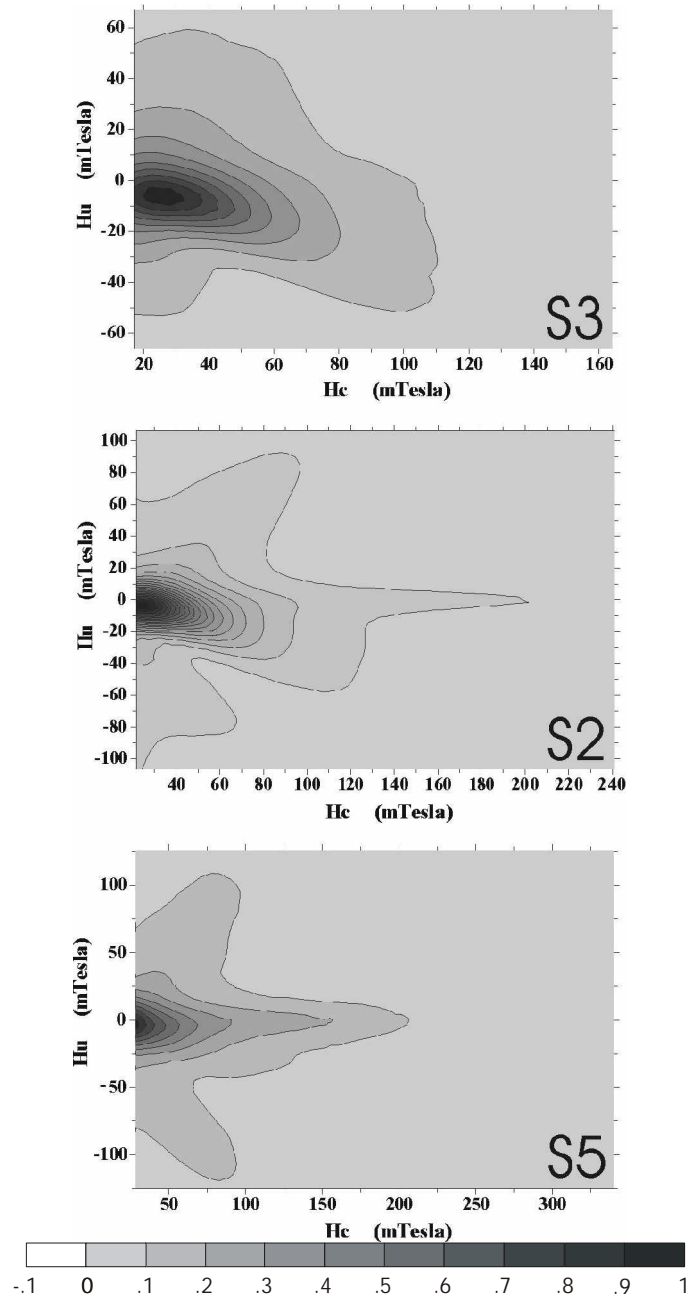


Figure 3.10: FORC diagrams from samples from the Isle of Skye, where different magnetic phases (pyrrhotite, magnetite) are present.

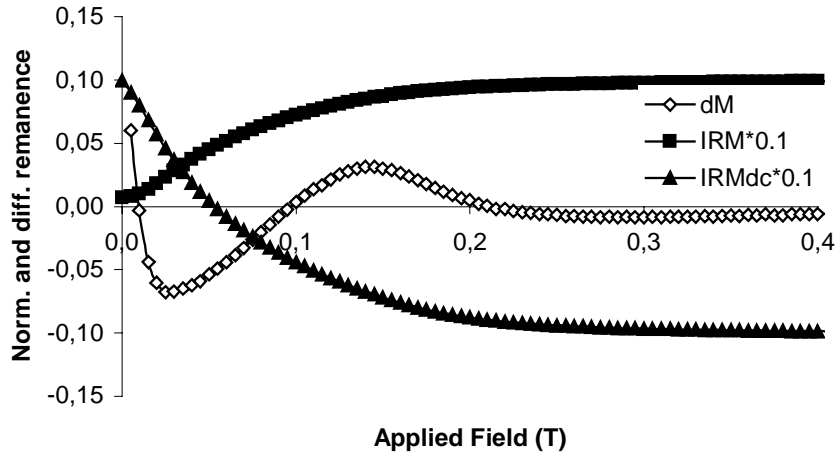


Figure 3.11: IRM, IRM_{dc} and ΔM curves for sample S5. The intensities of the IRM curves and the x-axis were changed for illustration.

the sample has a high coercive component up to 400 mT. The behaviour of this sample can be regarded as transitional one between S3 and S5, where bended counters are in the upper and lower half and the negative region is absent. Together with a long tail indicating a high coercive component this pattern is termed "bird-structure", where the bended areas are acting as the wings. The differential remanence ΔM for S3 und S2 (Tab. 3.1.) stands for a highly negative mean interaction field, which is supported by $W > 2$. Due to the broader grain-size distribution the calculated mean of the grain-size distribution is at $3\mu\text{m}$ for samples S2. On the contrary the ΔM for sample S5 contains a local minimum and maximum, both low in amplitude and located at high fields (Fig. 3.11).

A tentative interpretation for S3 and the $< 40\ \mu\text{m}$ TTE samples could be that both have a minor contribution of hexagonal pyrrhotite (not detected by other means) intergrown with the monoclinic phases in a sandwich like manner (one layer demagnetises the other), whereas the patterns of S2 and S5 are the consequence of the magnetic interaction with other phases like magnetite.

In the light of recording successive, independent pTRMs in pyrrhotite, the absence of magnetic interaction and the dominance of SD particles in samples from the regional metamorphic setting of Bourg d'Oisans support the rockmagnetic results made by Rochette et al. (1992) and Crouzet et al. (1999, 2001). The potential for TRM recording in contact metamorphic rocks as derived from the magnetic interaction analysis strongly depends on the different locations. In the Manaslu area, where clear non-interaction SD assemblages are

found, a violation of the laws of independent pTRMs (Thellier et Thellier, 1959) will not be expected. Under such conditions, for the Elba samples the restricted coercivity spectrum and a major domain state between SD to PSD grains confine their use as a pTRM recorder. In such a case their pTRM recording qualities should additionally be checked by pTRM experiments. In the samples from the Isle of Skye the recording of independent pTRMs during cooling of the rock can be excluded due to their high magnetic interaction content. The observations above support the use of magnetic interaction techniques as a preselective tool for Thellier like experiments as proposed by Wehland et al. (subm.) for basaltic samples.

3.5 Conclusion:

Both techniques used here, FORC and remanence based, are suitable to estimate the degree and nature of magnetic interaction in pyrrhotite bearing samples. The grain-size related change in the domain state is in good agreement with the literature and can be derived from FORC analysis as well as from the remanence and rock magnetic based techniques. The relationship between grain-size and SFD as derived from the artificial samples and expressed by FWHH-parameter can be described by a simple function, which helps to estimate the mean grain-size. Other parameters like the W-parameter, hysteresis parameters or the peak position of χ_r and χ_{dc} can enhance the understanding of the nature of the interaction field, grain-size distribution and domain state.

For natural systems we have shown that pyrrhotite can exist as an ideal non-interacting SD-particle assemblage in contact and regional metamorphic rocks. Nevertheless, intergrowths with other phases like magnetite or hexagonal pyrrhotite can often lead to high interaction fields of different nature. This seems to be more likely in contact metamorphic rocks, where the process of pyrrhotite formation often leads to mixed assemblages and a less pronounced grain-size distribution. In the context of pTRM experiments secondary pyrrhotite has the potential as a good recorder if the degree of interaction is checked by one of the methods used above.

Table 3.1

Sample	FWHH IRM _r	FWHH IRM _{dc}	Field _r	Field _{dc}	W	Equ. (4)	Equ. (5)	DS	M _{rs} /M _s	H _{cr} /H _c
<i>TTE150</i>	23.0	24.0	15.1	9.9	2.31	154.0	94.3	MD	0.24	0.89
<i>TTE75</i>	32.0	34.5	20.0	5.0	2.20	64.1	94.3	MD	0.26	1.01
<i>TTE55</i>	34.8	39.0	19.9	17.5	2.07	51.3	46.5	MD	0.29	0.89
<i>TTE40</i>	42.0	55.9	17.5	24.3	1.99	31.2	38.3	PSD	0.35	0.89
<i>TTE25</i>	59.7	73.5	28.3	35.0	1.73	12.3	18.5	PSD	0.36	0.74
<i>TTE10</i>	75.0	74.9	60.0	65.0	1.97	6.7	5.6	SD-PSD	0.44	0.96
<i>TTE5</i>	88.0	97.4	79.9	85.1	1.99	4.4	3.4	SD	0.47	0.97
<i>E2</i>	60	70	45	29.8	1.96	12.1	13.8	PSD	0.31	3.24
<i>E3</i>	61	70	60	40.1	1.97	11.6	8.3	PSD	0.26	2.66
<i>S3</i>	60	65	40	29.8	2.21	12.1	15.6	PSD	0.38	1.12
<i>S2</i>	115	103	60	35.0	2.34	2.2	9.1	SD	0.59	1.17
<i>S5</i>	62	63	25	15.0	2.27	11.1	41.4	PSD	0.39	1.45
<i>M1</i>	180	215	125	120.0	2.00	0.7	1.7	SD	0.66	1.53

Table 3.1: Parameters derived from the calculated susceptibility for selected samples. Field_{ac} and Field_{dc} denote the position of the calculated susceptibility peaks. The column with Equ. (4) and Equ. (5) give the calculated mean of the grain-size fraction after formula (4) and (5), respectively. DS stands for the interpreted dominating domain state in the assemblage. For FWHH and the W parameter see text. The rockmagnetic parameters of M_{rs}/M_s and H_{cr}/H_c are added for the sake of completeness.

3.6 References:

Cisowski, S. (1981): Interacting vs. non-interacting single domain behaviour in natural and synthetic samples. *Phys. Earth Planet. Inter.*, 26, 56-62.

Clark, DA. (1984): Hysteresis properties of sized dispersed monoclinic pyrrhotite grains, *Geophys. Res. Lett.*, 11 , 173–176.

Crouzet C., Ménard G. and Rochette P. (1999): High precision three dimensional paleothermometry derived from paleomagnetic data in an Alpine metamorphic unit, *Geology*, vol. 27, no. 6, p. 503-506.

Crouzet C., Rochette P. and Ménard G. (2001a): Experimental evaluation of thermal recording of polarity reversals during metasediments uplift. *Geophys. J. Int.* , 145, 771-785.

Crouzet C., Stang H., Appel E., Schill E. and Gautam P. (2001b): Detailed analysis of successive pTRMs carried by pyrrhotite in Himalayan metacarbonates: an example from Hidden Valley, Central Nepal. *Geophysical Journal International*, in press.

Daniel, E.D., Levine, I. (1960): Experimental and theoretical investigation of the magnetic properties of iron oxides recording tape. *J. Acoust. Soc. Am.*, 32, 1-15.

Dekkers, M.J. (1988a): Some rockmagnetic parameters for natural goethite, pyrrhotite and fine-grained hematite. (PhD Thesis, University of Utrecht), *Geologica Ultraiectina*, 51, 231 pp.

Dekkers, M.J.(1988b): Magnetic properties of natural pyrrhotite Part I: Behaviour of initial susceptibility and saturation-magnetization-related rock-magnetic parameters in a grain-size dependent framework, *Phys. Earth Plan. Inter.*, 52, 376-393.

Davis, P.M., Evans, M.E., (1976) : Interacting single-domain properties of magnetic intergrowths. *J. Geophys. Res.*,81, 989-994.

Dunlop, D.J. (1972): magnetite: behaviour near the single domain threshold. *Science*, 176, 41-43.

Dunlop, D.J., Westcott-Lewis, M.F., Bailey, M. (1990) : Preisach diagram and anhysteresis : do they measure interaction ?, *Phys. Earth Plan. Inter.*, 65, 62-77.

Fearon, M., Chantrell, R.W., Wohlfarth, E.P. (1990): A theoretical study of interaction effects on the remanence curves of particle dispersions, *J. Magn. Mater.*, 86: 197-206

Henkel, O. (1964): Remanenzverhalten und Wechselwirkungen in hartmagnetischen Teilchenkollektiven, *Phys. Status Solidi*, (b), 161: K41-K44

Kneller, E. (1969): Fine particle theory: In A.E. Berkowitz and E. Kneller (Editors), *Magnetism and Metallurgy*, Vol. I., Academic Press, NY, 365-471.

Lambert, I.B. (1973): Post-depositional availability of sulphur and metals and formation of secondary textures and structures in stratiform sedimentary sulphide deposits. *J. Geol. Soc. Australia*, 20, 205-215.

Mayergoyz, I.D., 1986. Mathematical model of hysteresis, IEEE Trans. Mag., MAG-22, 603-608.

Mayo, P. I., O'Grady, K., Chantrell, R.W., Cambridge, J.A., Sanders, I.L., Yogi, T., Howard, J.K. (1991a): Magnetic measurement of interaction effects in CoNiCr and CoPtCr thin film media, J. Mag. Mag. Mater., 95, 109-117.

Mayo, P.I., O'Grady, K., Kelly, P.E., Cambridge, J., Sanders, I.L., Yogi, T., Chantrell, R.W. (1991b): A magnetic evaluation of interaction and noise characteristics of CoNiCr thin films, J. Appl. Phys., 69 (8), 4733-4735

Petrovský, E., Hejda, P., Zelinka, T., Kropáček V., Šubrt. J. (1993): Experimental determination of magnetic interaction within a system of synthetic haematite particles, Phy. Earth Planet. Inter., 76,123-130

Pike, C.R., Roberts, A.P., Verosub, K.L., (1999): Characterizing interactions in fine magnetic particle systems using first order reversal curves, J. Appl. Phys. **85**, 6660

Roberts, A. P., Pike, C.R., Verosub, K.L. (2000): First-order reversal curve diagrams: A new tool for characterizing the magnetic properties of natural samples, J. Geophys. Res., 105, B12,28,461 – 28,475

Rochette, P. (1987) : Metamorphic control of the magnetic mineralogy of black shales in the Swiss Alps : towards the use of "magnetic isograds", Earth and Planetary Science Lett., 84, 446-456

Schill, E., Appel, E., Gautam, P. (2002): Towards pyrrhotite/magnetite geothermometry in low-grade metamorphic carbonates of the Tethyan Himalaya (Shiar Khola, Central Nepal). Journal of Asian Earth Science, 20, 195-201

Schill, E., Appel, E., Crouzet, C., Gautam, P., Wehland, F., Staiger, M. (Subm.): Oroclinal bending and regional significant clockwise rotations of the Himalayan arc - constraints from secondary pyrrhotite remanences. Geol. Soc. Am.

Soffel, H. (1977): Pseudo single domain effects and single domain - multidomain transition in natural pyrrhotite deduced from domain structure observations.- J. Geophys., 42, 351-359.

Soffel, H.C. (1981): Domain structure of natural fine-grained pyrrhotite in a rock matrix (diabase).- Phys. Earth Planet. Inter., 26, 98- 106.

Spratt, G.W.D, Bissel, P.R., Chantrell, R.W. (1988): Static and dynamic experimental studies of particulate recording media, J. Mag. Mag. Mater., 75, 309-318

Stancu, A., Stoleriu, L., Cerchez, M., (2001): Micromagnetic interaction of statistical and mean-field interactions in particulate ferromagnetic media, J. Mag. Mag. Mater., 225, 411-417

Stancu, A., Pike, C., Stoleriu, L., Postolache, P., Cimpoesu, D., (2003): Micromagnetic and Preisach analysis of the First Order Reversal Curves (FORC) diagram, J. Appl. Phys., 93, 10, 6620-6622.

Theillier, E., Theillier, O. (1959): Sur l'intensité du champ magnétique terrestre dans le passé historique et géologique. *Ann. Geophys.* (15), 285-376.

Veitch, R.J. (1990) :Anhysteretic susceptibility and static magnetic properties in interacting small particles, *IEEE Trans. Magn.*, MAG-26, 1876-1878.

Wohlfarth, E.P. (1958): Relations between different modes of the acquisition of the remanent magnetization of ferromagnetic particles, *J. Appl. Phys.*, 29, 595-596.

Woodward, J.G., Della Torre, E. (1960): Particle interaction in magnetic recording tapes, *J. Appl. Phys.*, 31, 56-62.

|

Magnetic interaction analysis of basaltic samples

Abstract:

For a successful paleointensity experiment a samples should only consist of non-interacting single domain (SD) particles. As this cannot be completely guaranteed for natural sample we applied different interaction test methods on basaltic samples from Fernando de Noronha, Brazil, in order to determine the degree of interaction and estimate their use as a preselection tool for paleointensity experiments. The occurrence of partial self-reversal in some of these samples is proven by continuous thermal demagnetization experiments and the characteristics of such samples are compared to non-interacting samples suitable for palaeointensity studies. First-order reversal curve (FORC) diagrams of the samples with partial self-reversal indicate an MD like behaviour and a typical asymmetry in the FORC diagram partly attributed to interacting PSD grains and a negative mean interaction field. Samples suitable for palaeointensity determination generally have a symmetrical FORC distribution with closed contours as expected from a SD particles assemblage. The character of the mean interaction field was also derived from the remanence based ΔM plots, where samples a MD contribution or with partial self-reversal have a ΔM minimum at low field values. As magnetic interaction can hamper palaeointensity measurements, both methods – FORC diagram and the ΔM plots – are suggested to be used as a pre-selection tool for Thellier-like experiments

4.1 Introduction:

Basaltic rocks are one of the major sources for palaeointensity determination using the Thellier-Thellier method (Thellier, 1959). Based on the independence of individual pTRMs the method requires amongst other things the existence of a non-interacting SD particle assemblage. Magnetic interactions in the assemblage hamper the method and can lead in extreme cases to processes like self-reversals.

For an non-interacting SD assemblage Wohlfahrt (1958) concluded, that the relationship of the different normalized remanence acquisitions can be described by

$$IRM_d(H) = 1 - 2 * IRM_r(H) \quad (1),$$

where IRM_r is the normalized remanence acquired from the initially demagnetized state and IRM_d the normalized remanence during the equivalent dc backfield demagnetization of the SIRM (saturation magnetization), respectively. Equation (1) also holds for MD particles provided that the density of pinning sites experienced by the domain-wall is the same for the ascending and descending branch of the remanence curve.

The Henkel plot is obtained by plotting IRM_r vs. IRM_{dc} (Henkel, 1964), where non-interacting SD particles will lead to a straight line with a slope of -2 . For an SD assemblage any deviation from this line can be expressed by the differential remanence parameter (Speliotis and Lynch, 1991)

$$\Delta M(H) = IRM_{dc}(H) - (1 - 2 IRM_r(H)) \quad (2)$$

Is ascribed to many-body effects and generally indicates the presence of magnetic interparticle interaction (Fearon et al., 1990; Mayo et al., 1990,a,b; 1991a,b). Positive values of ΔM are interpreted as a result of positive interaction, which tends to stabilize the magnetization, whereas a negative value would come from negative interaction yielding a net demagnetizing effect (see Petrovský et al., 1993). The Henkel plot can therefore be regarded as the analog of the Arai plot used in Thellier palaeointensity determinations.

A more detailed attempt to detect magnetic interaction is found in the recently developed FORC diagrams (Pike et al., 1999; Roberts et al., 2000). Derived from a set of first-order-reversal curves (Mayergoyz, 1984) the FORC distribution is obtained as the mixed second derivative:

$$\rho(H_a, H_b) \equiv - \frac{\partial^2 M(H_a, H_b)}{\partial H_a \partial H_b}, \quad (3)$$

where $\rho(H_a, H_b)$ is well defined for $H_b > H_a$. It is convenient for plotting the FORC distribution to use the coordinate system $\{H_b = (H_b - H_a)/2, H_u = (H_a + H_b)/2\}$ instead of the original $\{H_c = (H_b - H_a)/2, H_u = (H_a + H_b)/2\}$.

4.2 Samples and Methodology:

Samples were taken from ankaratritic lava flows and dykes from the island of Fernando de Noronha, Brazil (Leonhardt et al., submitted). Continuous demagnetizations were performed with a high temperature spinner magnetometer (HOTSPIN; described by Matzka et al. (2003)), which measures simultaneously two orthogonal components of the NRM at temperatures of up to 600°C. These measurements indicate the presence of partial self-reversal in samples of 5 volcanic units. The samples were repeatedly heated and cooled in HOTSPIN instrument with incrementally increasing maximum temperatures of 100°C, 200°C, 400°C and 600°C. This technique facilitates the recognition of reversibility of heating

and cooling cycles and the observation of possible blocking of remanences. Samples for the magnetic interaction analysis are grouped in: (A) four samples given suitable paleointensity results, (B) two samples indicating an MD contribution during Thellier experiments and (C) six samples containing self-reversed magnetization as proven by the HOTSPIN measurements. Twin specimens were taken from all of these samples and subjected to FORC analyses and IRM acquisition with subsequent backfield measurements. Prior to any treatment the specimens were subjected to AF demagnetization of 120mT to initialise the magnetic configuration using a 2G600 AF-demagnetiser. Ensuing IRM_r and IRM_d were performed up to 700mT with a field step of 5-10 mT followed by hysteresis measurements. Lastly FORC measurements (100 FORCs) were made using a saturation field of 500 mT and a smoothing factor (SF) of 2. All experiments were carried out by a Micromag 3900 Vibrating Sample Magnetometer.

4.3 Results and Discussion:

Continuous thermal demagnetisations:

The results of continuous thermal demagnetization are shown in Fig. 4.1. Sample FN-R1-2 (Fig. 1a) shows evidence for partial self-reversal. This sample is characterised by two ferromagnetic components with unblocking temperature (T_{UB}) of approximately 220°C and 580°C. The orthogonal projection, which contains only two components of magnetization,

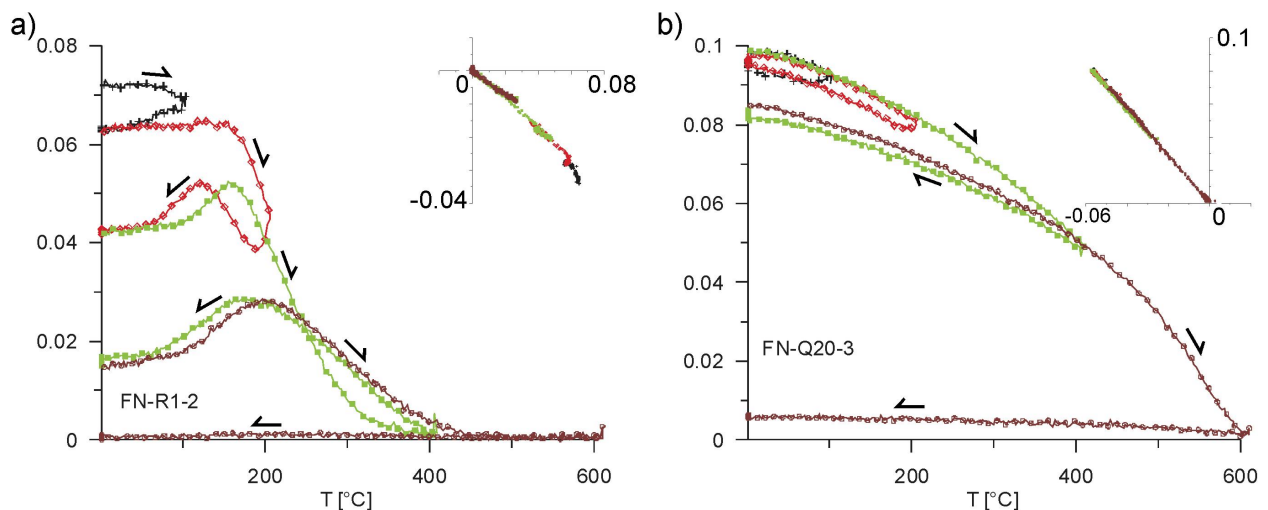


Figure 4.1: Continuous demagnetization diagrams of samples FN-R1-2 (a) and FN-Q20-3 (b) with incremental heating cycles. The insets on the upper right of each diagram show orthogonal projections of the measured z- and x-component. The reversible increase, respectively decrease of magnetization at heating steps above 200°C in (a) indicates the presence of interacting particles leading to partial self-reversal. Such feature is not found in (b).

indicates that during the first heating cycle a soft overprint, very likely of viscous origin, is removed. After heating to 200°C the cooling curve shows firstly an increase and then, at about 150°C, a characteristic decrease of magnetization towards room temperature. Thermomagnetic curves measured in a saturation field (Leonhardt et al., accept.) indicate that this feature is not controlled by the temperature dependence of the saturation magnetization. The reversible increase, respectively decrease of magnetization indicates a magnetic interaction between the two magnetic phases present in this sample. The maximum of magnetization is gradually shifted from lower temperatures to higher temperatures during repeated heating steps with increasing maximum temperature. This observation is interpreted as a results of a partial oxidation of the low temperature phase. Samples from sites FN-Q4 and FN-Q7 show similar characteristics as described for Fig 4.1a.

Fig. 4.1b shows the continuous thermal demagnetization results of sample FN-Q20-3 containing a ferrimagnetic phase with high T_{UB} . Rock magnetic investigations and ore microscopy revealed high temperature oxidized titanomagnetite as the dominating remanence carrying magnetic phase accompanied by a very limited amount of hematite (Leonhardt et al., submitted). Samples from site FN-Q20 proved to be suitable for palaeointensity determination. The orthogonal projection indicates a single component remanence. The decay diagram of the NRM intensity also points to a simple unblocking of a high-temperature component exhibiting no indications of magnetic interaction.

Interaction analysis:

In Fig. 4.2 examples of FORC diagrams for group A samples (FN-Q20; FN-Q22; FN-Q24) are compared with samples from group B (FN-Q3) and C (FN-Q13; FN-R1). The B and C samples show a higher percentage of open contour lines indicating an MD like behaviour and a strong asymmetry in the plot according the horizontal line (Pike et al., 1999). The shape of the lower half of the FORC diagram, which would lead to negative regions if more contours were used, can be attributed towards a negative mean interaction field (Stancu et al., 2003). Such negative mean interaction fields are generally interpreted as having a demagnetizing effect on the sample (Petrovsky et al., 1993). For the group A samples, such a strong asymmetry is only observed in sample FN-Q24. In the other samples the asymmetry in the FORC diagrams is negligible, although a certain degree of magnetic interaction can be observed.

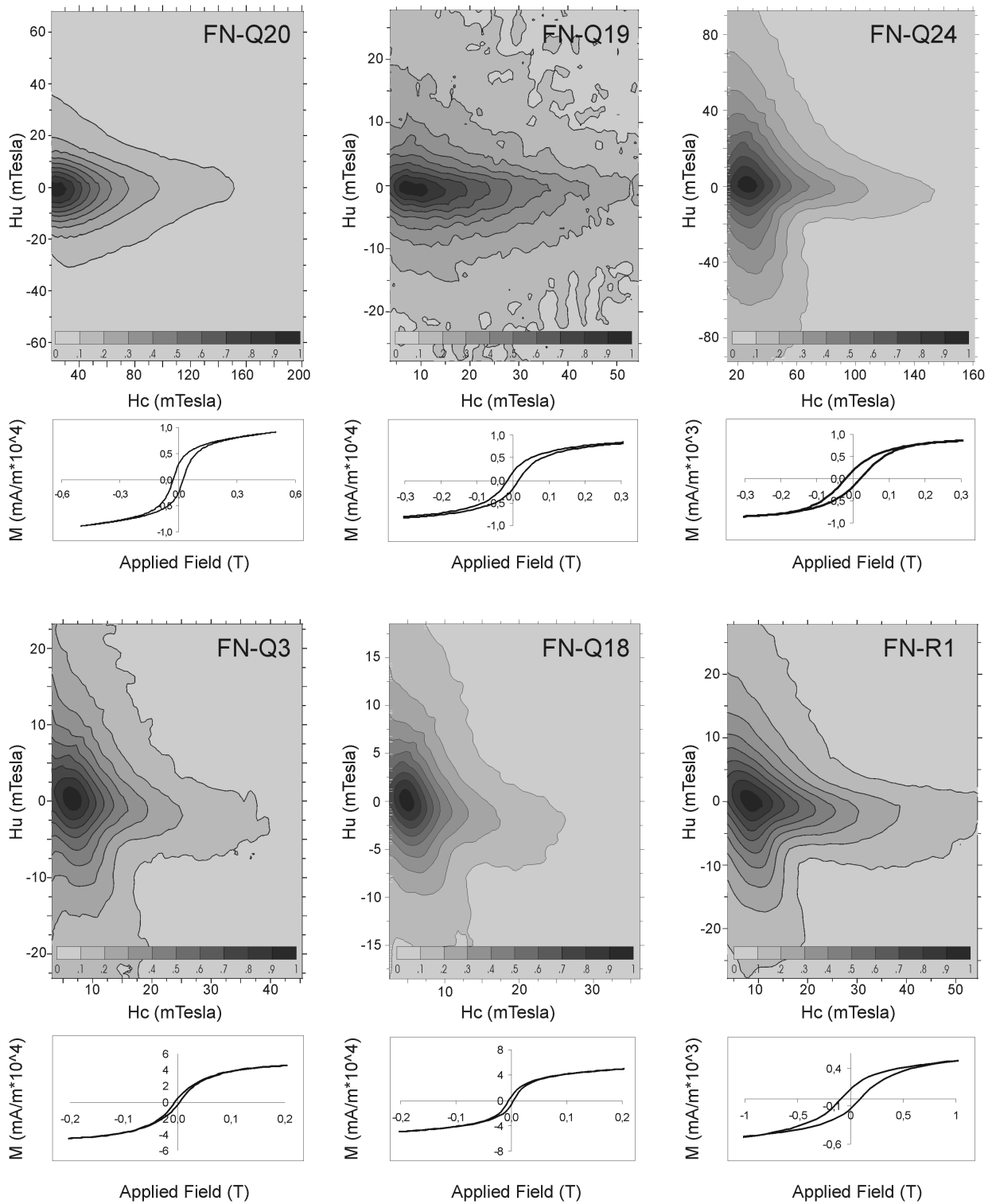


Figure 4.2: FORC diagrams of samples from group A (FN-Q20;FN-Q19;FN-Q24) , B (FN-Q3) and C (FN-Q18; FN-R1) together with their hysteresis loop. H_c stands for the coercivity distribution in the sample, whereas H_u indicates the strength of the interaction fields.

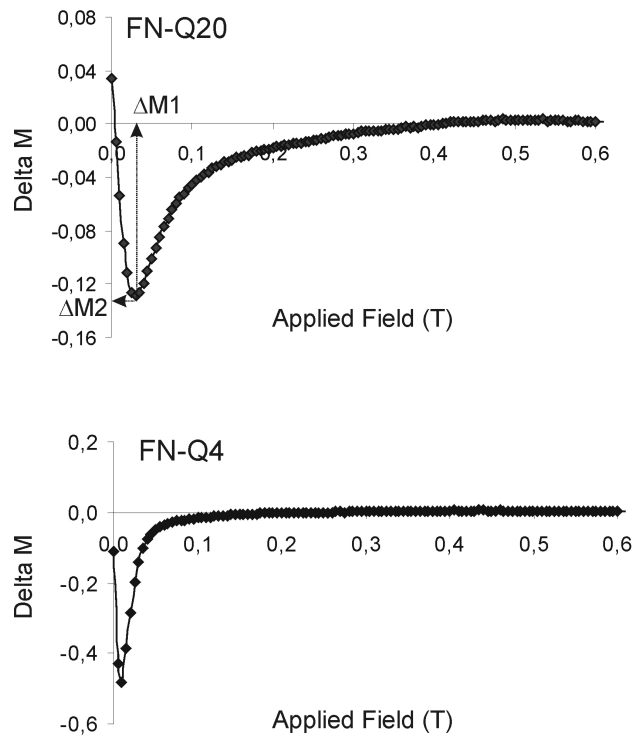


Figure 4.3: Two examples of ΔM plots. FN-Q20 belongs to group A and FN-Q4 to group C. The position of the parameters $\Delta M1$ and $\Delta M2$ are marked in the upper graph.

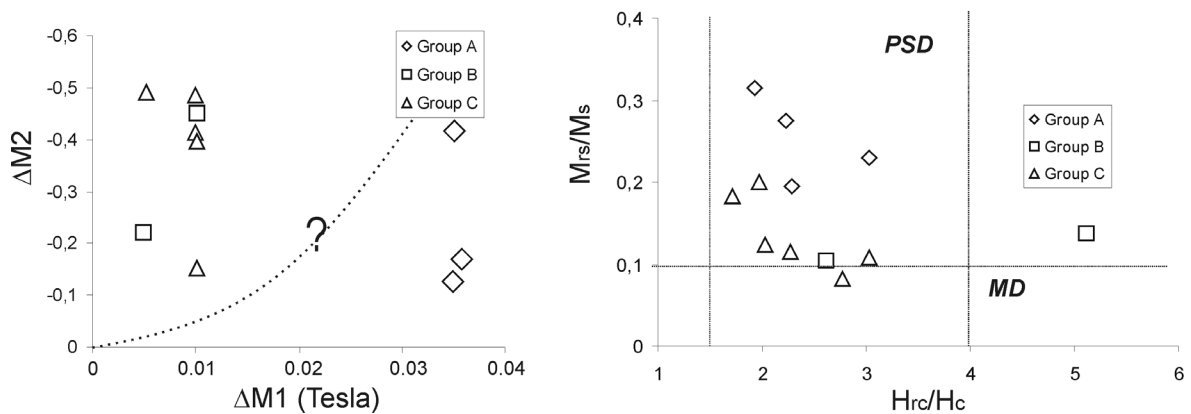


Figure 4.4: Comparison of the samples of all groups in the $\Delta M 1$ vs. $\Delta M 2$ plot and the conventional Day plot. The first one gives a better dissimination between group A and the other groups, whereas in the Day plot the transition between group A and B is gradual.

In the corresponding ΔM plots (Fig 4.3) we compared the results by using the position (called $\Delta M1$ parameter) and the intensity (called $\Delta M2$ parameter) of the minima (see Table 4.1). Samples of group B and C have lower $\Delta M1$ fields and tend to have higher negative $\Delta M2$ values indicating the dominance of negative mean interaction. Group A samples have

all higher $\Delta M1$ values The $\Delta M2$ shows an analogy with the asymmetry in the FORC diagrams based on the fact that both indicate the presence of negative mean interaction fields.

Sample	$\Delta M 1$ (T)	$\Delta M 2$	H_{cr}/H_c	M_{rs}/M_s	H_C Peak FORC (mT)	Group
<i>FN-Q19</i>	0,0358	-0,17	2,23	0,27	8	A
<i>FN-Q24</i>	0,0351	-0,417	2,28	0,20	26	A
<i>FN-Q20</i>	0,035	-0,127	1,93	0,31	23	A
<i>FN-Q22</i>	*		3,03	0,23	16	A
<i>FN-Q3</i>	0,0101	-0,452	2,61	0,10	7	B
<i>FN-Q1</i>	0,0049	-0,221	5,11	0,14	3,5	B
<i>FN-Q18</i>	0,00515	-0,49	2,27	0,12	5	C
<i>FN-Q23</i>	0,00995	-0,414	3,03	0,11	4,5	C
<i>FN-Q4</i>	0,0099	-0,484	2,77	0,08	5,5	C
<i>FN-R1</i>	0,0101	-0,395	1,97	0,20	9	C
<i>FN-R4</i>	0,0099	-0,485	1,71	0,18	8	C
<i>60I???</i>	0,0101	-0,152	2,03	0,12	5	C

Table 4.1: Summary of the rockmagnetic parameters and the parameters derived from the interaction methods. For sample FN-Q22 (*) the ΔM -plot was not calculated due to a high initial remanence.

In Fig. 4.4 the rockmagnetic values of the samples in a Day plot are compared with the results from the ΔM method. Whereas the three groups of samples are indistinguishable in the Day plot, the difference between group A samples and the samples of group B and C using the $\Delta M1$ parameter is obvious. As A samples with high mean coercivities and higher interaction fields resist self demagnetisation, it can be assumed that a stability field in the $\Delta M 1$ vs. $\Delta M 2$ plot exists (marked by the dashed line with the question mark). As samples of low coercivity, but no interaction fields should also behave like ideal SD grains, the stability field should start from the origin. The clear shape of that field has to be determined by more experiments.

4.4 Conclusion:

In terms of magnetic interaction, the qualitative and semi-quantitative classification of the FORC and $\Delta M1$ results indicate that the question whether or not a sample is suitable paleointensity experiments depends on the relationship between the degree in magnetic interaction and the main coercivity in the sample. Like for high mean interaction fields - as assessed by a strong asymmetry in the FORC diagram and a high intensity of the ΔM minima -, a particle assemblage of higher mean coercivity will lead to suitable paleointensity results, whereas in a sample of low coercivity it can lead to effects like self-reversal. For the ΔM

method, this can be quantitatively assessed using a combination of the $\Delta M1$ and $\Delta M2$ parameters, although more data will be needed to mark distinctive values for the suitability of samples for paleointensity measurements. Such parameters are harder to be found by the FORC method, where the shape of the distribution expresses the mean interaction field. The peak of the FORC distribution on its own as the mean coercivity of the sample will not be sufficient as a quality parameter.

4. 5 References:

Fearon, M., Chantrell, R.W., Wohlfahrt, E.P., 1990. A theoretical study of interaction effects on the remanence curves of particle dispersions, *J. Magn. Magn. Mater.*, 86, 197-206.

Henkel, O., 1964. Remanenzverhalten und Wechselwirkungen in hartmagnetischen Teilchenkollektiven, *Phys. Status Solidi*, (b), 161: K41-K44.

Leonhardt, R., Matzka J., Menor, E.A., Absolute palaeointensities and palaeodirections from Fernando de Noronha, Brazil, *Phys. Earth Planet. Inter.*, submitted.

Matzka et al., 2003

Mayergoyz, I.D., 1986. Mathematical model of hysteresis, *IEEE Trans. Mag.*, MAG-22, 603-608.

Mayo, P. I., Bradbury, A., Chantrell, R.W., Kelly, P.E., Jones, H.E., Bissel, P.R., 1990a. Interaction effects in the remanence curves of Co-Ti doped BaFe system. *IEEE Trans. Magn.*, 119, 228-230.

Mayo, P. I., Erkkila, R.M., Bradbury, A., Chantrell, R.W., 1990b. Interaction effects in longitudinally oriented and non-oriented barium hexaferrite tapes. *IEEE Trans. Magn.*, MAG-26, 1894-1896.

Mayo, P. I., O'Grady, K., Chantrell, R.W., Cambridge, J.A., Sanders, I.L., Yogi, T., Howard, J.K., 1991a. Magnetic measurement of interaction effects in CoNiCr and CoPtCr thin film media, *J. Mag. Mag. Mater.*, 95, 109-117.

Mayo, P.I., O'Grady, K., Kelly, P.E., Cambridge, J., Sanders, I.L., Yogi, T., Chantrell, R.W., 1991b. A magnetic evaluation of interaction and noise characteristics of CoNiCr thin films, *J. Appl. Phys.*, 69 (8), 4733-4735.

Petrovský, E., Hejda, P., Zelinka, T., Kropáček V., Šubrt, J., 1993. Experimental determination of magnetic interaction within a system of synthetic haematite particles, *Phys. Earth Planet. Inter.*, 76, 123-130.

Pike, C.R., Roberts, A.P., Verosub, K.L., 1999. Characterizing interactions in fine magnetic particle systems using first order reversal curves, *J. Appl. Phys.*, 85, 6660, 1999.

Roberts, A. P., Pike C.R., Verosub, K.L., 2000 First-order reversal curve diagrams: A new tool for characterizing the magnetic properties of natural samples, *J. Geophys. Res.*, 105, B12, 28,461 – 28,475.

Stancu, A., Pike, C., Stoleriu, L., Postolache, P., Cimpoesu, D., 2003. Micromagnetic and Preisach analysis of the First Order Reversal Curves (FORC) diagram, *J. Appl. Phys.*, 93, 10, 6620-6622.

Thellier, E., Thellier, O., 1959. Sur l'intensité du champ magnétique terrestre dans le passé historique et géologique. *Ann. Géophys.*, 15:285-376.

Wohlfahrt, E.P., 1958. Relations between different modes of the acquisition of the remanent magnetization of ferromagnetic particles, *J. Appl. Phys.*, 29, 595-596.

How to measure in a Cryogenic Magnetometer at elevated temperatures?

Abstract:

We have designed a heating device for a 2G Enterprise cryogenic magnetometer to measure the remanence of an inch sized sample at elevated temperatures. The technique is based on the transmission of thermal energy from outside the cryogenic magnetometer to the frontal parts of the sample by the means of a quartz glass bar. Two high-energy (1000Watt) lamps serve as the source of thermal energy. As no magnetic material (like thermocouples) can be used in the sensitivity area of the SQUIDs, the temperature of the sample is assessed by a time-temperature relation as derived from calibration experiments. The device was tested on a pyrrhotite-bearing sample containing laboratory induced TRMs of one and two antiparallel components. Heating to above the Curie temperature of pyrrhotite ($\sim 330^{\circ}\text{C}$) is achieved within 500s gaining one SQUID reading per second. The abnormal convex shape of the demagnetisation curve as well as the widening of the transition between two antiparallel components is explained by means of a simple remanence model. The results underlines that the furnace device is a low cost solution to measure remanences at elevated temperatures in short times.

5.1 Introduction:

The normal technique of thermal demagnetisation of a paleomagnetic sample in an external furnace is a time consuming task as heating and cooling has to be performed at each temperature step. Moreover, the repeated thermal treatment increases the possibility of alteration within the sample and – during cooling – the acquisition of laboratory induced thermal remanent magnetisations (TRMs). For strong magnetic, mainly basaltic samples, this problem was solved by the use of a heating system in a spinner magnetometer.

A realisation of such a technique for a more sensitive cryogenic magnetometer is aggravated by the geometry of the magnetometer itself, the problem of cooling requirement and the fact, that magnetic materials such as heating wires have to be avoided in the construction within the measurement zone. In this paper we like to discuss the applicability of such a heating device designed for cryogenic magnetometer.

5.2 Technical design:

The device uses a strong light source (1000 W lamps, Xerion GmbH, Freiberg i.Br., Germany). The energy is transmitted to the measurement position in the cryogenic magnetometer by means of quartz glass bars (23 x 900 mm, fire polished ends, SemiGuarz GmbH, Germany) used as light conductors (Fig. 5.1). With this technique, the energy brought into the magnetometer's measurement area is heating the sample's frontal parts. To avoid alteration at the sample's frontal part, a small slice of magnetically free gypsum is interposed. Energy loss – and therefore a heating up – along the whole inlet is negligible. Consequently, a cooling system is only required in direct vicinity of the sample.

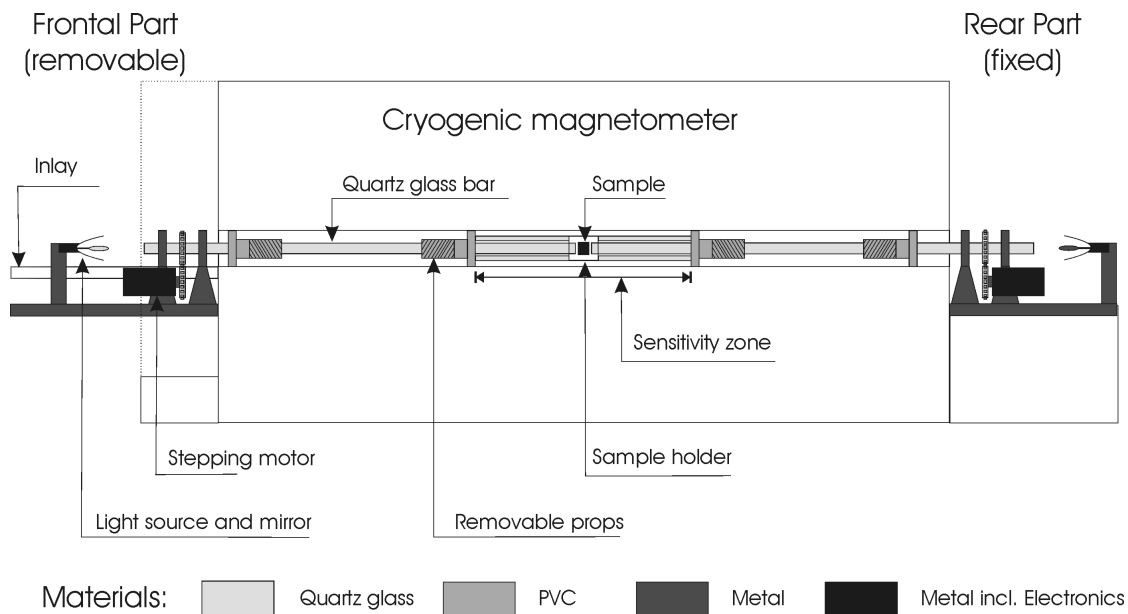


Figure 5.1: Conceptual sketch of the heating device for the cryogenic magnetometer

Crucial for the parts used inside the magnetometer's inlet is their pure diamagnetic property. Therefore, near the SQUIDS (sensitivity zone, Fig. 5.1) only quartz glass was used to construct the sample holder. The ends of the holder are mounted on a PVC cylinder, which also serves as the prop for the bars. Overall, four PVC made cylinders are used to stabilize the quartz glass bars inside the cryogenic magnetometer. The system is cooled by air using a thin quartz glass tube (not shown in Fig. 5.3) attached to a compressor.

For the outer parts, metal is used to build the holder for the light source and the stepping motor. With the stepping motor, the whole inlet can be rotated and thus the sample can be measured at different angles to improve the quality of the obtained data.

The device is loaded by removing the frontal part and replacing it with the inlay. Then the whole inlet is pulled out and – by opening the removable props – the sample handler can be opened.

5.3 Control and Calibration:

The homemade power supply for the lamps and the stepping motors are controlled by a LabView[®] written program in combination with a FieldPoint[®] system (Fig. 5.2). For the communication with the SQUID electronics a subroutine was used written in LabView[®] by Christan Hilgenfeld, Thorsten Frederichs and Karl Fabian from the University of Bremen.

As no metal parts are allowed in the sensitivity area during the measurements, the temperature can only be determined indirectly by means of a voltage-temperature calibration. Therefore, a dummy sample was prepared with two thermocouples – one at the frontal part and one in the centre of the sample – and placed in the device to record the temperature. The gradient after 1600 s of heating at 60% of the lamps full power is about 65°C (Fig. 5.2). Such a large

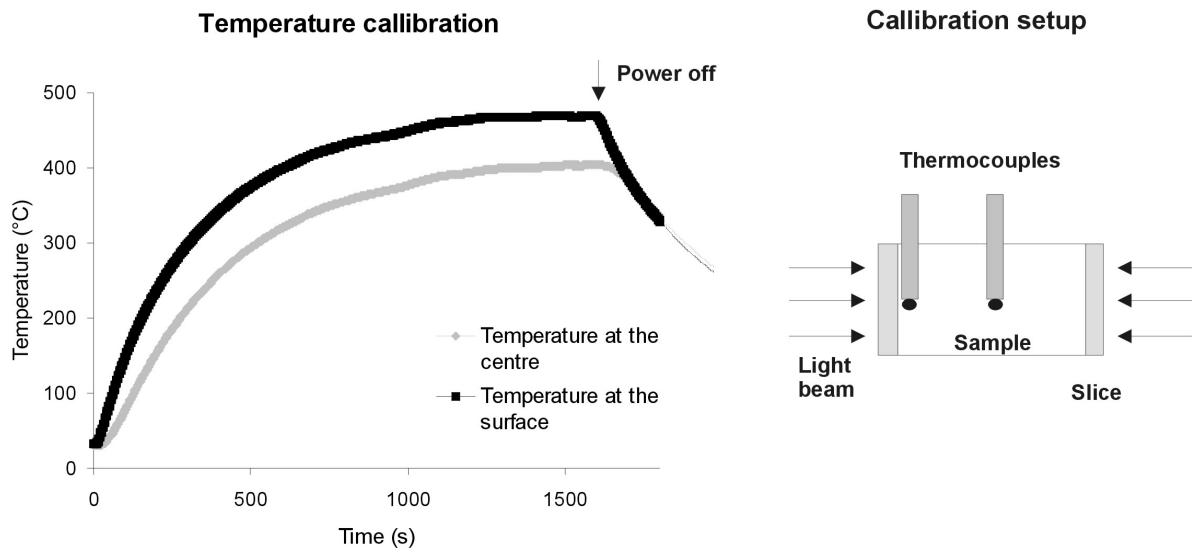


Figure 5.2: Left: Temperature behaviour in the centre and at the margin of a dummy sample. Applied power of the lamps = 600Watt. Right: Configuration of the thermocouples with the sample during the calibration.

gradient is the consequence of heating only the frontal parts of the sample. As the sample holder couldn't be closed during the calibration experiment, the temperatures in the cryogenic magnetometer will be reached earlier.

5.4 Demagnetisation Results:

To assess the quality and speed of thermal demagnetisation with the new device, demagnetisation experiments were performed on pyrrhotite bearing samples, carrying a laboratory induced thermoremanent magnetisation (TRM) or a natural remanent magnetisation (NRM). For a single component remanence, the result is explained by a simple demagnetisation model.

Demagnetization of a single- component TRM:

A unidirectional TRM was imparted on a pyrrhotite-bearing sample using a MMTD1 thermal demagnetiser (Magnetic Measurements) and an applied field of 90 μm . The demagnetisation curve using the new device using 60% (600Watt) of full power (Fig. 5.4) shows a rapid decrease

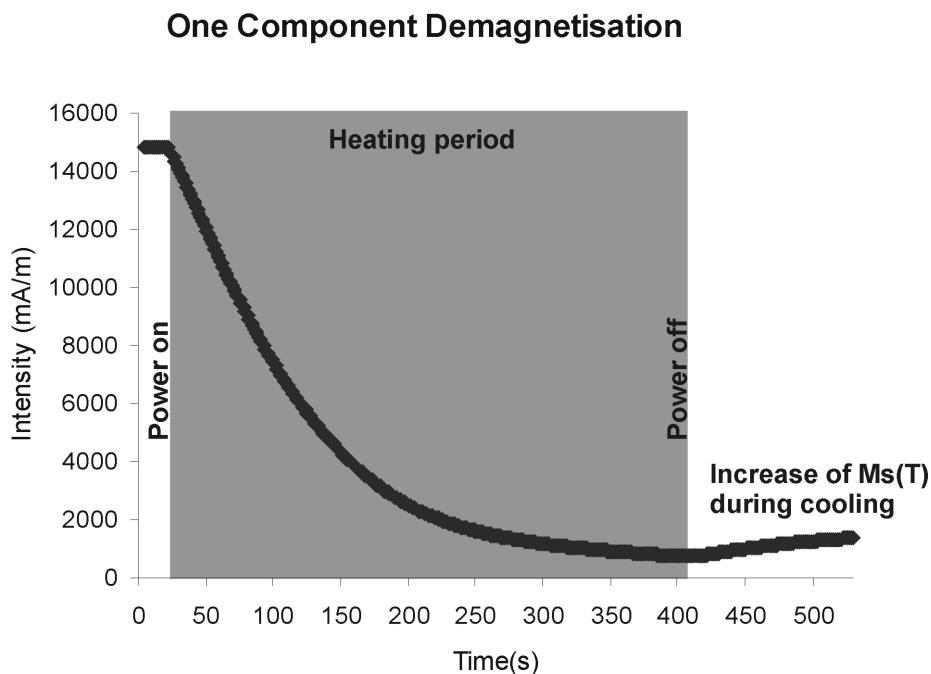


Figure 5.3: Thermal demagnetisation of a laboratory induced TRM (z-axis only) in a pyrrhotite-bearing sample. The grey area marks the time of heating. The remanence was measured every second.

of intensity during the first 100 seconds. The demagnetisation was stopped after ~400 s when a stable remanence was achieved. A complete demagnetisation with this technique is - at this stage - not possible, as the temperature distribution is not homogeneous. During cooling, the remanence slightly increases again because of its temperature dependence.

The concave shape of the thermal demagnetisation can be explained by a simple model: Due to the furnace design, heating of the sample starts from the frontal parts. Therefore the Curie temperature at the frontal part is reached earlier than in the centre of the sample (see Fig. 5.3). If we consider only one half of the sample and subdivide the sample in three equal volumes, the volume in direct contact to the light source will be heated faster than the one with the greatest distance from the light source (loss of temperature due to radial radiation and cooling is neglected in the model).

Number of grains		1	2	4	6	8	18	30	Sum
T(°C)	T_{ub}(°C)/	<150	150-200	200-250	250-270	270-290	290-300	300-330	
	30		1,03	2,06	4,12	6,18	8,24	18,54	30,90
60		0,98	1,96	3,91	5,87	7,82	17,61	29,34	67,49
90		0,92	1,85	3,69	5,54	7,39	16,62	27,70	63,70
120		0,86	1,73	3,46	5,19	6,92	15,57	25,94	59,67
150		0,80	1,60	3,21	4,81	6,41	14,43	24,06	55,33
180		0,00	1,47	2,93	4,40	5,87	13,20	22,00	49,87
210			0,00	2,63	3,94	5,26	11,83	19,72	43,39
240				2,28	3,43	4,57	10,28	17,13	37,68
270				0,00	2,81	3,74	8,43	14,04	29,02
300					0,00	0,00	6,00	10,00	16,00
330							0,00	0,00	0,00

Table 5.1: Example of the demagnetisation model for one volume element. Ordinate: Temperature T(°C) of the volume element. Abscissa: number of grains with the corresponding unblocking temperature T_{ub}(°C). Sum is the net magnetisation of the volume element at the temperature T(°C).

In each volume, we now store a set of SD particles with different unblocking temperatures, where the number of grains with unblocking temperatures increases towards the Curie temperature of pyrrhotite (~330°C; Table 5.1). Using the temperature dependence $M_s(T)/M_s(T_c)$ of pyrrhotite as formulated by Menyeh and O'Reilly (1997), the contribution of

each grain to the total remanence for a certain temperature can be calculated. The three volumes of the sample are assumed to heat up by 30°C/time unit (outer volume), 20°C/time unit (middle volume) and 10°C/time unit (inner volume), respectively. The results for the different volumes as well as the net remanence of the whole sample are shown in Fig 5.4. It explains the observed shape of the demagnetisation curve (Fig. 5.3) in principle.

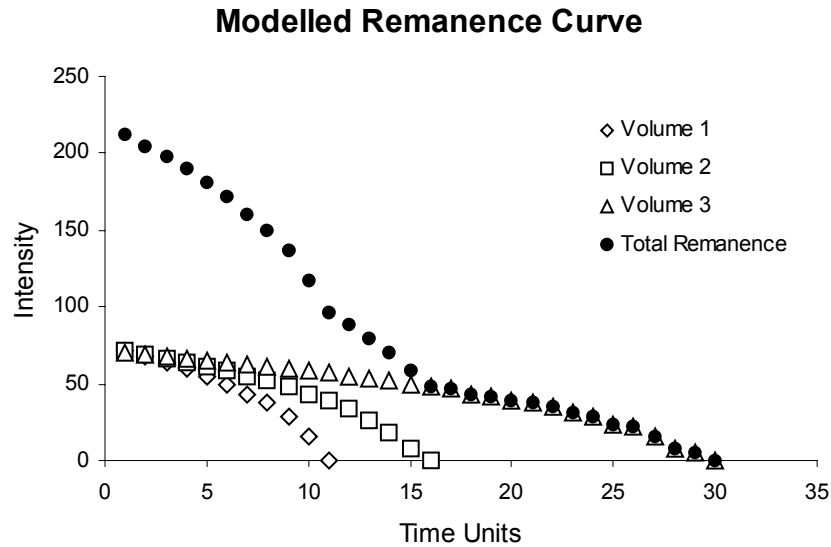


Figure 5.4: Results of the simple demagnetisation model: Open boxes indicate the intensity behaviour of the independent volume elements during heating. The black box stands for the net remanence, i.e. the sum of all three volume elements.

Demagnetisation of two antiparallel components:

The thermal inhomogeneity in the sample during heating has the consequence that different components with different unblocking ranges will be demagnetised at the same time with different positions within the sample. This is tested by demagnetising a sample where two antiparallel components with non-overlapping T_B ranges, i.e. a $pTRM_1$ (270°C-30°C) and a $pTRM_2$ (330°C-270°C) were imparted using the MMTD1 furnace and an applied field of 90µm.

The results of the demagnetisation are shown in Fig. 5.5 for using the new optical furnace and a conventional stepwise demagnetisation. For a better comparison, the time axis is transformed into a temperature axis using the transfer function from the calibration experiments described above. Consequently the transformation brings up two curves, which show the maximal temperature difference in the sample.

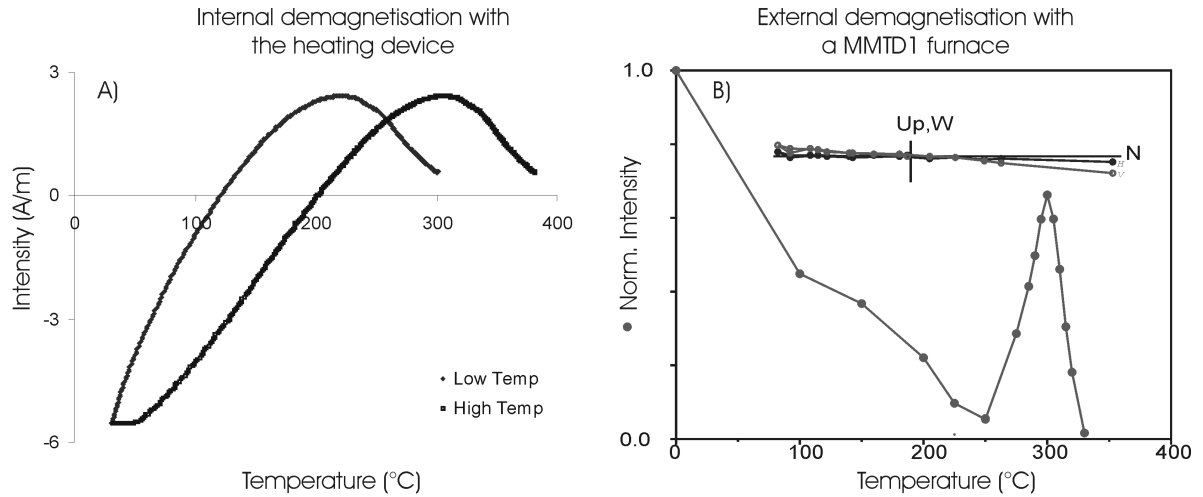


Figure 5.5: Thermal demagnetisation of two antiparallel components imparted at temperatures of 300°C-270°C and 270°C-30°C, respectively: A) using the new furnace device. The time axis is transformed into a temperature axis using the results from the experimental calibration. Dotted line depicts the two antiparallel components. B) Thermal demagnetisation of a sample from the same location using the MMTD1 thermal demagnetiser.

The comparison of both methods clearly shows that the transition is smoothed over a wide temperature range using the furnace device, whereas with conventional technique the transition is as sharp as one expects for a sample containing a single domain particle assemblage (see Wehland et al., subm., for samples from Bourg d’Oisans, France).

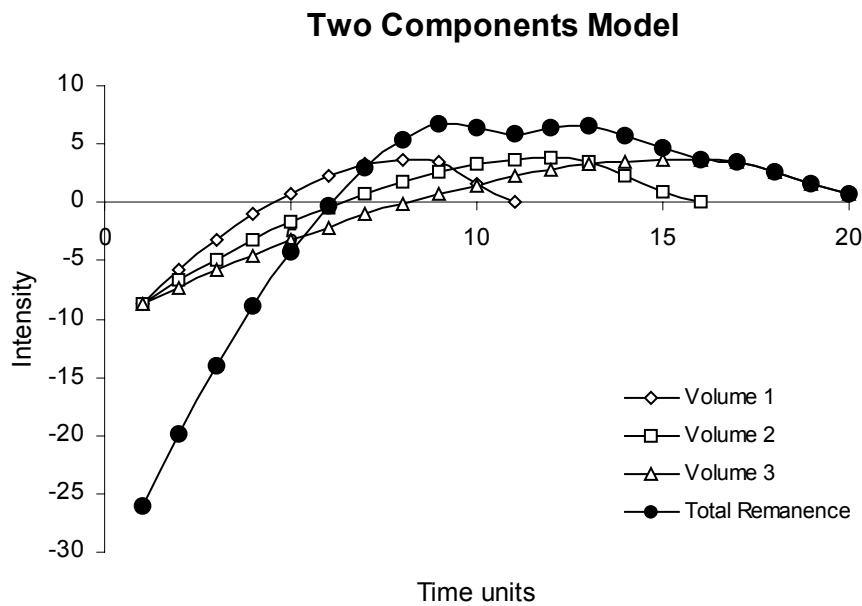


Figure 5.6: Simple model for the two components demagnetisation at elevated temperatures: for the total remanence the transition is smeared by the superposition of the single volumes.

The broadening of the transition is modelled using the same calculation described above with the difference that temperature intervals of 0-270°C and 270°C-330°C denote antiparallel directions. The blocking temperature range was narrowed to 10°C steps for better resolution. It becomes clear that already each individual volume shows a smeared transition (Fig. 5.6) due to the temperature dependence of the remanent magnetisation. Smearing increases by taking the sum of all volumes (total remanence, Fig. 5.6). It makes clear that two antiparallel components cannot be distinguished as easy as using the conventional demagnetisation technique, where remanences are measured at room temperature.

5.5 Conclusions:

The new furnace device opens the option for continuously measuring remanences during heating and cooling within a cryogenic magnetometer. Although tested here for pyrrhotite bearing samples only with a Curie temperature of $\sim 330^\circ\text{C}$ the device has the potential of heating up to 700°C covering the most prominent magnetic minerals like hematite and magnetite. For such higher temperatures, the cooling system has to be improved. The internal thermal gradient in the sample can be explained by simple remanence models and does not affect the analysis of unidirectional paleomagnetic remanences, thus making the technique suitable for many paleomagnetic applications. The time required to demagnetise a sample up to 350°C (pyrrhotite bearing sample) is about 10 minutes including sample loading and unloading

5.6 References:

Matzka, J., Krasa, D., Kunzmann, Th., Schult, A., Petersen, N., 2003. Magnetic state of 10 to 40 Ma old ocean basalts and its implication for natural remanent magnetization, *Earth. Planet. Sci Lett.*, 206(3-4), pp. 541-553.

Menyeh, A., O'Reilly, O., 1997: Magnetic hysteresis properties of fine particles of monoclinic pyrrhotite Fe_7S_8 , *J. Geomag. Geoelectr.*, 49, 965-976.

One inch of reversal or how a single sample can hold variations of the Earth magnetic field

magnetic field

Abstract:

The acquisition of partial thermoremanent magnetizations (pTRMs) during cooling of metamorphic rocks provides a new tool to continuously record variations of the Earth magnetic field in a single sample. Such a record determining absolute paleointensities is obtained from metamorphic limestones of central Elba. The quality of the record is ensured by rockmagnetic experiments like FORC analysis and Thellier experiments on laboratory TRMs. A transitional zone between antipodal remanence directions in the NRM record shows low paleointensities indicating a reversal period of the EMF. The duration for this field transition is estimated as less than 19kyr based on the thermal modeling of the cooling times. We thereby demonstrate that the pTRM method opens the way to new archives for paleointensity studies and allows to expand the information gained by common recorders like basaltic rocks and sediments.

6.1 Introduction:

The Earth's magnetic field (EMF) behavior during a reversal is usually studied in lava flows and sediments. Both rock types provide important knowledge but also have their specific uncertainties like unknown time gaps of the lava flows and the lock-in-depth problem in sediments. These uncertainties could be overcome by the replay of a continuous record of EMF variations residing in partial thermoremanent magnetizations (pTRMs) within single samples (Fig.6.1) from metamorphic rocks.

Crucial for a successful replay is the domain state of its magnetic particles in the sample.

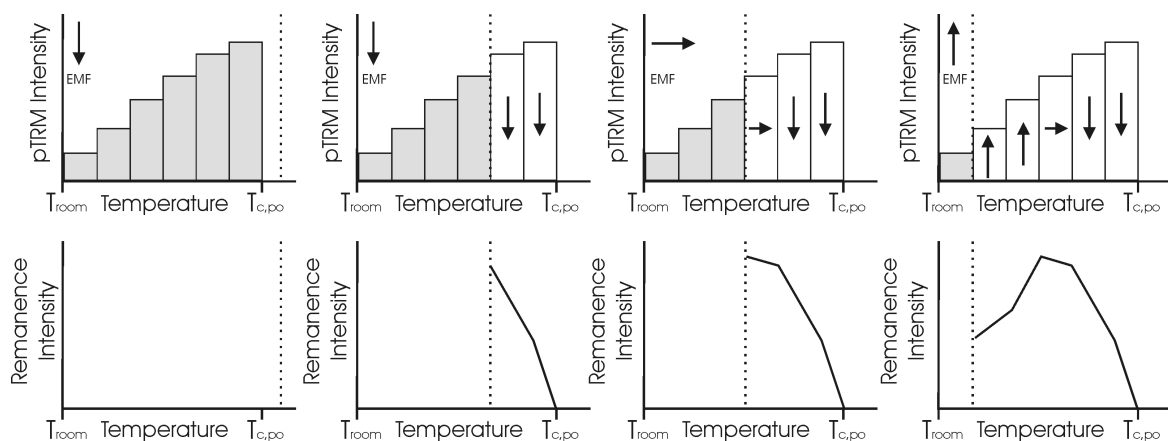


Figure 6.1: Principle of pTRM recording in a single sample during metamorphic cooling (from left to right): the different directions of the EMF are blocked in the respective TRMs. The direction of the EMF is marked with the arrow in the left upper half of the diagram. Gray boxes stand for individual unblocked pTRMs, white for blocked ones. The dashed line indicates the actual metamorphic temperature. The lower diagrams demonstrate the resulting net-intensity of the sample along the axis parallel to the primary EMF direction.

Only for single domain (SD) grains, the blocking temperature T_B is equivalent with the unblocking temperature T_{UB} thus allowing the existence of independent pTRMs. If multi domain (MD) particles are present or magnetic interaction exists the independence of pTRMs is lost and, hence, the information is blurred.

The cooling rate and the relevant blocking temperature interval of the remanence carriers determine the time period covered by a pTRM record. Suitable rocks should account for the duration of a reversal as the most prominent changes of the EMF, which is assumed to be not longer than 20 kyr¹. According to Merrill and McFadden² the mean duration is between 1000-8000 yr. With the intention to cover information also prior and after a reversal a pTRM record should span about 50-100 kyr. Cooling rates providing such periods can be only found in intrusions and in their related contact metamorphic aureole. In such settings pyrrhotite in contact metamorphic limestones is the most promising magnetic carrier as it forms mainly in the SD particle range during prograde metamorphism³. Its low Curie temperature of $\sim 330^\circ\text{C}$ allows recording of a full TRM. In addition, pyrrhotite in low grade metamorphic limestones has been proved to be a stable remanence carrier⁴. A suitable setting for such a scenario is found in Central Elba, where rapid cooling ($1-10^\circ\text{C}/\text{kyr}$) is assured by the intrusion of Miocene (7.4 Ma) laccolithic bodies^{5,6} (thickness < 700 m) into marly limestones (complex IV after ref.7).

6.2 Remanence directions:

Pyrrhotite and in a lesser amount magnetite were identified by the unblocking spectra of NRM and IRM using a 2G Enterprises RF SQUID magnetometer in combination with a MMTD1 thermal demagnetizer (Magnetic Measurements). Thermal demagnetization of the NRM of 18 samples (taken from one site across ~ 10 m) exhibits a two-component (characteristic remanences ChRM1 + ChRM2) behavior in the blocking temperature range of pyrrhotite in all measurements. Above the Curie temperature of pyrrhotite a residual remanence (ChRM3) exists, probably carried by magnetite (Fig. 6.2). The change of susceptibility measured after each temperature step is negligible.

The pyrrhotite components ChRM1 and ChRM2 are nearly antiparallel with a broad transition zone of up to 40°C ($250-290^\circ\text{C}$) in between. Both components show a negative fold test at 99% confidence level⁸ with a best grouping at 7% unfolding ($k_{\text{ChRM1}}=10.2$, $k_{\text{ChRM2}}=20.4$). It demonstrates that both components were recorded after folding and thus the TRM is secondary.

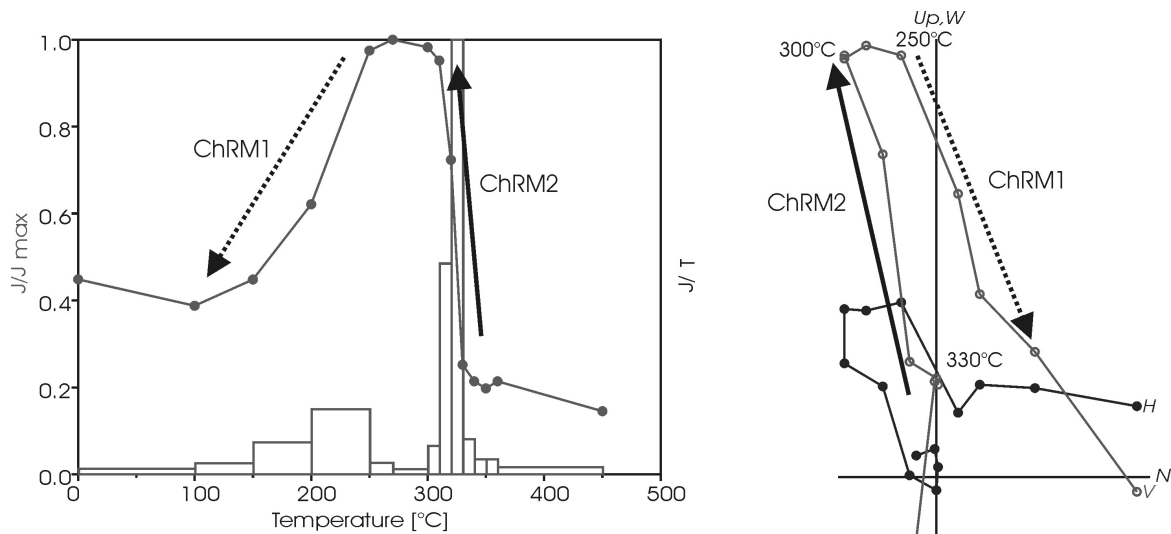


Figure 6.2: Thermal demagnetization of NRM. Left: Intensity variation. Right: Orthogonal vector plot. In the vertical projection the low (ChRM1) and high (ChRM2) unblocking components are indicated.

6.3 Quality of pTRM recording:

Thellier-Thellier tests on a laboratory induced TRMs ($90 \mu\text{T}$) including MD checks were performed to select suitable samples for further analysis of the NRM record. Chosen quality criteria were (i) MD contribution less than 5% and (ii) an accuracy within 10% for intensity determination obtained by laboratory TRM experiments. These criteria were fulfilled by about 50% of the samples tested. FORC analysis on selected samples indicate a SD to lower PSD grain-size distribution with a negligible amount of particle-particle interaction.

Laboratory TRMs with different field directions during cooling of the sample were performed using a homemade furnace. Designed for a single sample the temperature control in the furnace was monitored by two thermoelements in direct vicinity of the sample. The magnetic field was applied in an x-y plane and linked to the temperature obtained by the thermocouples using a self-written computer control. After heating to 350°C , an external field was applied in the +z direction while cooling. At 300°C and 250°C the field direction was changed by 90° (to +x and -z direction, respectively). During each change, the samples were brought into thermal equilibrium to avoid thermal gradients in the samples. The whole recording process took about 24h and was successfully performed on six samples with suitable recording qualities.

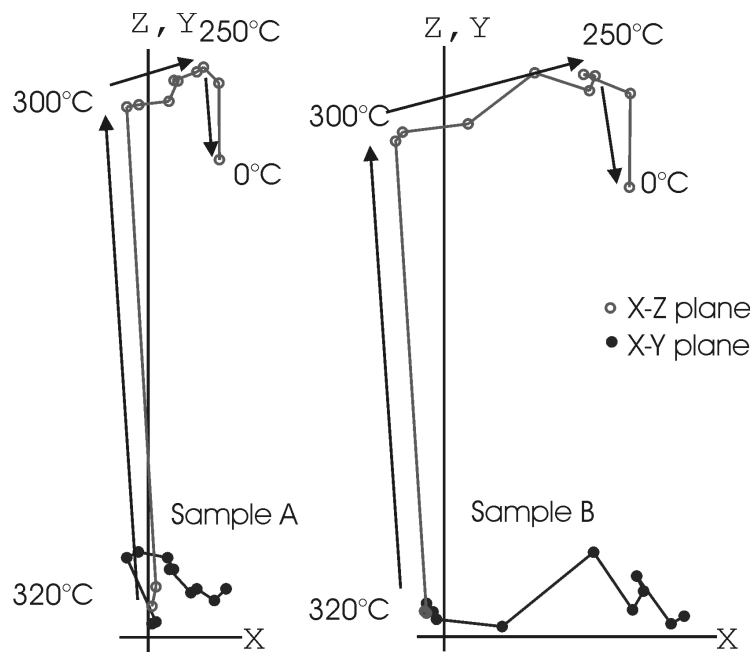


Figure 6.3: Two examples of the pTRM recording during laboratory experiments using different field direction. Arrows in the orthogonal vector plot indicate the directions of the applied fields.

The results (Fig. 6.3) show that in a directional sense the three perpendicular components were well recorded. It can be clearly seen that in comparison to the NRM record the low temperature component ($<250^{\circ}$) is small. This could be the consequence of the different recording times between the laboratory experiment (minutes) and the natural process (kyr), and also may reflect variations in the Earth magnetic field intensity. -

6.4 Thermal Modeling:

To convert the T_B spectra of pTRM acquisition into geological times it is important to know the metamorphic peak temperature of the sampling site and the temperature-time history after passing through the Curie temperature. A peak temperature above the Curie temperature is necessary to achieve a full TRM recording and to reject the possibility that the remanence is due to grain growth during prograde metamorphism (thermochemical).

For thermal modeling of the contact metamorphic temperature-time paths in the metacarbonates in respect of the distance towards the intrusive contact we used the one-dimensional stationary differential equation⁹ valid for conductive heat flow. The default

geological setting for this model is a vertical intrusive slab, extending infinitely in directions perpendicular to the profile (Appendix 1). The distance between the sampled site and the contact is about 70 m. As uplift and erosion will change the biasing country rock temperature (T_0), temperatures-time evolution was modeled with both, constant T_0 and an exponentially decreasing T_0 (from 120°C to about 50°C in 1Myr). Both results can be seen as two extreme cases for cooling.

In terms of the distance towards the contact, the model predicts the acquisition of a full TRM (Fig. 4) at 70 m distance towards the contact. In terms of cooling behavior, the different results are quite similar for the upper temperature interval, but diverge significantly for the lower part.

Using the results from T_0 =var., the temperature at 70 m distance in the system has dropped below 330°C after ≈ 2.8 kyr. Blocking ceases in the model around 100°C, which is reached

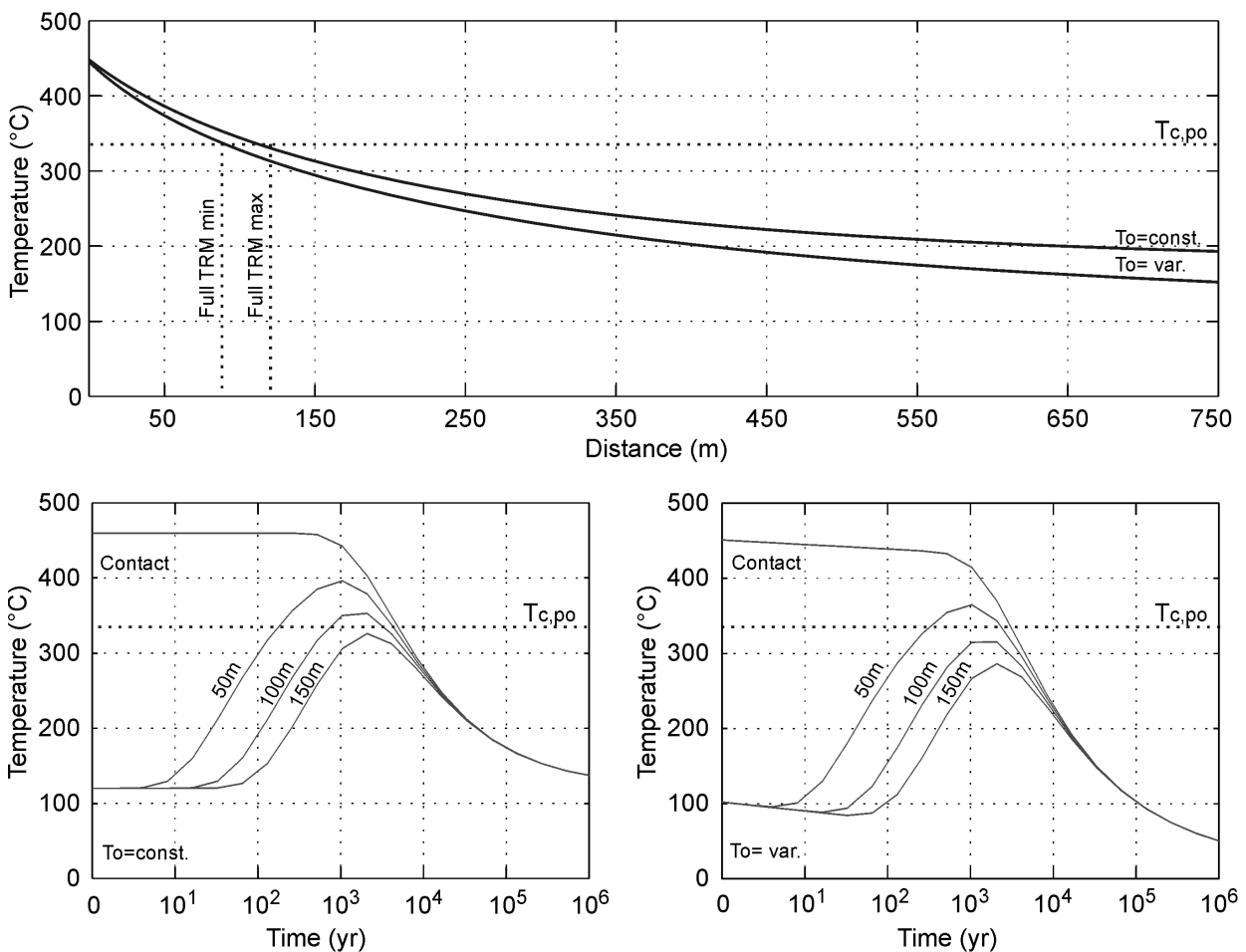


Figure 6.4: Thermal modeling of the temperature-time-distance behavior in the contact metamorphic aureole. Upper graph: Maximum temperatures versus distance to the contact towards the dyke with constant and variable country rock temperature T_0 . Lower Graphs: Temperature-time behavior at different distances towards the contact. At the left graph, T_0 is constant, whereas at the right one, T_0 decreases exponentially with time.

after $10^5 \approx 100$ kyrs. For the model with a fixed country rock temperature of 120°C (equivalent to a depth of about 2km), the model reaches the 150°C isotherm after about 300kyrs. In nature, where cooling also goes along with the uplift of the sequence, remanences acquisition at temperatures lower than 120°C are reasonable.

6.5 Paleointensity determination:

In general, paleointensity calculations are made on unidirectional components of the NRM. As in our case the NRM consists of a number of different components, common methods of intensity determination like the Thellier method¹⁰ or its derivatives¹¹ cannot be strictly applied. To overcome this, we calculated the intensity of each demagnetization step and, by adding all values up, recalculated the NRM intensity loss as it would be for a single component without changes in the EMF direction during recording.

The resulting NRM intensity decay was compared with the intensities obtained during the experiments on laboratory induced pTRMs. The latter were performed after NRM demagnetization using the same samples. But as cooling in the furnace is much faster than in nature we first transformed the unblocking temperatures from laboratory demagnetization into their natural equivalents (TRM trans., Fig. 6.5) using the time-temperature relation for pyrrhotite¹². The equivalent cooling times for each temperature step were taken from the thermal model. Finally, we interpolated the laboratory TRM curve (TRM inter, Fig. 6.5) to match with the demagnetization temperatures of the NRM demagnetization.

By comparing the NRM intensity loss with the transformed TRM gained one gets the paleofield strength by multiplying the slope between each temperatures step with the applied field during laboratory TRM acquisition ($90\mu\text{T}$).

Paleointensities of the low temperature range up to the 200°C - 250°C demagnetization step are similar to the present day value of the EMF for Elba ($46,15\mu\text{T}$ after IGRF 2000) and are corresponding to a mean VDM of $7.5 \cdot 10^{22} \text{ Am}^2$ (average of 100° , 150° and 200° , Fig. 5c). The relatively low paleointensity of the 30°C - 100°C component can be attributed to the presence of VRM overprints and, therefore, is regarded as unreliable. A pronounced intensity minimum ($< 10\%$ of the present field) can be seen at higher temperatures.

The intensity vs. time behavior is estimated using the cooling curves obtained by the thermal model (Fig. 6.5c) is added. As the reversal is not completely recorded, only a tentative estimate of its duration can be given by the time between the field minimum (300°C) and

normal field values (250°C). If the intensity behavior of the reversal is symmetrical, its duration is between 6 kyr and 19 kyr depending on the different thermal models.

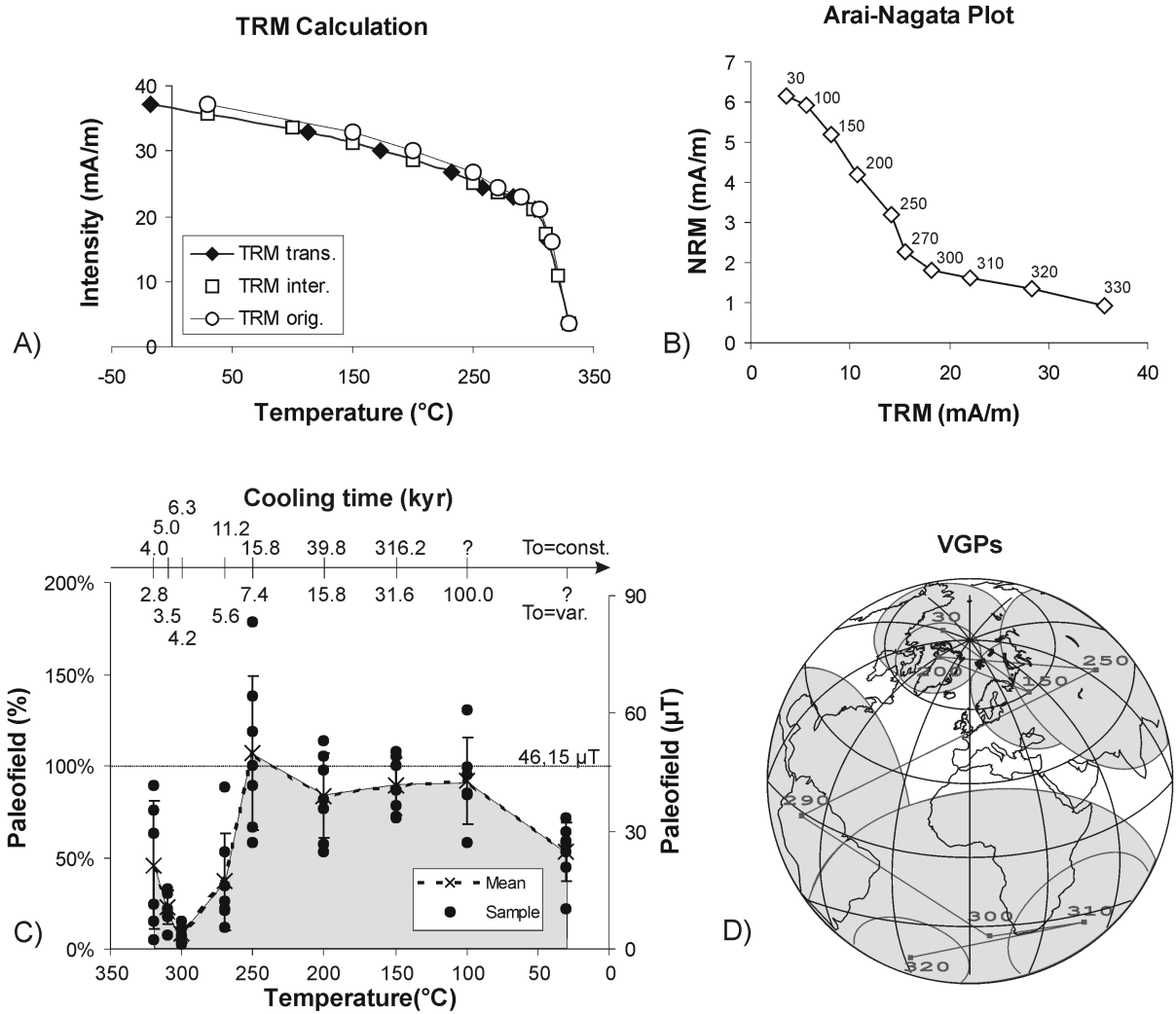


Figure 6.5 A: Laboratory TRM curve of one sample: The original temperatures (TRM orig.) were transformed according to natural cooling times (TRM trans.) after Dunlop et al. (2000). TRM inter. represents the temperature steps selected for NRM demagnetization. B: Example of an Arai-Nagata Plot, where the lined up NRM is compared with the transformed TRM. C: Paleointensities (in μT and % of present day field) obtained from the different demagnetization steps of the selected samples (black dots), where the temperature marks the lower demagnetization temperature of unblocking interval (i.e. component blocked between 200°C to 150°C is shown at 150°C, etc.). The mean and standard deviation of each temperature step is shown. The two cooling times on top are taken from the different thermal models (see Fig. 6.4). D: VGPs of the different components including α_{95} (gray circles).

6.6 Conclusions:

The NRM demagnetization spectra of contact metamorphic limestones for Central Elba exhibits a secondary TRM acquired during late Miocene cooling. Rock magnetic properties as derived from laboratory Thellier experiments (SD particle behavior) and FORC analysis (no

interaction) allow us to interpret the record as a succession of independent pTRMs. The existence of two major nearly antipodal components (ChRM1+ChRM2) with a transitional range of about 40°C opens the possibility to resolve a continuous record of an EMF reversal. This view is strengthened by the estimation of the paleointensities of the individual demagnetization steps, which are similar to the present EMF of Elba, but decrease within the interval to values below 10% of the present field during the transition. Using one-dimensional cooling models of a dyke and assuming a symmetrical behavior of the reversal allows us to estimate the duration of the reversal of about 6-19kyr. VGPs (Fig. 5d) calculated from the different demagnetization steps are following a reversed to normal direction. As the field transition is not completely covered by the NRM spectra the angle between the two major components is less than 180°C and the paleointensities at higher demagnetization temperatures are still below the normal field values.

6.7 References:

- (1) Leonhardt, R. & Soffel, H. A reversal of the Earth's magnetic field recorded in mid Miocene lava flows of Gran Canaria, Paleointensities. *J. Geophys. Res.* 107(B11), 2299 (2002) doi:10.1029/2001JB000949.
- (2) Merrill, R. T. & McFadden, P., L. Geomagnetic Polarity transitions. *Rev. Geophys.* 37 (2), 201-226 (1999).
- (3) Rochette, P. Metamorphic control of the magnetic mineralogy of black shales in the Swiss Alps: toward the use of "magnetic isogrades". *Earth Planet. Sci. Lett.*, 84, 446-456 (1987).
- (4) Crouzet, C., Stang, H., Appel, E., Schill, E. & Gautam, P. Detailed analysis of successive pTRMs carried by pyrrhotite in Himalayan metacharbonates: an example from the Hidden Valley, Nepal, *Geophys. J. Int.*, 146, 607-618 (2001).
- (5) Venzlaff, V. & Waldeck, H. Geochemical Investigations on the Island of Elba: 2. Age Dating of Central and Western Elba Granites – A Comparison. *N. Jahrb. Min. Ab.*, 120 (3), 315-323 (1974).
- (6) Rocchi, S., Westermann, D.S., Dini, A., Innocenti, F., & Toranin, F. Two-stage growth of laccoliths in Elba Island, Italy, *Geology*, 30 (11), 983-986 (2002).
- (7) Trevisan, L., 1950. L'Elba orientale e la sua tettonica di scivolamento per gravità, 15. Università, Istituto di Geologia e Paleontologia. Memorie, Padua, pp.40.
- (8) McFadden, P.L. & Jones, D.L. The fold test in palaeomagnetism. *Geophys. J. R. Astron. Soc.*, 67, 53-58 (1981).
- (9) Peacock, S.M. Thermal modeling of metamorphic pressure-time-temperature paths: a forward approach, in: *Metamorphic pressure-time-temperature paths*, 7, AGU (1989).
- (10) Thellier, E. & Thellier, O. Sur l'intensité du champ magnétique terrestre dan le passé historique et géologique, *Ann. Géophys. Res.*, 101, 25.029-25.044 (1959).
- (11) Coe, R.S. Paleointensities of the Earth's magnetic field determined from Tertiary and Quartery rocks, *J. Geophys. Res.*, 72, 3247-3267 (1967).
- (12) Dunlop, D.J., Özdemir, Ö., Clark, D.A. & Schmidt, P.W. Time-temperature relations for the remagnetization of pyrrhotite (Fe₇S₈) and their use in estimating paleotemperatures, *Earth Planet. Sci. Lett.*, 176 (1), 107-116 (2000).

Chapter VI

- (13) Daniel, J.-M. & Jolivet, L. Detachment faults and pluton emplacement: Elba Island (Tyrrhenian Sea). *Bull. Soc. Géo. France*, 166 (4), 341-354 (1995).
- (14) Angenheister, G. (editor) *Numerical Data and functional Relationship in Science and Technology*, Springer Verlag, 1a, 328-329 (1982)

The TRM furnace

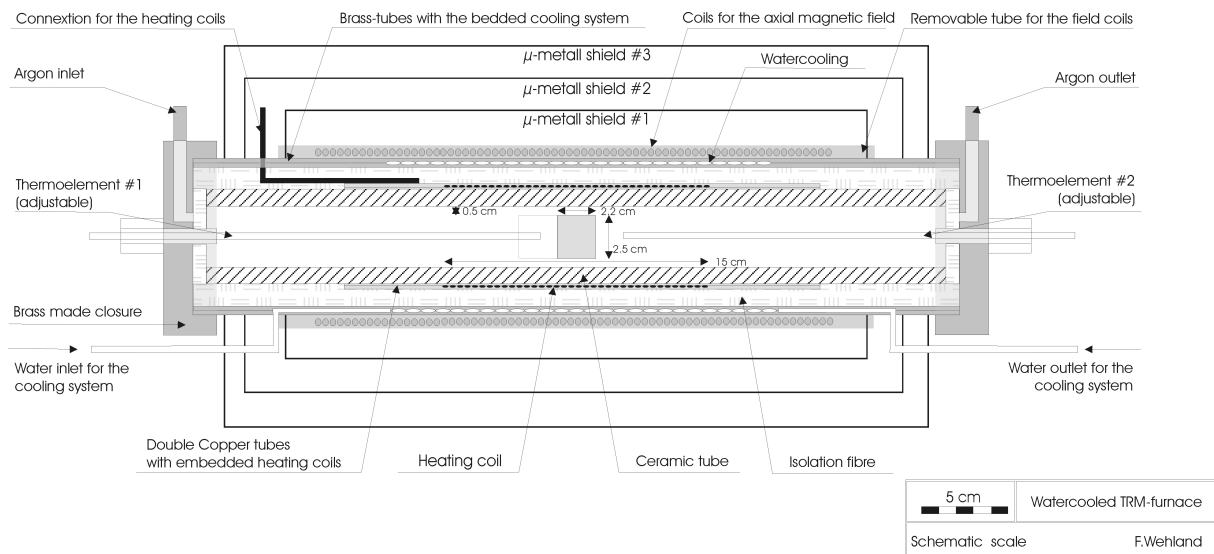


Figure A.1: Schematic drawing of the structural design of the furnace

The aim of the furnace development was realised by a symmetrical design around a single sample (Fig. A.1), which allows a perfect temperature control. The sample is placed into a quartz-glass holder, which is surrounded by a ceramic tube (polished Al_2O_3 -tube, Friatec AG, Germany). Coated on this is the heating system, which consists of a bifilar heating wire (Thermocoax GmbH, Germany) embedded into two copper tubes. The copper tubes are reduced in length compared to the full length of the furnace. This will assure a maximum of thermal homogeneity and a small thermal gradient within the sample area. The subsequent cooling system consists of two brass tubes in which the water cooling is milled. The cooling and heating system are separated by an isolation-layer of ceramic fibre (Rath GmbH, Germany) for enlarging the thermal gradient between them.

On top of it a removable tube carries the coils for the magnetic field. Number and extension of the windings was calculated in such a way that the gradient of the magnetic field in the vicinity of the sample is negligible. The whole system is protected against the influence of the Earth magnetic field by a three layered μ -metal shield (Magnetic Shields Ltd., UK). The length and diameter are calculated that the shielding is optimised for the sample area including the place for the dummy samples only. The shield can be removed for the sake of the second coil system. With the second coil system a field can be imparted perpendicular to the primary field. Both ends are closed with a brass made closure including the input for the adjustable thermoelements and the milled in Argon Inlet/Outlet. The thermoelements themselves can be placed along the entire length of the oven either open or imbedded in a

dummy sample. A third thermoelement is placed outside the furnace to check the proper functionality of the cooling system.

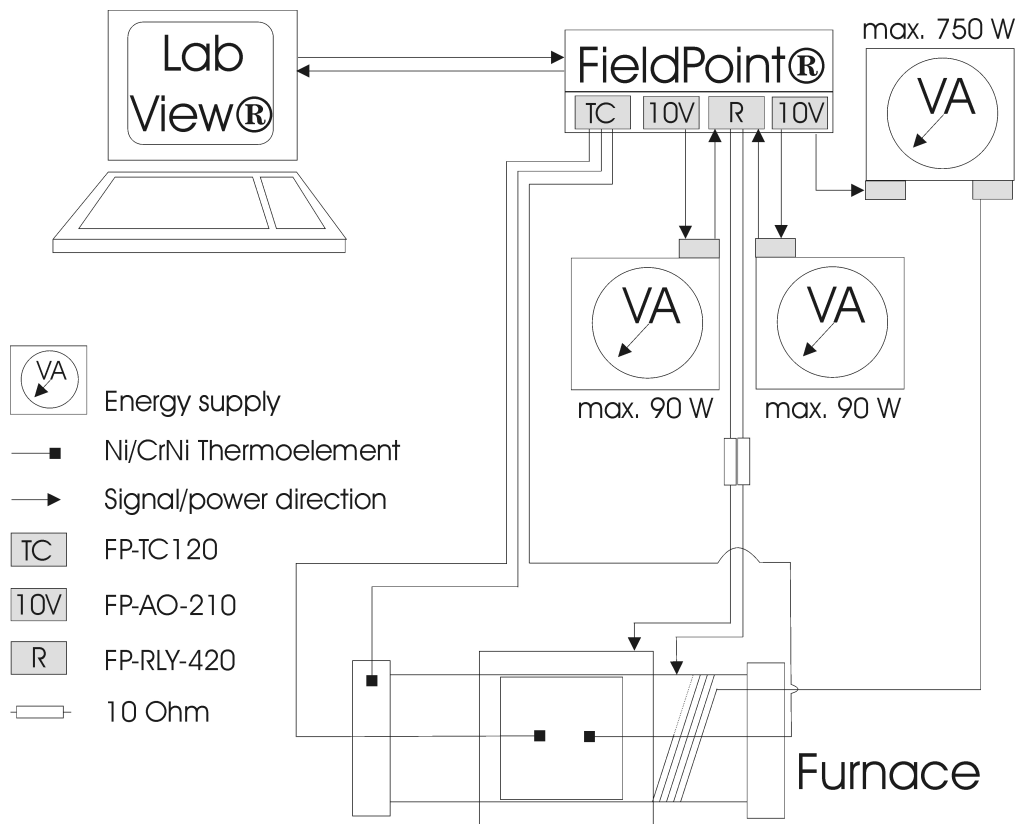


Figure A.2: Schematic configuration of the furnace control

To furnace is controlled by a LabView[®] (National Instruments) written program. An attached FieldPoint[®]-system (National Instruments) serves as the I/O and relay tool to communicate with the energy supply for the heating system and magnetic field coils (Fig. A.2). The software controls the temperature and the field strength by a simple V-T and V-H relationship. The output for the later one goes through a relay to switch the direction of the current and therefore of the magnetic field.

The voltage-temperature relation is obtained by various calibration experiments with a sample containing one thermoelement inside and one outside. The relation is given as

$$\text{Temperature (}^{\circ}\text{C)} = 50,807 * \text{Voltage (V)} - 138,92$$

with $R^2 = 0,9978$ (valid for a water flux of the cooling system of 0.5 l/min). A change in the water flux of the cooling does have a significant impact on the maximal temperatures reached (max. variation $\sim 40^\circ\text{C}$).

Vorrichtung zum punktuellen Aufheizen von Proben in einer sensitiven Umgebung

Die Erfindung betrifft eine Vorrichtung zum punktuellen Erhitzen von Proben in einer sensitiven Umgebung, wobei Energie von einer polychromatischen nichtkohärenten Energiequelle übertragen wird, die in einer Entfernung zur Probe positioniert ist.

Das Problem des Aufheizens von Proben in einer empfindlichen Umgebung ist lange bekannt. Zu den empfindlichen Umgebungen kann beispielsweise ein korrosives oder toxisches Umfeld oder auch ein magnetisch feldfreier Raum gezählt werden.

Bekannte Heizverfahren bedienen sich entweder einer gewöhnlichen Heizwendel oder der Lasertechnologie. Ersteres besitzt aufgrund des angelegten Stroms und des verwendeten Materials ein hohes magnetisches Moment und kann somit nicht verwendet werden, wenn eine Aufrechterhaltung von magnetisch feldfreiem Raum erwünscht ist. Außerdem kann eine Heizwendel wegen einer geringen chemischen Resistenz in einer chemisch aggressiven Umgebung, wie beispielsweise einem stark oxidierenden oder reduzierenden Umfeld, nicht eingesetzt werden. Ein weiterer Nachteil von Heizwendeln ist ihre schlechte Fokussierbarkeit der abgegebenen Wärmestrahlung. Die Lasertechnologie ermöglicht zwar eine gute Fokussierung des Wärmestrahls sowie eine Energieübertragung über eine Distanz, ist jedoch relativ teuer.

Die Erfindung stellt sich demzufolge die Aufgabe, eine preiswerte Vorrichtung zum punktuellen Aufheizen von Proben in einer sensitiven Umgebung bereitzustellen, welche die Nachteile der bekannten Vorrichtungen überwinden soll.

Diese Aufgabe wird durch die Vorrichtung mit den Merkmalen des Anspruchs 1 gelöst. Bevorzugte Ausführungsformen dieser Vorrichtung sowie ihre Verwendung sind in den abhängigen Ansprüchen 2 bis 10 beschrieben. Der Wortlaut sämtlicher Ansprüche wird hiermit durch Bezugnahme zum Inhalt dieser Beschreibung gemacht.

Die Aufgabe wird durch eine Vorrichtung gelöst, die als Kernkomponente einen Stab oder eine Faser aus einem für infrarote Strahlen durchlässigen Material enthält, wobei dieser Stab oder die Faser zwischen einer polychromatischen nichtkohärenten Lichtquelle und der zu erhitzenden Probe positioniert ist.

In einer besonders bevorzugten Ausführung werden als Material für den Stab oder die Faser Quarz oder Quarzglas verwendet. Die an einem Ende des Stabs bzw. der Faser einfallende

Wärmestrahlung von einer Lichtquelle wird an der Grenze Material / Luft im Inneren des Stabes bzw. der Faser mehrfach reflektiert. Die am anderen Ende des Stabes bzw. der Faser austretende Strahlung enthält Infrarotstrahlen von relativ großer Intensität. Diese Intensität reicht aus, um Proben, die am anderen Ende des Stabs bzw. der Faser positioniert sind, auf mehrere Hundert Grad zu erhitzen. Im Falle von z.B. Quarzglas sind die Absorptionsbanden im Infrarot relativ schmal, sodass dies z.B. bei einem zylindrischen Stab mit einem Durchmesser von 23 cm zu einem Aufheizen von nur den ersten 10 cm des Stabes führt. Der Rest des Stabes bleibt kühl, so dass die Umgebungsluft nicht erwärmt wird.

Die erfindungsgemäße Vorrichtung funktioniert somit nach dem Prinzip eines Lichtleiters zur Übertragung von insbesondere Infrarotstrahlen. Weil mit dem vorliegenden Verfahren Infrarotstrahlen über weitere Distanzen fast verlustfrei übertragen werden können, kann eine Energie- oder Lichtquelle verwendet werden, die im Gegensatz zum teureren Lasergerät ein polychromatisches nicht kohärentes Licht ausstrahlt. In einer einfachsten Ausführung kann eine Heizlampe oder gewöhnliche Glühbirne die Lichtquelle darstellen.

Die Intensität und die spektrale Zusammensetzung des einfallenden Lichtes sowie die Wahl des Materials beeinflussen die Intensität und die Länge der austretenden Strahlen. Eine Variation dieser Parameter kann erfindungsgemäß dazu genutzt werden, die gewünschte Temperatur der zu erheizenden Probe einzustellen. Die einfachste Methode zur Einstellung der gewünschten Temperatur ist dabei die Regulierung der Intensität der thermischen Quelle.

In einer bevorzugten Ausführung hat die erfindungsgemäße Vorrichtung eine zylindrische Form. Alternativ kann sie jedoch auch andere Formen aufweisen, beispielsweise konische Form, wobei der Durchmesser des Stabes von der Lichtquelle ausgehend kontinuierlich leicht abnimmt.

Die Verwendung eines Stabes bzw. einer Faser mit einem kleinen Durchmesser ermöglicht eine sehr gute Fokussierung der Strahlen, so dass die Probe punktuell erhitzt werden kann. Dies kann insbesondere vorteilhaft sein, wenn eine Erhitzung der umgebenden Luft bzw. des umgebenden Mediums oder von Gegenständen vermieden werden soll, z.B. beim Vorliegen von toxischen oder explosiven Substanzen. Durch eine Variation des Durchmessers des Stabes bzw. der Faser kann die Größe der zu erheizenden Fläche beeinflusst werden.

Bei schwer zugänglichen Proben empfiehlt sich, eine biegsame Faser als Strahlenleiter zu verwenden. Auf diese Weise können selbst Proben erreicht werden, die durch weitere Gegenstände verdeckt oder ungünstig positioniert sind.

Die Entfernung zwischen der Energiequelle und der zu erhitzenden Probe kann zwischen wenigen Millimetern und mehreren Metern betragen. Dementsprechend können der lichtleitende Stab bzw. die lichtleitende Faser, die zwischen der Energiequelle und der Probe platziert sind, abhängig vom Versuchsaufbau unterschiedliche Längen aufweisen, von wenigen Millimetern bis zu mehreren Metern.

Da die bevorzugt verwendeten Materialien, insbesondere das Quarzglas, chemisch stark resistent sind, bietet sich eine Reihe von Anwendungen der erfindungsgemäßen Vorrichtung, die mit herkömmlichen Vorrichtungen nicht oder stark eingeschränkt möglich sind. Im Gegensatz zur bekannten Heizspule kann die erfindungsgemäße Vorrichtung wegen der chemischen Resistenz der Strahlenleiter-Komponente auch in einem stark oxidierenden oder reduzierenden Umfeld eingesetzt werden. Dabei kann das Umfeld sowohl ein Gas oder ein Gasgemisch als auch eine Flüssigkeit sein.

Von den in Frage kommenden Materialien für den Strahlenleiter zeichnet sich das Quarzglas auch wegen seiner unmagnetischen Eigenschaften aus. Dies ermöglicht seine Verwendung als Strahlenleiter bei Fragestellungen, bei denen Proben in einem magnetisch feldfreier Raum erhitzt werden sollen (s. Beispiel unten).

Im Vergleich zum Laser wird die Anwendung der erfindungsgemäßen Vorrichtung nicht durch atmosphärische Veränderungen wie Staub, Dämpfe o. ä. gestört. Daraus ergeben sich Anwendungen insbesondere im Bereich der verarbeitenden Industrie, wie z.B. Oberflächenbehandlung bei verschiedenen Atmosphären oder in flüssigen Medien. Zum weiteren Vorteil der erfindungsgemäßen Vorrichtung gegenüber einer Laservorrichtung zählt auch ihr geringer Preis.

Das Aufheizen des Probematerials mit der erfindungsgemäßen Vorrichtung auf mehrere Hundert Grad kann dazu genutzt werden, über eine Distanz gewünschte Veränderungen im Probematerial gezielt hervorzurufen, wie beispielsweise Verformung, Thermolyse, Ein- oder Auslöten von Teilen o. ä. Die dazu notwendige thermische Energie kann dabei über einen berührungslosen Vorgang von der Energiequelle auf die zu verändernde Probe punktuell übertragen werden.

Zusammenfassend liegen die Vorteile der Vorrichtung darin, dass sie relativ verlustfrei ohne Einfluss auf die chemische Zusammensetzung und magnetischen Zustand im Proberaum thermische Strahlung über längere Distanzen übertragen kann und dabei preiswert ist.

Weitere Vorteile, Merkmale und Anwendungsmöglichkeiten der Erfindung werden nachstehend anhand eines Ausführungsbeispiels mit Bezug auf die Zeichnung beschrieben:

Abb. 1: Eine Ausbildung der erfindungsgemäßen Vorrichtung zur Erhitzung einer Probe in einem magnetisch feldfreier Raum in einem SQUID Magnetometer

Ausführungsbeispiel

Thermische Behandlung im magnetfeldfreien Raum mittels eines Quarzglasstabes

Ziel dieser Ausführung der Erfindung ist das Aufheizen einer Probe zur Messung der magnetischen Remanenz in einem magnetisch feldfreien Raum bei verschiedenen Temperaturen.

Zur Aufheizung der Probe muss die thermische Energie über eine Strecke von ca. 80 cm übertragen werden, ohne dabei magnetische Felder zu erzeugen oder das Messgerät zu beschädigen. Dies wurde mittels eines Quarzglasstabes bewerkstelligt, der nach dem Prinzip der Lichtleitung die thermische Energie einer Heizlampe auf die Probe überträgt.

*Die Realisierung des Wärmetransports von der Hochtemperaturlampe (1000 W Lampe der Firma Xerion GmbH, Freiberg i.Br.) erfolgte mittels eines zylindrischen Quarzglasstabes (\emptyset 23 mm, Länge 900 mm, feuerpolierte Enden, SemiQuarz GmbH) entsprechend dem Aufbau in **Abb. 1**. Bei dieser Lösung ist die Übertragung der thermischen Energie auf die Probe beschränkt. Der Quarzglasstab wird dabei nur innerhalb der ersten Zentimeter erhitzt.*

Wichtig für die Umsetzung war die Voraussetzung, dass alle Bauteile unmagnetisch sind, um die Messergebnisse nicht zu stören. Aufgrund der vernachlässigbaren Wärmeabgabe des Quarzglasstabes konnten die internen Halterungen (removable props) aus einfachen PVC gefertigt werden.

Im Vergleich zur bisherigen Lösung, bei der die thermische Behandlung extern erfolgt, ist diese Technik besonders zeitsparend. Die Demagnetisierung einer Probe im Normalverfahren dauert ca. 1-3h für 10 Datenpunkte im gewählten Temperaturbereich. Mit der neuen Methode lässt sich eine Probe in 500 sec demagnetisieren mit der Gewinnung von 500 Datenpunkten.

Die beschriebene Ausführung der Vorrichtung ermöglicht zum ersten Mal das Messen von magnetischer Remanenz bei variablen Temperaturen in einem cryogenen Magnetometer.

Die bevorzugten Ausführungsformen und Beispiele für die erfindungsgemäße Vorrichtung sind lediglich als beschreibende, keineswegs als in irgendeiner Weise limitierende Offenbarung aufzufassen.

Patentansprüche

1. Vorrichtung zum punktuellen Erhitzen einer Probe in einer sensitiven Umgebung, wobei die zum Erhitzen notwendige Energie von einer polychromatischen nichtkohärenten Lichtquelle enthaltend infrarote Strahlung übertragen wird, die in einer Entfernung zur Probe positioniert ist, **dadurch gekennzeichnet**, dass die Energieübertragung nach dem Lichtleiterprinzip über einen Stab oder eine Faser aus einem für infrarote Strahlen durchlässigen Material erfolgt, wobei dieser Stab bzw. die Faser zwischen der Lichtquelle und der zu erhitzenden Probe positioniert ist.
2. Vorrichtung nach Anspruch 1, dadurch gekennzeichnet, dass das Material für den Stab oder die Faser Quarz oder Quarzglas, ist.
3. Vorrichtung nach einem der vorhergehenden Ansprüche, dadurch gekennzeichnet, dass der Stab oder die Faser eine zylindrische oder leicht konische Form aufweist.
4. Vorrichtung nach einem der vorhergehenden Ansprüche, dadurch gekennzeichnet, dass der Stab oder die Faser eine Länge zwischen wenigen Millimetern und mehreren Metern aufweisen kann.
5. Vorrichtung nach einem der vorhergehenden Ansprüche, dadurch gekennzeichnet, dass die Lichtquelle eine Heizlampe oder eine Glühbirne ist.
6. Vorrichtung nach einem der vorhergehenden Ansprüche, dadurch gekennzeichnet, dass die Temperatur der zu erhitzenden Probe durch die Intensität und die spektralen Eigenschaften der verwendeten Lichtquelle und die Wahl des Materials des Stabes bzw. der Faser einstellbar ist.
7. Vorrichtung nach einem der vorhergehenden Ansprüche, dadurch gekennzeichnet, dass die Größe der zu erhitzenden Fläche der Probe durch den Durchmesser des Stabes bzw. der Faser an dem der Probe zugewandten Ende einstellbar ist.
8. Vorrichtung nach einem der vorhergehenden Ansprüche, dadurch gekennzeichnet, dass bei einer schwer zugänglichen zu erhitzenden Probe zur Energieübertragung eine biegsame Faser verwendet wird.
9. Verwendung der Vorrichtung nach einem der vorhergehenden Ansprüche in einer sensitiven Umgebung, insbesondere in einem chemisch aggressiven, z.B. stark

oxidierenden oder reduzierenden, einem toxischen, explosiven Umfeld oder in einem magnetisch feldfreiem Raum.

10. Verwendung der Vorrichtung nach einem der vorhergehenden Ansprüche zur Veränderung der zu erhitzenden Probe, insbesondere zu Verformung, Thermolyse, Ein- oder Auslöten von Probeteilen.

Zusammenfassung

Die Erfindung betrifft eine Vorrichtung zum punktuellen Erhitzen einer Probe in einer sensitiven Umgebung, wobei die zum Erhitzen notwendige Energie von einer polychromatischen nichtkohärenten Lichtquelle enthaltend infrarote Strahlung übertragen wird, die in einer Entfernung zur Probe positioniert ist. Die Vorrichtung ist dadurch gekennzeichnet, dass die Energieübertragung nach dem Lichtleiterprinzip über einen Stab oder eine Faser aus einem für infrarote Strahlen durchlässigen Material erfolgt, wobei dieser Stab bzw. die Faser zwischen der Lichtquelle und der zu erhitzenden Probe positioniert ist. Als bevorzugtes Material für den Stab bzw. die Faser wird Quarz oder Quarzglas verwendet. Die Erfindung kann dazu genutzt werden, um Proben in einer sensitiven Umgebung, wie z.B. in einem chemisch aggressiven, toxischen, explosiven Umfeld oder in einem magnetisch feldfreiem Raum, aufzuheizen und / oder durch thermische Energie zu verändern.

1 / 1

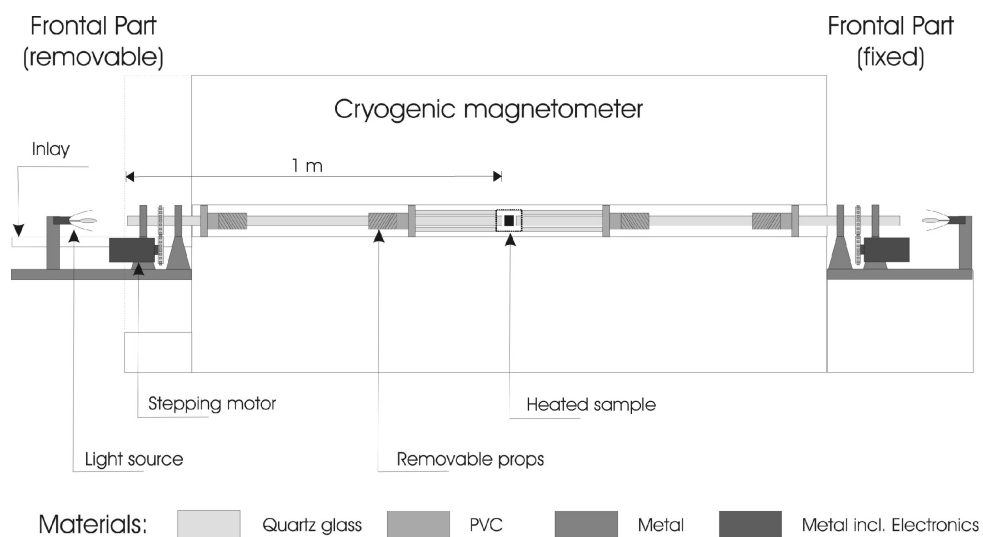


Abb. 1

29-MAR-04 MO 13:55

ABT. FORSCHUNGSKONTAKTE

FAX NR. +49 7071 295866

S. 1

W-6.4.04

An das
Deutsche Patent- und Markenamt
80297 München

DEUTSCHES PATENT- UND MARKENAMT

(1) In der An-
schrift Straße,
Haus-Nr. und
ggf. Postfach
angeben

Sendungen des Deutschen Patent- und Markenamts sind zu richten an:
Universität Tübingen
Abteilung Forschungskontakte
Wilhelmstr. 5
72074 Tübingen

Antrag
auf Erteilung
eines Patents

1

Wahrmark nicht
bei PTT-Vor-
schriften ver-
wenden
Rückseite

TELEFAX vorab am 29.03.2004
Aktenzahl
10 2004 015 732.4

(2) Zeichen des Anmelders/Vertreters (max. 20 Stellen)
038F>Wehländ

Telefon des Anmelders/Vertreters
07071/2976788

Datum
29.03.2004

(3) Der Empfänger in Feld (1) ist der

Anmelder Zustellungsbevollmächtigte Vertreter

ggf. Nr. der Allgemeinen Vollmacht

nur auszu-
füllen, wenn
streichend
von Feld (1)
Hauptregis-
trations-
nummer
oder bei Firmen
angeben

(4) **Anmelder**
Universität Tübingen
Wilhelmstr. 5
72074 Tübingen

Vertreter

Der Anmelder ist eingetragen im Handelsregister Nr. _____ beim Amtsgericht _____

(5) Anmeldercode-Nr.

Vertretercode-Nr.

Zustelladressecode-Nr.

ABT.

ERP

(6) Bezeichnung der Erfindung
s. auch
Rückseite
IPC-Vorschlag
ist unbedingt
anzugeben,
sofern bekannt

Vorrichtung zum punktuellen Aufheizen von Proben in
einer sensitiven Umgebung

IPC-Vorschlag d. Anmelders

(7) Erläuterung
u. Kosten-
hinweise
auf der
Rückseite

(7) Sonstige Anträge

Aktenzeichen der Hauptanmeldung (des Hauptpatents)

- Die Anmeldung ist **Zusatz** zur Patentanmeldung (zum Patent) →
- Prüfungsantrag** - Prüfung der Anmeldung mit Ermittlung der öffentlichen Druckschriften (§ 44 Patentgesetz)
- Rechercheantrag** - Ermittlung der öffentlichen Druckschriften ohne Prüfung (§ 43 Patentgesetz)
- Aussetzung des Erteilungsbeschlusses** auf _____ Monate (§ 49 Abs. 2 Patentgesetz)
(Max. 15 Mon. ab Anmelde- oder Prioritätstag)

(10) Erläuterung
und Kosten-
hinweise
Rückseite

(10) **Gebührenzahlung** in Höhe von **60** EUR

Einzugsermächtigung
Vordruck (A 9507) ist beigelegt

Überweisung (nach Erhalt
der Empfangsbescheinigung)

Abbuchung von meinem/unsrem Abbuchungskonto bei der
Dresdner Bank AG, München
Abbuchungsauftrag (V 1244) ist beigelegt

Wird die Anmeldegebühr nicht innerhalb von 3 Monaten nach dem Tag des Eingangs der Anmeldung gezahlt, so gilt die Anmeldung als zurückgenommen

(11) Anlagen
Anlagen 3 - 6,
max. 3-fach
s. auch
Rückseite

- | | | | |
|-------------|--|-------------|-------------------------------|
| 1. _____ | Vertretervollmacht | 5. <u>2</u> | Seite(n) Patentansprüche |
| 2. <u>1</u> | Erfindernennung | 6. <u>1</u> | Anzahl Patentansprüche |
| 3. <u>1</u> | Zusammenfassung
(ggf. mit Zeichnung Fig. _____) | 7. _____ | Blatt Zeichnungen |
| 4. <u>5</u> | Seite(n) Beschreibung
(ggf. mit Bezugszeichenliste) | 8. _____ | Abschrift(en) d. Voranmeld. |
| | | 9. _____ | Zitierte Nichtpatentliteratur |

Bracke Universität Tübingen
Abteilung Forschungs- Kontakte
Wilhelmstraße 5
72074 Tübingen
(Dr. F. Stracke)
(12) Unterschrift(en)

Nur von der Antragsstelle auszufüllen
Diese Patentanmeldung ist dem ...
Dieser Aktenzettel ist ...
Nummer (3 Rückseiten zu Feld (1)) zu versehen.

P 2007
12.02

Bitte beachten Sie die Hinweise
auf der Rückseite
der zurückgehaltenen Antragsdurchschrift

M 6
über Patentanträge eingegangen
an das Deutsche Patent-
und Markenamt

AXG3 Nr: 354611 von NVS:FAXG3.I0.0101/07071295866 an NVS:PRINTER.0101/HPLJMRS2 (Seite 1 von 11)
atum 29.03.04 14:50 - Status: Server MRSDPAM02 (MRS 4.00) übernahm Sendeauftrag
treff: 11 Seite(n) empfangen

Glossary:

A.F.	<i>Alternating field</i>
CEF	<i>Central Elba fault</i>
CRM	<i>Chemical remanent magnetization</i>
ChRM	<i>Characteristic remanent magnetisation</i>
DS	<i>Domain state</i>
EBF	<i>Eastern Border Fault (Elba)</i>
EMF	<i>Earth magnetic field</i>
f(X)	<i>Fugacity of fluid X</i>
FeO	<i>Iron oxides</i>
FORC	<i>First order reversal curves</i>
FWHH	<i>Full-width-at-half-height</i>
H _a	<i>Reversed field during FORC measurements</i>
H _b	<i>Measurement field during FORC measurements</i>
H _c	<i>Magnetic coercivity</i>
H _{paleo}	<i>Laboratory fieldstrength</i>
H _{paleo}	<i>Paleofieldstrength</i>
H _u	<i>Magnetic interaction in the FORC plane</i>
I _{po}	<i>Intensity of the magnetization carried by pyrrhotite</i>
IRM	<i>Isothermal remanent magnetization</i>
IRM _r	<i>Acquisition of IRM</i>
IRM _{dc}	<i>dc backfield demagnetisation of SIRM</i>
M(H _a ,H _b),	<i>Magnetization during FORC measurement</i>
MAD	<i>Mean angular deviation</i>
MD	<i>Multi domain</i>
M _{rs}	<i>saturation remanence</i>
M _s	<i>saturation magnetization</i>
NRM	<i>Natural remanent magnetization</i>
Po	<i>Pyrrhotite</i>
PSD	<i>Pseudo single domain</i>
PTRM	<i>Partial thermoremanent magnetization</i>
Pyr	<i>Pyrite</i>
SD	<i>Single domain</i>

SEM	<i>Scanning electron microscopy</i>
SF	<i>Smoothing factor during FORC processing</i>
SFD	<i>Switching field distribution</i>
SIRM	<i>Saturation remanence magnetization</i>
t_{avr}	<i>Averaged time during FORC measurements</i>
T_C	<i>Curie temperature</i>
T_B	<i>Blocking temperature</i>
$T_{max,po}$	<i>Upper pyrrhotite window temperature</i>
$T_{min,po}$	<i>Lower pyrrhotite window temperature</i>
T_{UB}	<i>Unblocking temperature</i>
TEM	<i>Transition electron microscopy</i>
TRM	<i>Thermoremanent magnetization</i>
TSS	<i>Tethyan Sedimentary Series</i>
W	<i>The ratios of χ_r and χ_{dc}</i>
ZDF	<i>Zucchale Detachment Fault</i>
$\rho(H_a, H_b)$	<i>FORC distribution</i>
χ_{dc}	<i>Differential susceptibility calculated from the IRM_{dc}</i>
χ_r	<i>Differential susceptibility calculated from the IRM_r</i>
ΔM	<i>Remanence based interaction parameter</i>
$\Delta M1$	<i>Position of the minima in the ΔM-plot</i>
$\Delta M2$	<i>Intensity of the minima in the ΔM-plot</i>
Δmag	<i>Difference in the remanent magnetisation during MD checks</i>
Δang	<i>Directional deviation during thermal demagnetisation</i>

Figure Captions:

- Figure I.1: Principle of pTRM recording in a single sample during metamorphic cooling (from left to right): the different directions of the EMF are recorded in the respective pTRMs. The direction of the EMF is marked with the arrow in the left upper half of the diagram. Gray boxes stand for individual unblocked pTRMs, white for blocked ones. The dashed line indicates the actual metamorphic temperature during cooling. The middle diagrams demonstrates the resulting net-intensity of the sample. $T_{c,po}$ is the Curie temperature of pyrrhotite. The lower diagram represents an orthogonal vector plot for demagnetisation. III
- Figure I.2: Steps to be taken in order to ensure pTRM recording within a single sample VII
- Figure I.3: Processing of metamorphic data. VIII
- Figure 1.1: (A) Cluster of framboidal pyrite grains (partly polished), (B) individual idiomorphic pyrrhotite grain (white arrow). Both pictures were made by SEM analysis. 3
- Figure 1.2: Pyrrhotite under TEM. The continuous structure (white arrow) in the pyrrhotite grain indicates chemical homogeneity. 4
- Figure 1.3: Elba limestones in transmitted light microscopy: A) large idiomorphic ore crystals in a blurry matrix. B) refilled crack with two generations of calcite crystals. 5
- Figure 1.4: Pyrrhotite (A) and pyrite (B) in the samples from Central Elba (Italy) using SEM. 6
- Figure 1.5: Reflected light microscopy of the samples of Isle of Skye. A) Large aggregates of pyrrhotite patches. B) Preserved cell structure of a plant. The carbon is transformed to graphite. 6
- Figure 1.6: Pyrrhotite in the samples from Isle of Skye. A) Abundance and grain-size spectrum. B) Pyrrhotite around an iron rich grain (possibly an iron carbonate). 7
- Figure 1.7: Transmitted light microscopy on samples from the contact metamorphic (A) and the regional metamorphic part (B). 7
- Figure 1.8: Cluster iron sulfids (A) and individual pyrrhotite grains (B) from the Manaslu area. 8
- Figure 1.9: Relative blocking temperature spectra derived from Thellier experiments on a laboratory induced TRM. A) Wide spectrum up to the Curie temperature of pyrrhotite. B) Narrow blocking temperature spectrum restricted to the lower unblocking range. 9
- Figure 2.1: Principle of pTRM recording in a single sample during metamorphic cooling (from left to right): the different directions of the EMF are blocked in the respective pTRMs. The direction of the EMF is marked with the arrow in the left upper half of the diagram. Gray boxes stand for individual unblocked pTRMs, white for blocked ones. The dashed line indicates the actual metamorphic temperature during cooling. The lower diagrams demonstrates the resulting net-intensity of the sample along the axis parallel to the primary EMF direction. $T_{c,po}$ is the Curie temperature of pyrrhotite. 13

- Figure 2.2:** Geological map of the eastern contact metamorphic area of the Manaslu granite (Nepal) modified after Fuchs and Paudel (1998). The geological profile of the central ridge (sampling positions 100-121) is made by own observation. Sampling positions are indicated with square boxes. The circles and arrows represent sampling sites and remanence directions as reported by Schill et al. (inpress). 15
- Figure 2.3:** Overview of the sampling area at the Isle of Skye (Scotland). A and B are profiles sampled with increasing distance towards the contact. C is the position of the conglomerate. D and E are individual sites. 16
- Figure 2.4:** Simplified geological map of the contact metamorphic parts of Elba Island (from W to E): Mt. Capanne, central Elba and Mt. Calamita. The cross-section through central Elba is redrawn after Rocchi et al. (2002), EBF- Eastern Border Fault; CEF – Central Elba Fault. 17
- Figure 2.5:** Examples of normalised IRM acquisition and thermal demagnetisation of the SIRM from different locations. The maximum applied field is 1500mT. 20
- Figure 2.6:** Successive thermomagnetic runs of sample 142 from the northern profile of the Manaslu area showing that besides initial differences pyrrhotite destruction starts at temperatures greater 420°C. 21
- Figure 2.7:** Magnetic susceptibility and pyrrhotite/magnetite ratio ($I_{pyr}/I_{mag+pyr}$) derived from thermal demagnetisation of the NRM and SIRM along different profiles. Dashed lines show inferred trends in respect to the distance of the intrusion. 22
- Figure 2.8:** Thellier type experiments on laboratory TRMs: Arai-Nagata plot (left side), corresponding Zijderveld diagram (middle) and the intensity during demagnetisation (right). Histograms showing intensities of MD checks (white bars) and directional deviations of pTRMs from the external field directions (gray bars). 24
- Figure 2.9:** Time temperature relation for different depths and positions: in the centre the intrusion (upper curves), in a distance of 200 m from the contact (middle curves) and in a distance of 1000 m from the contact (lower curves). The gray boxes marks the pyrrhotite window (Schill et al., 2002). Lighter gray stands for the temperatures above the Curie temperature of pyrrhotite (where a full TRM is acquired). 26
- Figure 2.10:** Examples of pyrrhotite bearing sample carrying different, partly antiparallel components. 27
- Figure 3.1:** FORC diagrams of all grain-size fractions from the TTE series (M. Dekkers, 1988). The samples show a decreasing asymmetry regarding their horizontal axis and a vanishing of the negative area with an increasing grain-size. Note that the coordinates are different for the sake of illustration. 42
- Figure 3.2:** Position of the distribution maxima in the FORC diagram. The coercivity (H_c) shows a decrease with increasing grain size. The deviation from the horizontal line (H_u) shows a more linear dependence. 43
- Figure 3.3:** Differential remanence parameter ΔM (see text for explanation) as a function of the applied field for selected grain-size fractions (in μm). A clear change in the type of interaction can be seen at the 30-40 μm fraction (upper limit of the PSD range). 43
- Figure 3.4:** Normalized IRM acquisition curve for the <5 μm fraction. The incomplete a.f. demagnetisation causes a residual remanence at zero fields. 44
- Figure 3.5:** FWHH and peak position ($Field_r$ and $Field_{dc}$) of the calculated differential susceptibility. The thick black line is the exponentially fitted trendline for the FWHH IRM_r curves. 45

Figure 3.6: IRM, IRM_{dc} and ΔM (grey) for the M1 sample. The IRM-values are reduced by .1 for a better illustration.	47
Figure 3.7: FORC diagram of sample M1 (SF=2, $t_{avr}=0.25s$, 100 FORCs). The distribution shows a clear SD particle assemblage. Interaction seems to be absent.	47
Figure 3.8: FORC diagrams from samples of Bourg d'Oisans. The elongated and closed contours along H_c up to 400 mT standing for a pure SD particles distribution with high coercivities. (picture with SF=3).	49
Figure 3.9: FORC diagrams from samples from the Elba. The closed contours and the peak position around 30 mT indicates a dominantly PSD assemblage. Signs of mean interaction field are absent. (both pictures with SF=3).	49
Figure 3.10: FORC diagrams from samples from the Isle of Skye, where different magnetic phases (pyrrhotite, magnetite) are present.	50
Figure 3.11: IRM, IRM_{dc} and ΔM curves for sample S5. The intensities of the IRM curves and the x-axis were changed for illustration.	51
Figure 4.1: Continuous demagnetization diagrams of samples FN-R1-2 (a) and FN-Q20-3 (b) with incremental heating cycles. The insets on the upper right of each diagram show orthogonal projections of the measured z- and x-component. The reversible increase, respectively decrease of magnetization at heating steps above 200°C in (a) indicates the presence of interacting particles leading to partial self-reversal. Such feature is not found in (b).	59
Figure 4.2: FORC diagrams of samples from group A (FN-Q20;FN-Q19;FN-Q24) , B (FN-Q3) and C (FN-Q18; FN-R1) together with their hysteresis loop. H_c stands for the coercivity distribution in the sample, whereas H_u indicates the strength of the interaction fields.	61
Figure 4.3: Two examples of ΔM plots. FN-Q20 belongs to group A and FN-Q4 to group C. The position of the parameters $\Delta M1$ and $\Delta M2$ are marked in the upper graph.	62
Figure 4.4: Comparison of the samples of all groups in the ΔM 1 vs. ΔM 2 plot and the conventional Day plot. The first one gives a better dissimination between group A and the other groups, whereas in the Day plot the transition between group A and B is gradual.	62
Figure 5.3: Conceptual sketch of the heating device for the cryogenic magnetometer	68
Figure 5.4: Left: Temperature behaviour in the centre and at the margin of a dummy sample. Applied power of the lamps = 600 Watt. Right: Configuration of the thermocouples with the sample during the calibration.	69
Figure 5.3: Thermal demagnetisation of a laboratory induced TRM (z-axis only) in a pyrrhotite-bearing sample. The grey area marks the time of heating. The remanence was measured every second.	70
Figure 5.4: Results of the simple demagnetisation model: Open boxes indicate the intensity behaviour of the independent volume elements during heating. The black box stands for the net remanence, i.e. the sum of all three volume elements.	72
Figure 5.5: Thermal demagnetisation of two antiparallel components imparted at temperatures of 300°C-270°C and 270°C-30°C, respectively: A) using the new furnace device. The time axis is transformed into a temperature axis using the results from the experimental calibration. Dotted line depicts the two antiparallel components. B) Thermal demagnetisation of a sample from the same location using the MMTD1 thermal demagnetiser.	73

Figure 5.6: Simple model for the two components demagnetisation at elevated temperatures: for the total remanence the transition is smeared by the superposition of the single volumes.	73
Figure 6.1: Principle of pTRM recording in a single sample during metamorphic cooling (from left to right): the different directions of the EMF are blocked in the respective TRMs. The direction of the EMF is marked with the arrow in the left upper half of the diagram. Gray boxes stand for individual unblocked pTRMs, white for blocked ones. The dashed line indicates the actual metamorphic temperature. The lower diagrams demonstrate the resulting net-intensity of the sample along the axis parallel to the primary EMF direction.	77
Figure 6.2: Thermal demagnetization of NRM. Left: Intensity variation. Right: Orthogonal vector plot. In the vertical projection the low (ChRM1) and high (ChRM2) unblocking components are indicated.	79
Figure 6.3: Two examples of the pTRM recording during laboratory experiments using different field direction. Arrows in the orthogonal vector plot indicate the directions of the applied fields.	80
Figure 6.4: Thermal modeling of the temperature-time-distance behavior in the contact metamorphic aureole. Upper graph: Maximum temperatures versus distance to the contact towards the dyke with constant and variable country rock temperature T_0 . Lower Graphs: Temperature-time behavior at different distances towards the contact. At the left graph, T_0 is constant, whereas at the right one, T_0 decreases exponentially with time.	81
Figure 6.5A: Laboratory TRM curve of one sample: The original temperatures (TRM orig.) were transformed according to natural cooling times (TRM trans.) after Dunlop et al. (2000). TRM inter. represents the temperature steps selected for NRM demagnetization. B: Example of an Arai-Nagata Plot, where the lined up NRM is compared with the transformed TRM. C: Paleointensities (in μT and % of present day field) obtained from the different demagnetization steps of the selected samples (black dots), where the temperature marks the lower demagnetization temperature of unblocking interval (i.e. component blocked between 200°C to 150°C is shown at 150°C , etc.). The mean and standard deviation of each temperature step is shown. The two cooling times on top are taken from the different thermal models (see Fig. 6.4). D: VGPs of the different components including α_{95} (gray circles).	83
Figure A.5: Schematic drawing of the structural design of the furnace	i
Figure A.6: Schematic configuration of the furnace control	ii

Table Captions:

Table 2.1: Benchmarks of the thermal modeling. $T_{\min,po}$ and $T_{\max,po}$ are the lower and upper limit of the pyrrhotite window.	31
Table 2.2: Recording potential tested by Thellier type experiments on a laboratory TRM (90μT): <u>Field</u> is the calculated field strength derived from the experiments; <u>Std.-dev</u> its standard deviation. <u>T_{Min}</u> and <u>T_{Max}</u> are the lower and upper temperature step, <u>N</u> the number of temperature steps used for field calculation. <u>MAD</u> is the mean angular deviation of the TRM direction. <u>Class</u> is the classification as mentioned in the text. <u>Δmag</u> and <u>Δang</u> are the maximal deviations from the intensity (MD checks) and the direction for an individual temperature step.	32
Table 3.1: Parameters derived from the calculated susceptibility for selected samples. $Field_{ac}$ and $Field_{dc}$ denote the position of the calculated susceptibility peaks. The column with Equ. (4) and Equ. (5) give the calculated mean of the grain-size fraction after formula (4) and (5), respectively. DS stands for the interpreted dominating domain state in the assemblage. For FWHH and the W parameter see text. The rockmagnetic parameters of M_{rs}/M_s and H_{cr}/H_c are added for the sake of completeness.	53
Table 4.1: Summary of the rockmagnetic parameters and the parameters derived from the interaction methods. For sample FN-Q22 (*) the ΔM-plot was not calculated due to a high initial remanence.	63
Table 5.1: Example of the demagnetisation model for one volume element. Ordinate: Temperature T($^{\circ}$C) of the volume element. Abscissa: number of grains with the corresponding unblocking temperature T_{ub}($^{\circ}$C). Sum is the net magnetisation of the volume element at the temperature T($^{\circ}$C).	71